GROUND STATES OF THE CLASSICAL ANTIFERROMAGNET ON THE PYROCHLORE LATTICE

By

Matthew Lapa

An Honors Thesis Submitted to the Department

of Applied and Engineering Physics

in Partial Fulfillment of the

Requirements for the Degree of

BACHELOR OF SCIENCE

Major Subject: ENGINEERING PHYSICS

Approved:

Christopher Henley, Project Adviser

Cornell University
Ithaca, New York

May 2012
(For Graduation May 2012)

CONTENTS

LIST OF TABLES iv

LIST OF FIGURES v

ACKNOWLEDGMENT vi

ABSTRACT vii

1. Introduction, Background and Methods 1

1.1 General Introduction 2

1.1.1 Frustrated Magnetism 2

1.1.2 Why study classical frustrated magnets? 4

1.2 Background Material 5

1.2.1 Some Notation 5

1.2.2 Heisenberg Hamiltonian 6

1.2.3 What is a classical spin? 6

1.2.4 The Pyrochlore Lattice 7

1.3 Methods 13

1.3.1 Iterative Minimization 14

1.3.2 Fourier Transforms and the Spin Structure Factor 15

1.3.3 Luttinger-Tisza (L.T.) Method 16

1.3.3.1 Derivation of the Method 17

1.3.3.2 The Special Case of a Bravais Lattice 18

1.3.4 Least Squares Fits 19

1.3.5 Projection of Stacked or Columnar States onto Lower Dimensional Lattices 21

1.3.6 Finding a Good Basis in Spin Space 23

1.3.6.1 Row Sums in Simple Cubic Sublattices 23

1.3.6.2 If Spins Point Towards the Corners of a Cube 24

2. The J_1-J_2 Phase Diagram 25

2.1 Simple States 29

2.1.1 Ferromagnetic State 29

2.1.2 Pure $J_1 < 0$ 30

2.1.3 $\mathbf{q} = \mathbf{0}$ State(s) 31
2.1.4 Pure $J_2 < 0$ 33
2.1.5 $\{q00\}$ Planar Spiral ($J_2 < 0$ and $J_1 > 0$ or $J_1 < 0$) 35
2.2 Cuboctahedral Stack ($J_1 > 0$, $J_2 < 0$) 36
2.3 Kawamura States 39
2.3.1 Kawamura Sextuplet-q State 41
2.4 A New Variety of Double-Twist State 47
2.5 Multiply-Modulated Commensurate Spirals 52
3. Beyond first and second nearest neighbor interactions 57
3.1 Cuboctahedral Stack in the J_1, J_3, J_3' Phase Diagram 57
3.2 A New Kind of Alternating Conic Spiral State 58
3.3 States Stacked Along a $\langle 111 \rangle$ Axis in Real Space 61
4. Conclusion 64
BIBLIOGRAPHY 66
APPENDICES
A. Taking Fourier Transforms on an F.C.C. Lattice 67
B. The Luttinger-Tisza Matrix for the Pyrochlore Lattice 70
C. Degeneracy of the Luttinger-Tisza eigenvalues for a pure first neighbor interaction J_1 72
D. Equivalence of small $J_2 > 0$ and small $J_3 < 0$ (and vice-versa) for large $J_1 < 0$. . . 74
E. Unit cells of the six sublattices of the Kawamura Sextuplet-q State 77

LIST OF TABLES

2.1 Summary of States Found in the J_1-J_2 Phase Diagram. 26

2.2 Site Energies of the Kawamura Sextuplet-q State with $J_1 = -1$, $J_2 = 0.1$, $seed = 67$. 42

2.3 Site Energies of the Kawamura Sextuplet-q State with $J_1 = -1$, $J_2 = 0.5$, $seed = 84$. 45

LIST OF FIGURES

1.1 The Pyrochlore Lattice. 8

1.2 View of the cubic unit cell of the Pyrochlore lattice down the z-axis. 9

1.3 One *up* and one *down* tetrahedron meet at a vertex. 10

1.4 The Kagome Lattice. 11

1.5 Stacking of triangular and Kagome lattice layers along a $\langle 111 \rangle$ axis. 12

2.1 The J_1-J_2 Phase Diagram for the Pyrochlore Lattice. 25

2.2 Largest L.T. eigenvalues vs. $J_2/|J_1|$ for the ferromagnetic and Kawamura states in the region $J_1 < 0$, $J_2 > 0$. 27

2.3 Largest L.T. eigenvalues vs. J_2/J_1 for the five ground states in the region $J_1 > 0$, $J_2 < 0$. 28

2.4 Largest L.T. eigenvalues vs. $J_2/|J_1|$ for the $\mathbf{q} = \mathbf{0}$ and $\{q00\}$ planar spiral states found in the region $J_1 < 0$, $J_2 < 0$. 29

2.5 L.T. eigenvalues plotted in the Brillouin zone of the F.C.C. lattice for $J_1 = -1$, $J_2 = -0.25$. 33

2.6 L.T. eigenvalues plotted in the Brillouin zone of the F.C.C. lattice for $J_1 = 1$, $J_2 = -0.2$. 39

2.7 L.T. eigenvalues plotted in the Brillouin zone of the F.C.C. lattice for $J_1 = -1$, $J_2 = 0.1$. 41

2.8 L.T. eigenvalues plotted in the Brillouin zone of the F.C.C. lattice for $J_1 = 1$, $J_2 = -0.6$. 52

D.1 Location of the spin $\mathbf{s}_0$ and the eight tetrahedra containing its first and second nearest neighbors. 75

ACKNOWLEDGMENT

We'd like to thank S. Sklan for helpful communications and calculations, Z. Lamberty for his help with the programming aspect of this project, and also S. Ghosh, H. Changlani and S. Pujari for helpful discussions. C.L.H. was supported by NSF grant DMR-1005466.

ABSTRACT

We study the classical ground states of the Heisenberg Hamiltonian on the Pyrochlore lattice, a lattice made of corner-sharing tetrahedra. We have explored all regions of the phase diagram for first and second nearest neighbor interactions. In this phase diagram we find a number of interesting coplanar and non-coplanar states. Examples include a 120° planar spiral state which is stacked in a $\langle 100 \rangle$ direction and the Cuboctahedral Stack state in which the spins point towards the eight corners and 12 edge-midpoints of a cube in spin space. We also find more complicated non-coplanar states like the Kawamura States and Double-Twist state, in which more wavevectors than just the optimal Luttinger-Tisza wavevectors are needed to normalize the states.

We also briefly look at states which incorporate the two kinds of third nearest neighbor interactions on the Pyrochlore lattice, and in that region of parameter space we again find the Cuboctahedral Stack state, as well as a new kind of alternating conic state. Our study suggests that the Heisenberg Hamiltonian has many interesting non-coplanar ground states for many different sets of interactions between nearest neighbors, next-nearest neighbors, etc. This should motivate future studies to find and characterize the ground states of the Heisenberg Hamiltonian on the Pyrochlore lattice with interactions beyond second nearest neighbors.

1. Introduction, Background and Methods

The goal of this project is to study the lowest energy states, or ground states, of the classical Heisenberg antiferromagnet on the Pyrochlore lattice. By a classical Heisenberg antiferromagnet, we mean a magnet whose total energy is given by the Heisenberg Hamiltonian,

$$\mathcal{H} = -\frac{1}{2}\sum_{i=1}^{N}\sum_{j\neq i} J_{ij}\mathbf{s}_i \cdot \mathbf{s}_j \tag{1.1}$$

where the N spins $\mathbf{s}_i$ are classical unit vectors (i.e. $|\mathbf{s}_i|^2 = 1$) which sit on the sites i of a crystal lattice. The spins are three-component vectors and the energy of the interaction between two spins is proportional to their dot product. The J_{ij} are constants which determine the strength and character of the interactions between the two spins $\mathbf{s}_i$ and $\mathbf{s}_j$. A $J_{ij} > 0$ corresponds to a ferromagnetic interaction and a $J_{ij} < 0$ corresponds to an antiferromagnetic interaction (because of the minus sign out front in the expression for $\mathcal{H}$). The factor of $\frac{1}{2}$ before the sum ensures that we don't double count the energy of interaction between two spins (just as one does not double count the electrostatic energy between two point charges in a collection of stationary point charges). We discuss a few of the elementary mathematical properties of (1.1) in detail in subsection 1.2.2.

We are particularly interested in finding non-coplanar ground states of (1.1). These are states in which the spins $\mathbf{s}_i$ have components in all three directions of spin space, the three-dimensional vector space that the spins "live" in. One can prove a theorem (see [6]) that every ground state of (1.1) on a Bravais lattice is coplanar. So we need to work with a non-Bravais lattice if we want to find ground states which are non-coplanar.

The Pyrochlore lattice is a non-Bravais lattice consisting of four face-centered cubic (F.C.C.) sublattices. We can think of the Pyrochlore lattice as being made up of corner-sharing tetrahedra. Because of the heavy presence of triangles of spins on this lattice (each tetrahedron has four triangular sides), many sets of interactions J_{ij} are geometrically frustrated, meaning that the geometry of the lattice makes it so that one cannot simultaneously satisfy all the interactions. Besides this geometric frustration, one can also get frustration from a set of competing interactions. An example of this kind of frustration occurs on the

square lattice with both antiferromagnetic first and second nearest neighbor interactions. We discuss the concept of frustration in general in 1.1.1.

Our work is based heavily on the work of Sophia Sklan (see [1]), a former student in the Applied & Engineering Physics department. In her honors thesis Sklan studied the ground states of a classical Heisenberg antiferromagnet on the Octahedral lattice, a non-Bravais lattice with three simple cubic sublattices. One can think of this lattice as a simple cubic lattice where the lattice sites sit on the 12 edge-midpoints of a cube. Most of the methods we use to search for grounds states on the Pyrochlore lattice, including Iterative Minimization and projection of stacked states onto one-dimensional lattices were all developed by Sklan to find the grounds states of (1.1) on the Octahedral lattice. We give a description of these methods and others in section 1.3.

In our study we have focused mostly on the case of first and second nearest neighbor interactions J_1 and J_2. We quickly found that the J_1-J_2 phase diagram already contains a number of interesting non-coplanar ground states, without any need to incorporate further neighbor interactions. The states we found in the J_1-J_2 plane are discussed in detail in chapter 2.

We also looked briefly at states beyond the J_1-J_2 phase diagram. In particular, we looked at a number of non-coplanar states involving J_3 and J_3', the two kinds of third nearest neighbor interactions on the Pyrochlore lattice. We discuss these states in detail in chapter 3.

1.1 General Introduction

In this section we discuss the concept of frustrated magnetism and indicate the reasons why we are interested in pursuing the classical ground states of (1.1) on the Pyrochlore lattice.

1.1.1 Frustrated Magnetism

One encounters frustrated magnetic systems when there are triangular geometries or competing interactions between neighboring spins in a material. A classic example is the case of a triangular lattice with an antiferromagnetic first nearest neighbor interaction. In

this case, the three spins on the vertices of each triangle cannot all point opposite each other and so the system is frustrated. In the context of the classical Heisenberg model, the ground state of this triangular lattice system is one in which the three spins on the vertices of every triangle all lie in the same plane but point 120° away from each other. One might call this situation geometrical frustration, because it is the geometry of the triangular lattice which prevents each spin from being able to satisfy all of its interactions.

Another kind of magnetic frustration can occur when one incorporates multiple different kinds of interactions, say J_1 between first nearest neighbors, J_2 between second nearest neighbors, J_3 between third nearest neighbors, etc. and these interactions compete with each other. A typical example of this kind of frustration occurs on the square lattice with an antiferromagnetic first neighbor interaction J_1 and an antiferromagnetic second neighbor interaction J_2. With only an antiferromagnetic first nearest neighbor interaction the square lattice is not frustrated because it is bipartite. When the second nearest neighbor interaction is added, however, the spins cannot point opposite all of their first nearest neighbors and all of their second nearest neighbors, so the system is frustrated.

Here is a way to identify frustration on a lattice with a set of competing interactions J_1, J_2, J_3, etc. First make a sketch of the lattice and draw lines connecting spins which have an interaction between them. If any three spins are connected in such a way that they form the vertices of a topological triangle then one should count the number of negative signs in the interactions around this triangle (positive signs for ferromagnetic interactions and negative signs for antiferromagnetic interactions). If there is an odd number of negative signs in the triangle then the interaction between these three spins is frustrated, hence the interaction between spins on this lattice is frustrated. In this way, frustration due to competing interactions can still be thought of as a frustration due to triangular geometry. To check an entire lattice for frustrated interactions, one needs to repeat this analysis for every set of three spins which are all connected by interactions. This is not difficult to do (although it may be time consuming). Given a set of interactions, one can easily find the triangles a given spin is a part of by looking to see which of that spin's neighbor's neighbors are also neighbors of that spin.

Whenever any kind of frustration is involved, the ground state of a system of spins

is always some kind of compromise between the competing interactions. In most of the states we look at, the competing interactions are all of comparable strength, so the resulting state does not favor any one interaction in particular. There are certain states, however, where one interaction is much stronger than all the others. Once we have understood the geometry of such a state, we try to understand how that state favors the dominant interaction between spins. Next we try to see how the state manages to still partially satisfy the weaker interactions. In this way we develop a qualitative understanding of why certain sets of interactions produce certain states.

There are a number of interesting categories of non-collinear magnetic states which occur in frustrated magnets, including coplanar states, in which the spins all lie in the same plane, and non-coplanar states, in which they do not. An example of a coplanar state is the helimagnetic or spiral state, in which spins along a line of sites in a material are each rotated by the same angle with respect to the previous spin in the line. An example of a non-coplanar state is the asymmetric conic state, found in the chain lattice (a one-dimensional lattice with a basis of two sites), in which spins of one type describe a cone opening upwards (with respect to some plane in the material) while spins of the second type describe a cone opening downwards (with respect to the same plane) but with a different cone angle. In this work we will mainly be interested in finding and characterizing non-coplanar states.

1.1.2 Why study classical frustrated magnets?

A good understanding of the classical ground states of frustrated magnetic systems is important for two reasons. When experimentalists doing neutron diffraction studies of magnetic materials find a new state, they might like to know what kind of magnetic interactions in the material work to produce that state (e.g. is the first neighbor interaction ferromagnetic or antiferromagnetic?). By working out the structure of the phase diagram for these materials, theorists can provide a kind of road map that can be used to identify the interactions causing the different kinds of magnetic ordering observed in neutron diffraction studies of magnetic materials. When a certain magnetic ordering is observed one simply looks for the area of the phase diagram in which that ordering is expected to be and makes note of the sign and strength of the exchange interactions in that area of the phase diagram. In this way one can get at least a qualitative sense of the character of the magnetic interactions

in that material. In fact, this project was partially motivated by the desire to know which sets of interactions on the Pyrochlore lattice can give a ground state like the one found in neutron diffraction experiments carried out by Lee, et al in [2].

There are also a number of very interesting physical properties which frustrated magnetic materials can display. For example, frustrated magnetic materials can have a non-zero entropy, even when cooled to temperatures near absolute zero. This is because frustrated magnets tend to have a large number of degenerate ground states. Since the entropy of a system is proportional to the logarithm of the number of microstates the system has, these frustrated materials have a non-zero entropy, even when cooled down to temperatures near absolute zero (see [12]). Eventually, at low enough temperatures, the quantum mechanical nature of the spins becomes important and quantum fluctuations will tend choose a particular ground state. This is one example of the concept of "ordering due to disorder", in which quantum fluctuations, thermal fluctuations, or structural disorder in the material select a specific ground state out of a set of degenerate states (see [3]).

1.2 Background Material

1.2.1 Some Notation

Let $\mathcal{E}_i$ denote the site energy of the spin $\mathbf{s}_i$. We define the site energy of the spin $\mathbf{s}_i$ to be

$$\mathcal{E}_i = -\frac{1}{2}\sum_{j\neq i} J_{ij}\mathbf{s}_i \cdot \mathbf{s}_j \ . \tag{1.2}$$

We call the average of this quantity over all the spins in the lattice the "energy per site" and denote it by $\bar{\mathcal{E}} = \frac{1}{N}\sum_i \mathcal{E}_i$. The total energy of the system can then be written as $\mathcal{H} = N\bar{\mathcal{E}}$. Let the unit vectors $\hat{\mathbf{A}}_0$, $\hat{\mathbf{B}}_0$ and $\hat{\mathbf{C}}_0$ form a fixed right-handed orthonormal basis, with $\hat{\mathbf{C}}_0 = \hat{\mathbf{A}}_0 \times \hat{\mathbf{B}}_0$. Because equation (1.1) is invariant under rotations in spin space, it will be useful to write parameterizations of ground states in terms of an orthonormal basis which has no special orientation relative to the crystal lattice. Matrices will be represented by bold, capital letters with a double underline, for example $\underline{\underline{\mathbf{M}}}$. Fourier Transforms of functions will have a tilde over the variable, for example $\mathcal{F}[f(\mathbf{r})] = \tilde{f}(\mathbf{q})$. Any further notation will be discussed when it becomes relevant, for example when we derive the Luttinger-Tisza Method.

1.2.2 Heisenberg Hamiltonian

The Heisenberg Hamiltonian for a set of N spins on a lattice is shown in equation (1.1). The coupling J_{ij} is a function of the vector separating the spins $\mathbf{s}_i$ and $\mathbf{s}_j$. We write $J_{ij} = J(\mathbf{R}_{ij})$ where $\mathbf{R}_{ij} = \mathbf{r}_i - \mathbf{r}_j$. Moreover, the coupling is an even function of $\mathbf{R}_{ij}$, so that $J(-\mathbf{R}_{ij}) = J(\mathbf{R}_{ij})$. In general it is not true that the coupling J_{ij} is a function of the magnitude of $\mathbf{R}_{ij}$, i.e. $J_{ij} \neq J(|\mathbf{R}_{ij}|)$. This is especially important on the Pyrochlore lattice where each site has two kinds of third nearest neighbor. Both kinds of a site's third nearest neighbors are the same distance from that site but they are not equivalent by symmetry. For this reason, J_{ij} is a function of the vector $\mathbf{R}_{ij}$.

It is not difficult to prove that (1.1) is invariant under a uniform rotation of all the spins. Suppose we apply the rotation $\underline{\underline{\mathbf{R}}}$ to each spin $\mathbf{s}_i$. Then $\mathbf{s}_i \cdot \mathbf{s}_j \to (\underline{\underline{\mathbf{R}}}\mathbf{s}_i) \cdot (\underline{\underline{\mathbf{R}}}\mathbf{s}_j)$. Using elementary matrix algebra we find

$$\begin{aligned} (\underline{\underline{\mathbf{R}}}\mathbf{s}_i) \cdot (\underline{\underline{\mathbf{R}}}\mathbf{s}_j) &= (\underline{\underline{\mathbf{R}}}^T \underline{\underline{\mathbf{R}}}\mathbf{s}_i) \cdot \mathbf{s}_j \\ &= (\underline{\underline{\mathbf{I}}}\mathbf{s}_i) \cdot \mathbf{s}_j \\ &= \mathbf{s}_i \cdot \mathbf{s}_j \end{aligned} \tag{1.3}$$

where the second step follows from the fact that $\underline{\underline{\mathbf{R}}}^T \underline{\underline{\mathbf{R}}} = \underline{\underline{\mathbf{I}}}$ since $\underline{\underline{\mathbf{R}}}$ is a rotation matrix. So the total energy of the system does not change if we apply the same rotation to all of the spins.

1.2.3 What is a classical spin?

Since the spin of a particle is a quantum mechanical concept, it is natural for one to wonder what exactly is meant by a classical spin. Here we provide a partial answer to this question. Consider a quantum mechanical particle of spin S. We know that the z-component of the spin, S_z, can take on any value m in the set $-S, -S+1, \ldots, S-1, S$. If this particle is in the eigenstate of S_z with $S_z = m$, denoted by $|S, m\rangle$ then as the spin fluctuates quantum mechanically, the tip of the vector $\mathbf{S}$ is free to wander around on the circle in spin space parallel to the S_x-S_y plane with radius $\sqrt{S(S+1) - m^2}$ and center at $S_z = m$.

In the largest eigenstate of S_z with $m = S$, the radius of this circle is $\sqrt{S}$ and the ratio of the radius of this circle to the size of the spin, S, is $\frac{1}{\sqrt{S}}$. In the limit $S \to \infty$, this ratio

tends to zero, so that the spin points in a definite direction in the three-dimensional spin space. So the classical spins which we are dealing with, which point in definite directions, can be thought of as the largest eigenstate of a quantum mechanical particle of spin S in the limit $S \to \infty$.

1.2.4 The Pyrochlore Lattice

As we mentioned in the introduction, the Pyrochlore lattice (figure 1.1) is a non-Bravais lattice consisting of four F.C.C. sublattices. One may visualize the Pyrochlore lattice in a variety of different ways, each of which is useful for understanding the geometry of the various ground states that we find. Perhaps the simplest way of describing the Pyrochlore lattice is to give the locations of the origins of its four F.C.C. sublattices, which we have numbered $0, \ldots, 3$. We take the edge-length of the cubic unit cell of the Pyrochlore lattice to be 1, so the edge-length of the cubic unit cell of each FCC sublattice is also 1. In our work the origins of the four F.C.C. sublattices are taken to be $(0,0,0)$, $(0,\frac{1}{4},\frac{1}{4})$, $(\frac{1}{4},0,\frac{1}{4})$ and $(\frac{1}{4},\frac{1}{4},0)$, respectively. The cubic unit cell of the Pyrochlore lattice, viewed down the z-axis, is shown in figure 1.2. First we review a few facts about the F.C.C. lattice (see [11] as a reference).

The F.C.C. lattice is a cubic Bravais lattice consisting of the points at the corners and the face-centers of the underlying simple cubic lattice. In fact, the F.C.C. lattice itself consists of four simple cubic sublattices. Any point in the F.C.C. sublattice has a position vector of the form

$$\mathbf{R} = n_1\mathbf{a}_1 + n_2\mathbf{a}_2 + n_3\mathbf{a}_3 \tag{1.4}$$

where n_1, n_2 and n_3 are integers and $\mathbf{a}_1$, $\mathbf{a}_2$ and $\mathbf{a}_3$ are the *direct lattice vectors* for the F.C.C. lattice. They are defined to be

$$\mathbf{a}_1 = \frac{1}{2}(\hat{\mathbf{y}} + \hat{\mathbf{z}}) \tag{1.5a}$$

$$\mathbf{a}_2 = \frac{1}{2}(\hat{\mathbf{x}} + \hat{\mathbf{z}}) \tag{1.5b}$$

$$\mathbf{a}_3 = \frac{1}{2}(\hat{\mathbf{x}} + \hat{\mathbf{y}}) \tag{1.5c}$$

where $\hat{\mathbf{x}}$, $\hat{\mathbf{y}}$ and $\hat{\mathbf{z}}$ are the usual Cartesian basis vectors for real space. Since we want to discuss the periodicity of spin arrangements on the Pyrochlore lattice, we also need to know

Figure 1.1: The Pyrochlore Lattice.

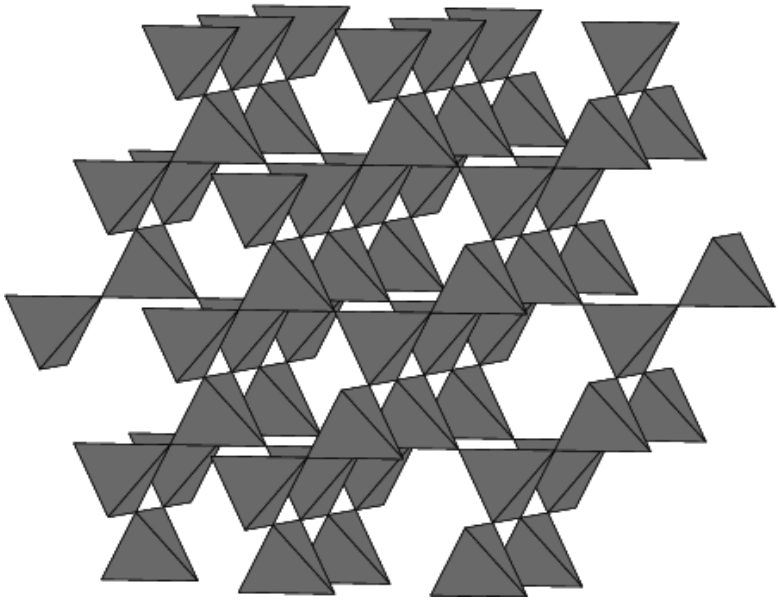

(Ph. D. thesis of Uzi Hizi, 2006.)

the reciprocal lattice vectors for the F.C.C. lattice. It will sometimes be helpful to express the wavevectors our spin configurations are composed of in the basis formed by the reciprocal lattice vectors of the F.C.C. lattice, instead of the usual cubic basis for reciprocal space.

The reciprocal lattice vectors for the F.C.C. lattice can be computed as follows:

$$\mathbf{g}_1 = 2\pi \frac{\mathbf{a}_2 \times \mathbf{a}_3}{\mathbf{a}_1 \cdot (\mathbf{a}_2 \times \mathbf{a}_3)} \tag{1.6a}$$

$$\mathbf{g}_2 = 2\pi \frac{\mathbf{a}_3 \times \mathbf{a}_1}{\mathbf{a}_1 \cdot (\mathbf{a}_2 \times \mathbf{a}_3)} \tag{1.6b}$$

$$\mathbf{g}_3 = 2\pi \frac{\mathbf{a}_1 \times \mathbf{a}_2}{\mathbf{a}_1 \cdot (\mathbf{a}_2 \times \mathbf{a}_3)} \tag{1.6c}$$

We find

$$\mathbf{g}_1 = 2\pi \left(-\hat{\mathbf{x}} + \hat{\mathbf{y}} + \hat{\mathbf{z}}\right) \tag{1.7a}$$

$$\mathbf{g}_2 = 2\pi \left(\hat{\mathbf{x}} - \hat{\mathbf{y}} + \hat{\mathbf{z}}\right) \tag{1.7b}$$

$$\mathbf{g}_3 = 2\pi \left(\hat{\mathbf{x}} + \hat{\mathbf{y}} - \hat{\mathbf{z}}\right) \tag{1.7c}$$

Figure 1.2: View of the cubic unit cell of the Pyrochlore lattice down the z-axis.

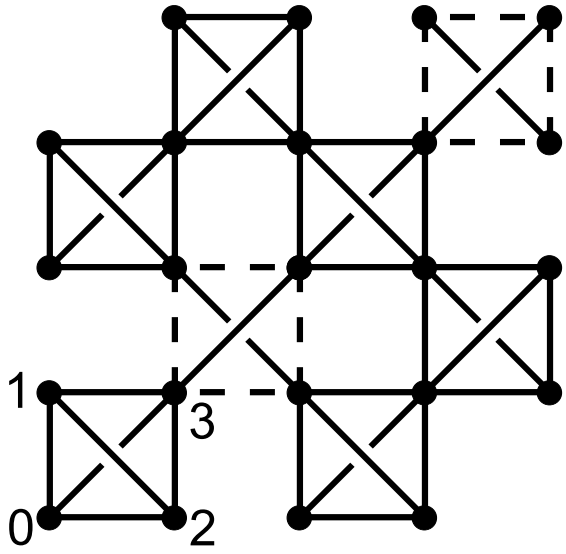

We see that the Brillouin zone of the F.C.C. lattice is twice the size of the Brillouin zone of the simple cubic lattice. The reason for this is that functions defined on the F.C.C. lattice can have twice the frequency of functions on the simple cubic lattice because there are sites in the F.C.C. lattice which have half-integer coordinates. As an example, the function $\cos(2\pi x)$ has the same value on every site in the simple cubic lattice (it always equals 1), but in the FCC lattice it is alternately plus or minus 1 depending on whether x is an integer or half-integer.

Some particular points of importance in the Brillouin zone of the F.C.C. lattice are the Γ point, $(0,0,0)$, the X point, $2\pi(1,0,0)$, the W point, $2\pi(1,\frac{1}{2},0)$, the K point, $2\pi(\frac{3}{4},\frac{3}{4},0)$ and the L point, $2\pi(\frac{1}{2},\frac{1}{2},\frac{1}{2})$. When one plots the band structure of a dispersion relation on the F.C.C. lattice, one typically plots it on the following route through the Brillouin zone (see [11], figure 9.5): $\Gamma \to X \to W \to L \to \Gamma \to K \to X$. In chapter 2 we plot the Luttinger-Tisza eigenvalues for a given set of interactions J_{ij} along this route in the Brillouin zone of the F.C.C. lattice to show the wavevector where the largest Luttinger-Tisza eigenvalue is maximized.

With this knowledge of the F.C.C. lattice in hand, we return to our discussion of the

Pyrochlore lattice.

The Pyrochlore lattice can also be thought of as the network of sites at the vertices of corner-sharing regular tetrahedra. In this picture the Pyrochlore lattice is made up of two kinds of tetrahedra, which we will call *up* and *down* tetrahedra. An *up* tetrahedron meets a *down* tetrahedron at each of its four vertices and the reverse is true for the *down* tetrahedra. Figure 1.3 shows one *up* and one *down* tetrahedron meeting at a vertex, like they do at every site in the Pyrochlore lattice.

Figure 1.3: One *up* and one *down* tetrahedron meet at a vertex.

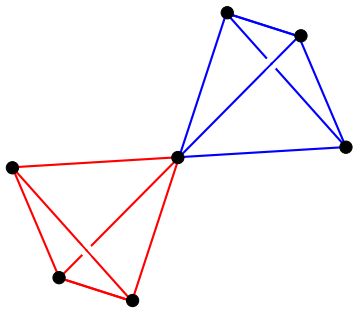

A third way to construct the Pyrochlore lattice is by placing lattice sites at the bond midpoints of the diamond lattice (the diamond lattice is itself made up of two F.C.C. sublattices, displaced from each other a distance $\frac{\sqrt{3}}{4}$ along the [111] direction, see [11]).

Finally, one can think of the Pyrochlore lattice as a stacking of alternating triangular lattice and Kagome lattice layers in a $\langle 111 \rangle$ direction. The Kagome lattice is a two-dimensional non-Bravais lattice with three triangular sublattices. It is shown in figure 1.4. In this stacking picture, the triangular lattice layers are made up of sites from one of the F.C.C. sublattices and the Kagome lattice layers are made up of sites from the other three F.C.C. sublattices. In the geometry we have chosen, if we thought of the lattice as a stacking of such layers in the [111] direction, then the triangular lattice layers would consist of sites in the 0^{th} F.C.C. sublattice and the Kagome lattice layers would consist of sites in F.C.C. sublattices 1, 2 and 3. Figure 1.5 shows one Kagome lattice layer sandwiched between two triangular lattice layers along a $\langle 111 \rangle$ direction.

Every site on the Pyrochlore lattice has six first nearest neighbors. The first nearest neighbors of a site can be reached by traveling along an edge of either of the two tetrahedra

that that site is a part of. There are six such edges connected to each site so each site has six first nearest neighbors. Since we take the cubic unit cell of the Pyrochlore lattice to have edge length equal to one, the edges of the tetrahedra have length $\delta_1 = \sqrt{(\frac{1}{4})^2 + (\frac{1}{4})^2} = \frac{1}{2\sqrt{2}}$, so the first nearest neighbors of a site are a distance δ_1 away. From now on, we refer to a site's first nearest neighbors as its "J_1 neighbors", where J_1 is the interaction between sites which are first nearest neighbors.

Each site also has 12 second nearest neighbors. These can be reached from any site by first moving along one of the six edges of the two tetrahedra that that site belongs to, and then along one of the two edges of the next tetrahedron which is not collinear with the first edge traveled on. Because there are six options for the first edge to take and then two options for every next edge to travel along, each site has 12 second nearest neighbors. Since the two edges one travels on to get to a second nearest neighbor have an angle of $\frac{2\pi}{3}$ between them, a site's second nearest neighbors are a distance $\delta_2 = \delta_1\sqrt{2(1 - \cos(\frac{2\pi}{3}))} = \delta_1\sqrt{3}$ away. We refer to a site's second nearest neighbors as its "J_2 neighbors", where J_2 is the interaction between sites which are second nearest neighbors.

Each site on the Pyrochlore lattice also has 12 third nearest neighbors, but these third nearest neighbors come in two kinds which are not equivalent by symmetry. Each site has six of each kind of third nearest neighbor. The six third nearest neighbors of the first kind of a site can be reached from that site by traveling along two collinear tetrahedron edges. There are six such routes from each site so there are six of the first kind of third nearest

Figure 1.4: The Kagome Lattice.

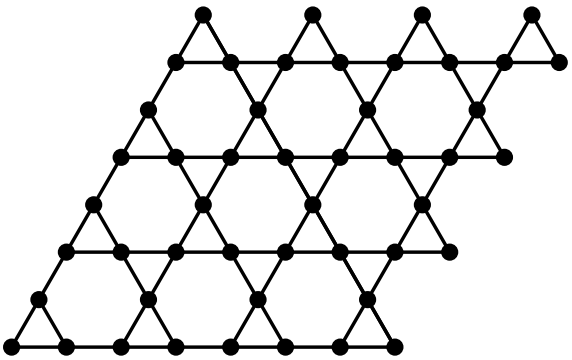

Figure 1.5: Stacking of triangular and Kagome lattice layers along a $\langle 111 \rangle$ axis.

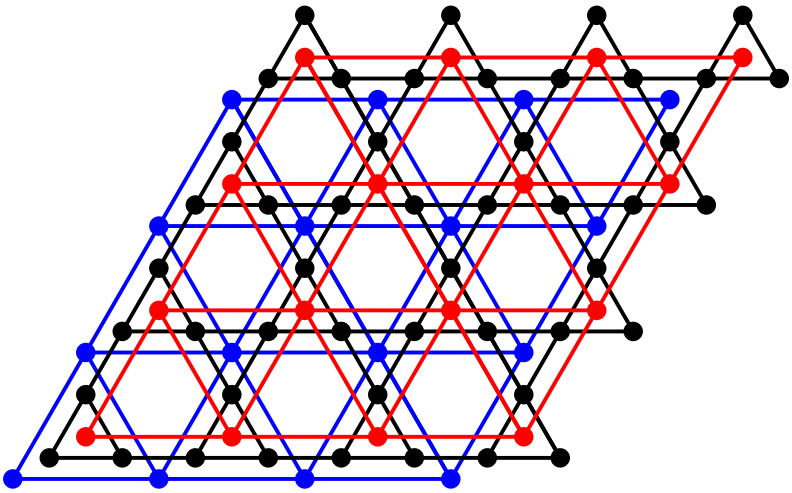

neighbor. The six third nearest neighbors of the second kind of a site can be reached by hopping from that site across a hexagon in the Kagome lattice layers that that site is in. One can see that these two kinds of third nearest neighbors are inequivalent by symmetry because they are reached in very different ways. In particular, there is always a first nearest neighbor on the line between a site and one of its third nearest neighbors of the first kind but there are no other neighbors on the line between a site and one of its third nearest neighbors of the second kind. Both kinds of third nearest neighbor are a distance $\delta_3 = 2\delta_1$ away, and this distance is just twice the length of an edge of a tetrahedron. We refer to a site's third nearest neighbors of the first kind as "J_3 neighbors" and the third nearest neighbors of the second kind as "J_3' neighbors", where J_3 and J_3' are the interactions between sites which are third nearest neighbors of the first and second kind, respectively.

Each site on the Pyrochlore lattice also has 12 fourth nearest neighbors. These can be reached by hopping across a hexagon in a Kagome layer and then traveling along one edge of a tetrahedron which is perpendicular to the direction of the hop. The fourth nearest neighbors also connect up sites that are in different FCC sublattices. Since one first travels the third nearest neighbor distance δ_3 and then the first nearest neighbor distance δ_1 (in a direction perpendicular to the first hop), the distance from a site to its fourth nearest

neighbors is $\delta_4 = \sqrt{\delta_1^2 + \delta_3^2} = \delta_1\sqrt{5}$. We refer to a site's fourth nearest neighbors as its "J_4 neighbors", where J_4 is the interaction between spins which are fourth nearest neighbors.

1.3 Methods

In this section we describe a number of methods which we relied on heavily for finding and interpreting the ground states. Our main method for finding the ground states was the Iterative Minimization simulation, an iterative computational method which can find the ground states of a finite set of spins on a lattice with some given boundary conditions. Once we find a ground state using iterative minimization, the next thing we do is take a Fourier Transform of that state in each F.C.C. sublattice. We compute the Spin Structure Factor, the absolute square of the Fourier Transform of the spins in each F.C.C. sublattice, to determine which wavevectors a state is mostly composed of.

The Luttinger-Tisza method (see [6]) is a theoretical method which can be used to determine which wavevectors a state will be mostly composed of. We refer to these wavevectors as the "optimal Luttinger-Tisza wavevectors". Comparing these wavevectors to those found in the Fourier Transform of the result of an Iterative Minimization simulation is a useful way of determining whether the simulation has found the true ground state.

To get a rough idea of the parameterization of a ground state, we do a least squares fit of the configuration found in an Iterative Minimization simulation to sines and cosines of the wavevectors found in the Fourier Transform of that state. We can then analyze this parameterization and try to find an idealization of it to completely characterize a state.

We sometimes find stacked or columnar states, in which all the spins the same plane perpendicular to a certain direction, or all the spins in the same line parallel to a certain direction, are parallel to each other. In cases like this we can project our problem on the three-dimensional Pyrochlore lattice onto an equivalent problem on a one- or two-dimensional lattice with a corresponding set of interactions. We can then try to solve this lower dimensional problem for the ground state of the three-dimensional lattice.

Finally, it is very useful to write the parameterization of a state using a basis for spin space in which the spins point in high symmetry directions. Below, we discuss the technique of taking row sums of spins in each simple cubic sublattice, as a method for finding the

distinguished directions in spin space. We also show how one can construct a symmetrical basis for spin space if the spins point towards the eight corners of a cube in spin space.

1.3.1 Iterative Minimization

As in the previous work of Sophia Sklan (see [1]), our main method of searching for ground states is the Iterative Minimization simulation. Given a set of interactions J_{ij} and set of spins in a random configuration, one can use this simulation to numerically determine the ground state of (1.1). This method is based on the idea of the local field $\mathbf{h}_i$, of a spin $\mathbf{s}_i$. Given a Hamiltonian $\mathcal{H}(\mathbf{s}_1, \ldots, \mathbf{s}_N)$ that is a function of the spins $\mathbf{s}_1, \ldots, \mathbf{s}_N$, the local field of the spin $\mathbf{s}_i$ is defined to be

$$\mathbf{h}_i = \left(\frac{\partial \mathcal{H}}{\partial s_i^a}, \frac{\partial \mathcal{H}}{\partial s_i^b}, \frac{\partial \mathcal{H}}{\partial s_i^c} \right) \tag{1.8}$$

where s_i^a, s_i^b, and s_i^b are the three components of the spin $\mathbf{s}_i = s_i^a \hat{\mathbf{A}}_0 + s_i^b \hat{\mathbf{B}}_0 + s_i^c \hat{\mathbf{C}}_0$. It is the gradient of the Hamiltonian with respect to the spin coordinates. For the Heisenberg Hamiltonian, the local field for the spin $\mathbf{s}_i$ is

$$\mathbf{h}_i = -\sum_{j \neq i} J_{ij} \mathbf{s}_j \ . \tag{1.9}$$

Then we can rewrite equation (1.1) in the following way:

$$\mathcal{H} = \frac{1}{2} \sum_{i=1}^{N} \mathbf{h}_i \cdot \mathbf{s}_i \ . \tag{1.10}$$

This expression implies that any state state in which every spin points opposite its local field is a ground state. To see this, suppose that we had a state in which one spin $\mathbf{s}_k$ was not pointing opposite its local field. Then we could immediately construct a lower energy state by keeping fixed every spin $\mathbf{s}_j$, $j \neq k$, and rotating $\mathbf{s}_k$ to point opposite it's local field. This observation suggests an iterative method for finding the ground state of a set of spins initially pointing in random directions. One could try to find the ground state by choosing spins at random and reorienting them so that they point opposite their local field.

The Iterative Minimization simulation works in the following way. We start with the N spins on the lattice pointing in random directions. Next, we run a large loop for an

unspecified number of iterations. On each iteration of the loop we choose N spins at random and reorient them to point opposite their local field. The loop stops when the difference between the new set of spin vectors and the old set is smaller than some specified tolerance.

This procedure does not always find the true ground state but it usually comes pretty close. If we think that the simulation has not found the true ground state, we usually try projecting the state down onto the dominant Fourier modes composing it and then perform the Iterative Minimization procedure on that configuration to see if it produces a configuration with lower energy.

We typically perform these simulations on an $L \times L \times L$ block of Pyrochlore lattice unit cells (where L is an integer). We use periodic boundary conditions so that the spins at $\mathbf{r} + L\hat{\mathbf{x}}$, $\mathbf{r} + L\hat{\mathbf{y}}$ and $\mathbf{r} + L\hat{\mathbf{z}}$ are all the same as the spin at $\mathbf{r}$. One cubic unit cell of the Pyrochlore lattice contains 16 sites, so an $L \times L \times L$ block of Pyrochlore lattice unit cells contains $N = 16L^3$ spins. The parameter *seed*, which is mentioned later on when we refer to the results of specific Iterative Minimization simulations, is the initial number supplied to the random number generator which generates our initial set of N randomly oriented spins and later picks spins at random to set opposite their local field.

1.3.2 Fourier Transforms and the Spin Structure Factor

Once we have found a spin configuration using Iterative Minimization, we take Fourier Transforms of that spin configuration in each F.C.C. sublattice. Next we compute the Spin Structure Factor in each F.C.C. sublattice to determine which wavevectors the configuration mostly consists of. Let $\mathbf{s}_0(\mathbf{r})$, $\mathbf{s}_1(\mathbf{r})$, $\mathbf{s}_2(\mathbf{r})$ and $\mathbf{s}_3(\mathbf{r})$ be functions representing the spin configuration in the four FCC sublattices. The Fourier Transform of the spin configuration in the α^{th} sublattice is given by

$$\tilde{\mathbf{s}}_\alpha(\mathbf{q}) = \frac{2}{\sqrt{N}} \sum_{\mathbf{r}} \mathbf{s}_\alpha(\mathbf{r}) e^{-i\mathbf{q}\cdot\mathbf{r}} \tag{1.11}$$

where $\mathbf{q}$ is a wavevector in the Brillouin zone of the F.C.C. lattice and the sum is taken over all sites in the α^{th} F.C.C. sublattice. The factor $\frac{2}{\sqrt{N}}$ is just one divided by the square root of the number of spins in the F.C.C. sublattice (each F.C.C. sublattice has $N/4$ spins in it). In practice we compute these Fourier Transforms one spin component at a time. We discuss in

detail the process of taking the Fourier Transform of a scalar function defined on an F.C.C. lattice in appendix A.

The Spin Structure Factor of the spin configuration in the α^{th} F.C.C. sublattice is

$$S.S.F._{\alpha}(\mathbf{q}) = |\tilde{\mathbf{s}}_{\alpha}(\mathbf{q})|^2 \ . \tag{1.12}$$

It is just the absolute square of the Fourier Transform of the spin configuration in the α^{th} F.C.C. sublattice. Analyzing the values of $S.S.F._{\alpha}(\mathbf{q})$ helps us determine which wavevectors a given state is mostly composed of.

1.3.3 Luttinger-Tisza (L.T.) Method

By taking the Fourier Transform of the spin configuration in each Bravais sublattice of a non-Bravais lattice, one can write the Heisenberg Hamiltonian, (1.1) as a sum of the Fourier Transform of the interactions J_{ij} over all wavevectors $\mathbf{q}$ in the Brillouin zone of the underlying Bravais lattice. Minimizing (1.1) by writing it in this fashion is known as the Luttinger-Tisza Method (this method is reviewed in [6]).

Suppose the lattice has M Bravias sublattices and let the sublattices be labeled by the index α, with $0 \leq \alpha \leq M-1$. If the lattice has N spins in total then there will be $n = \frac{N}{M}$ spins in each Bravais sublattice. Let $\mathbf{r}_i^{\alpha}$ denote the position of the i^{th} spin in the α^{th} sublattice, where $1 \leq i \leq n$. Define $\mathbf{R}_{ij}^{\alpha\beta} = \mathbf{r}_i^{\alpha} - \mathbf{r}_j^{\beta}$ as the displacement vector between the i^{th} spin in the α^{th} sublattice and the j^{th} spin in the β^{th} sublattice. Finally let $\mathbf{s}_i^{\alpha}$ denote the i^{th} spin in the α^{th} sublattice. Then we may write the Heisenberg Hamiltonian, equation (1.1) in the following way:

$$\mathcal{H} = -\frac{1}{2}\sum_{i}\sum_{j}\sum_{\alpha}\sum_{\beta} J(\mathbf{R}_{ij}^{\alpha\beta})\mathbf{s}_i^{\alpha}\cdot\mathbf{s}_j^{\beta} \tag{1.13}$$

with the constraint that $i \neq j$ if $\alpha = \beta$ (so that spins do not interact with themselves).

1.3.3.1 Derivation of the Method

To begin the derivation of the L.T. method, we first write $\mathbf{s}_i^\alpha$ as a sum of Fourier modes,

$$\mathbf{s}_i^\alpha = \frac{1}{\sqrt{n}} \sum_{\mathbf{q}} \tilde{\mathbf{s}}^\alpha(\mathbf{q}) e^{i\mathbf{q}\cdot\mathbf{r}_i^\alpha} \tag{1.14}$$

where $\tilde{\mathbf{s}}^\alpha(\mathbf{q})$ is the Fourier Transform of $\mathbf{s}_i^\alpha$ and $\mathbf{q}$ is a wavevector in the Brillouin zone of the F.C.C. lattice. We now plug this expression in for $\mathbf{s}_i^\alpha$ and $\mathbf{s}_j^\beta$ in the above equation. We get

$$\mathcal{H} = -\frac{1}{2} \sum_i \sum_j \sum_\alpha \sum_\beta J(\mathbf{R}_{ij}^{\alpha\beta}) \left(\frac{1}{\sqrt{n}} \sum_{\mathbf{q}} \tilde{\mathbf{s}}^\alpha(\mathbf{q}) e^{i\mathbf{q}\cdot\mathbf{r}_i^\alpha} \right) \cdot \left(\frac{1}{\sqrt{n}} \sum_{\mathbf{q}'} \tilde{\mathbf{s}}^\beta(\mathbf{q}') e^{i\mathbf{q}'\cdot\mathbf{r}_j^\beta} \right) \tag{1.15}$$

Next we pull the sums over $\mathbf{q}$ and $\mathbf{q}'$ out to the front, and we set $\mathbf{r}_j^\beta = \mathbf{r}_i^\alpha - \mathbf{R}_{ij}^{\alpha\beta}$ to get

$$\mathcal{H} = -\frac{1}{2n} \sum_i \sum_j \sum_\alpha \sum_\beta \sum_{\mathbf{q}} \sum_{\mathbf{q}'} J(\mathbf{R}_{ij}^{\alpha\beta}) \tilde{\mathbf{s}}^\alpha(\mathbf{q}) \cdot \tilde{\mathbf{s}}^\beta(\mathbf{q}') e^{i(\mathbf{q}+\mathbf{q}')\cdot\mathbf{r}_i^\alpha} e^{-i\mathbf{q}'\cdot\mathbf{R}_{ij}^{\alpha\beta}} \tag{1.16}$$

Since we have exchanged $\mathbf{r}_j^\beta$ for $\mathbf{r}_i^\alpha - \mathbf{R}_{ij}^{\alpha\beta}$, the sum over j is now really a sum over all separations between spins. This means that we can perform the sum over i while holding all of the other variables constant. This sum only "picks up" the exponential term involving $\mathbf{q}$ and $\mathbf{q}'$. Using the usual orthogonality relations for discrete Fourier transforms we have

$$\sum_i e^{i(\mathbf{q}+\mathbf{q}')\cdot\mathbf{r}_i^\alpha} = n\delta_{-\mathbf{q},\mathbf{q}'} \tag{1.17}$$

where $\delta_{-\mathbf{q},\mathbf{q}'}$ is the Kronecker delta symbol. After performing the sum over $\mathbf{q}'$, the Hamiltonian becomes

$$\mathcal{H} = -\frac{1}{2} \sum_j \sum_\alpha \sum_\beta \sum_{\mathbf{q}} J(\mathbf{R}_{ij}^{\alpha\beta}) \tilde{\mathbf{s}}^\alpha(\mathbf{q}) \cdot \tilde{\mathbf{s}}^\beta(-\mathbf{q}) e^{i\mathbf{q}\cdot\mathbf{R}_{ij}^{\alpha\beta}} \tag{1.18}$$

Next we define the quantity $\tilde{J}^{\alpha\beta}(\mathbf{q})$, the Fourier transform of the coupling $J(\mathbf{R}_{ij}^{\alpha\beta})$ between sublattice α and sublattice β, to be

$$\tilde{J}^{\alpha\beta}(\mathbf{q}) = \frac{1}{2} \sum_j J(\mathbf{R}_{ij}^{\alpha\beta}) e^{i\mathbf{q}\cdot\mathbf{R}_{ij}^{\alpha\beta}} \ . \tag{1.19}$$

Now we may write $\mathcal{H}$ as

$$\mathcal{H} = -\sum_{\mathbf{q}} \sum_{\alpha} \sum_{\beta} \tilde{J}^{\alpha\beta}(\mathbf{q}) \tilde{\mathbf{s}}^{\alpha}(\mathbf{q}) \cdot \tilde{\mathbf{s}}^{\beta}(-\mathbf{q}) \tag{1.20}$$

where we have again rearranged the sums out front. The summand of the sum over $\mathbf{q}$ in this expression is just a quadratic form involving the matrix whose elements are $\tilde{J}^{\alpha\beta}(\mathbf{q})$. We call this matrix $\underline{\underline{\tilde{\mathbf{J}}}}(\mathbf{q})$. To minimize $\mathcal{H}$ then, we should choose the wavevector $\mathbf{q}^*$ which maximizes the largest eigenvalue of $\underline{\underline{\tilde{\mathbf{J}}}}(\mathbf{q})$. In what follows, we will sometimes denote the largest eigenvalue of $\underline{\underline{\tilde{\mathbf{J}}}}(\mathbf{q})$ by $\lambda_{L.T.^*}$.

We show the form of $\underline{\underline{\tilde{\mathbf{J}}}}(\mathbf{q})$ for the Pyrochlore lattice with interactions out to fourth nearest neighbors in Appendix B. In Appendix C we exactly diagonalize $\underline{\underline{\tilde{\mathbf{J}}}}(\mathbf{q})$ for the case of a pure first neighbor interaction $J_1 < 0$.

1.3.3.2 The Special Case of a Bravais Lattice

In the special case of a Bravais lattice, the number of sublattices M is equal to one. This means that in equation (1.13) the sums over α and β disappear and we must take $j \neq i$ in the sum over j. Then equation (1.19), the Fourier transform of the couplings, becomes a scalar quantity

$$\tilde{J}(\mathbf{q}) = \frac{1}{2} \sum_{j \neq i} J(\mathbf{R}_{ij}) e^{i\mathbf{q}\cdot\mathbf{R}_{ij}} \tag{1.21}$$

The Heisenberg Hamiltonian as a sum over $\mathbf{q}$, equation (1.20), becomes

$$\mathcal{H} = -\sum_{\mathbf{q}} \tilde{J}(\mathbf{q}) \left|\tilde{\mathbf{s}}(\mathbf{q})\right|^2 \tag{1.22}$$

since $\tilde{\mathbf{s}}(\mathbf{q}) \cdot \tilde{\mathbf{s}}(-\mathbf{q}) = \left|\tilde{\mathbf{s}}(\mathbf{q})\right|^2$. Once we have the wavevector $\mathbf{q}^*$ which minimizes $\tilde{J}(\mathbf{q})$, we can write the total energy of the system as

$$\mathcal{H} = -N\tilde{J}(\mathbf{q}^*) \tag{1.23}$$

since $\left|\tilde{\mathbf{s}}(\mathbf{q}^*)\right|^2 = N$ if the spins are normalized. In fact, because the optimal L.T. wavevector has the same amplitude on all sites of a Bravais lattice, we may write out the final form of

the ground state. It is a coplanar spiral involving only the wavevector $\mathbf{q}^*$.

$$\mathbf{s}_i = \cos(\mathbf{q}^* \cdot \mathbf{r}_i + \phi)\hat{\mathbf{A}}_0 + \sin(\mathbf{q}^* \cdot \mathbf{r}_i + \phi)\hat{\mathbf{B}}_0 \tag{1.24}$$

where ϕ is an arbitrary phase factor.

1.3.4 Least Squares Fits

One method which proved very useful for getting a rough idea of the parameterization of a state in each F.C.C. sublattice was to do a least squares fit of that state to sines and cosines of the optimal L.T. wavevectors. To get the best results from a fit like this it is helpful if one has already rotated the spin configuration into a convenient basis in spin space (finding the right basis to rotate each state into is a tricky problem in itself, more on this later).

The problem here is to do a least squares fit of a numerical spin configuration (the output of an Iterative Minimization simulation) to a set of functions which are sines and cosines of the wavevectors which that configuration is mostly comprised of (we determine the wavevector content of a state by taking Fourier Transforms of the spin configuration in the four F.C.C. sublattices, see appendix A). We do this fit one F.C.C. sublattice at a time and one spin component at a time, so one has to perform 12 = (4 F.C.C. sublattices)$\times$(3 spin components) fits to get a complete parameterization for a state.

The spin configuration is a function of three independent variables (the x, y and z coordinates of the spins) so we need to do a least squares fit for functions of three independent variables. The computation is a much simpler here though since we have placed all the spin vectors and position vectors into single arrays of length N, so each position in the lattice (and each spin) is indexed by one integer i, with $1 \leq i \leq N$. This makes the performing the fit exactly the same as performing a least square fit to functions of only one independent variable (in fact, since one can always index any data set this way, one can see that a least squares fit to functions of n independent variables is exactly the same as a least squares fit to functions of just one independent variable). Then the data for each spin component can be represented as a function of only the index i, $w_i \equiv w(x_i, y_i, z_i)$.

The least square fit of the data set w_i begins by trying to express w_i as a linear

combination of the fitting functions f_j (sines and cosines of the wavevectors the state is composed of) using a set of M unknown coefficients c_j.

$$w_i \approx \sum_{j=1}^{M} c_j f_j(x_i, y_i, z_i) \tag{1.25}$$

We then find the set of coefficients c_j which minimize the sum of the squared differences between the actual data w_i and the approximation, equation (1.25), at all coordinates in the lattice (x_i, y_i, z_i). We want to minimize

$$\Delta = \sum_{i=1}^{N} \left(w_i - \sum_{j=1}^{M} c_j f_j(x_i, y_i, z_i) \right)^2 \tag{1.26}$$

To do this we take derivatives of the expression (1.26) with respect to the coefficients c_k and then set these derivatives equal to zero. This gives us a set of M equations in M unknowns to solve for the coefficients which provide the best fit to the data w_i. We have

$$\frac{\partial \Delta}{\partial c_k} = -2 \sum_{i=1}^{N} \left(w_i - \sum_{j=1}^{M} c_j f_j(x_i, y_i, z_i) \right) f_k(x_i, y_i, z_i) = 0 \tag{1.27}$$

So for each value of $k = 1, \ldots, M$ we have to solve an equation of the form

$$\sum_{i=1}^{N} w_i f_k(x_i, y_i, z_i) = \sum_{j=1}^{M} c_j \left(\sum_{i=1}^{N} f_j(x_i, y_i, z_i) f_k(x_i, y_i, z_i) \right) \tag{1.28}$$

We can simplify the appearance of this equation by defining the quantities

$$b_k = \sum_{i=1}^{N} w_i f_k(x_i, y_i, z_i) \tag{1.29}$$

$$A_{kj} = \sum_{i=1}^{N} f_j(x_i, y_i, z_i) f_k(x_i, y_i, z_i) \ . \tag{1.30}$$

With these new definitions equation (1.28) becomes

$$b_k = \sum_{j=1}^{M} A_{kj} c_j \tag{1.31}$$

The equations for all values of k can be neatly summed up in vector notation by defining the $M \times 1$ vectors $\mathbf{b}$ with components b_k, $\mathbf{c}$ with components c_j, and the $M \times M$ matrix $\underline{\underline{\mathbf{A}}}$ with components A_{kj}. We get

$$\underline{\underline{\mathbf{A}}}\mathbf{c} = \mathbf{b} \tag{1.32}$$

which can be solved easily in Matlab for the unknown coefficients c_j. One only needs to invert the matrix $\underline{\underline{\mathbf{A}}}$.

To measure the error in the fit we compute the residual at each lattice point, where the residual at a point (x_i, y_i, z_i) is defined as

$$res_i = \left| w_i - \sum_{j=1}^{M} c_j f_j(x_i, y_i, z_i) \right| \tag{1.33}$$

1.3.5 Projection of Stacked or Columnar States onto Lower Dimensional Lattices

Another technique which was helpful was projecting the problem down onto an equivalent problem on a lower dimensional lattice in cases where we know that the ground state is a stacked or columnar configuration (usually we know this from the results of Iterative Minimization simulations). This method was used by Sklan and Henley to study stacked ground states on the Octahedral lattice (see [1]). If the lower dimensional lattice is a Bravais lattice then we can use the Luttinger-Tisza method to rigorously find the ground state. Even if the lower dimensional lattice is not a Bravais lattice, the problem has still been made simpler because solving a one- or two-dimensional problem is generally easier than solving a three-dimensional problem. Before illustrating this method we should first explain what we mean by stacked and columnar states.

A stacked state is a state in which there is a certain direction in real space, say $\hat{\mathbf{n}}$, such that all spins in the same plane perpendicular to $\hat{\mathbf{n}}$ are parallel to each other. In this case, we can project the three-dimensional lattice and the interactions between spins in the

three-dimensional problem down the $\hat{\mathbf{n}}$ direction onto an equivalent one-dimensional lattice with a corresponding set of interactions. Each spin in this equivalent one-dimensional lattice is then a representative of an entire plane of spins in the original three-dimensional lattice.

A columnar state is a state in which there is a certain direction in real space, again let's call it $\hat{\mathbf{n}}$, such that all spins on the same line parallel to $\hat{\mathbf{n}}$ are parallel to each other, so that the spin configuration is made up of columns of spins in which all spins in the same column are parallel to each other. In this case we can project the three-dimensional lattice and its interactions down onto an equivalent two-dimensional lattice and a corresponding set of interactions on that lattice. Each spin in this two-dimensional lattice is then a representative of an entire line of spins in the original three-dimensional lattice.

We now demonstrate this procedure with a simple example. Consider a state on the simple cubic lattice which is stacked along the [001] direction and suppose that we include interactions between spins out to third nearest neighbors (so we have interactions J_1, J_2 and J_3). Denote the corresponding interactions in the one-dimensional lattice by j_1, j_2, j_3, etc.

The first nearest neighbor interaction in the equivalent one-dimensional lattice must include all the interactions that a spin in a (001) plane has with spins in the adjacent (001) planes. A spin in the simple cubic lattice has six nearest neighbors but only one of these first nearest neighbor spins lie in each adjacent (001) plane (the other four lie in the same plane as that spin). Each spin in the simple lattice also has 12 second nearest neighbors, four in each adjacent (001) plane and four in its own plane. Finally, each spin in the simple cubic lattice has eight third nearest neighbors, four in each adjacent (001) plane and zero in its own plane. So the corresponding first nearest neighbor interaction in the one-dimensional lattice is

$$j_1 = J_1 + 4J_2 + 4J_3 \ . \tag{1.34}$$

Since the J_1, J_2 and J_3 interactions in the simple cubic lattice don't act between spins that are separated by more than a distance of 1 in the (001) direction, the only interaction in the equivalent one-dimensional lattice is this first nearest neighbor interaction j_1. In this case, the one-dimensional lattice is a Bravais lattice, so one could immediately use the Luttinger-Tisza method to rigorously find a parameterization for the ground state.

In the case of the Pyrochlore lattice, states stacked in a $\langle 100 \rangle$ direction project down

onto a one-dimensional Bravais lattice and states layered in a $\langle 100 \rangle$ direction project down onto a two-dimensional non-Bravais lattice which we call the Checkerboard lattice. Recent neutron diffraction studies (see [2]) on a magnetic material with the Pyrochlore structure have discovered a state which is stacked along a $\langle 111 \rangle$ direction in which spins in the same triangular lattice layer are all parallel to each other and spins in the same Kagome lattice layer are all parallel to each other. This state can be mapped down onto an equivalent one-dimensional non-Bravais lattice with a basis of two sites, known as the chain lattice. The ground states of the chain lattice for various sets of interactions have been studied extensively by Sklan and Henley, as they found a number of stacked states on the Octahedral lattice which could be projected down onto the chain lattice (see [1]). The first site in each unit cell of this chain lattice represents the spins in an entire triangular lattice layer of the three-dimensional material and the second site in each unit cell represents an entire Kagome lattice layer of spins in the three-dimensional material. We will discuss these and other projections in detail in the sections where they are most relevant.

1.3.6 Finding a Good Basis in Spin Space

In this subsection we discuss a few ways one can try to find a good basis in spin space to express a given spin configuration in. This can often be quite a challenge, but finding the right basis to express a state in is very helpful for understanding the geometry of that state. Our goal is always to find a basis in which the spins point in some kind of important or high-symmetry directions. For example, we express the Cuboctahedral Stack state (section 2.2) in a basis in which the spins point in $\langle 111 \rangle$ and $\langle 110 \rangle$ directions.

1.3.6.1 Row Sums in Simple Cubic Sublattices

A general technique that one can use to find distinguished directions in spin space is the technique of taking row sums of spins the 16 simple cubic sublattices of the Pyrochlore lattice.

By taking row sums in each simple cubic lattice, we mean that in each simple cubic lattice we first add up all the spins in each row parallel to the x-direction, then we add up all the spins in each row parallel to the y-direction and finally we add up all the spins in each row parallel to the z-direction. So if we had a state on an $L \times L \times L$ block of Pyrochlore

lattice unit cells, then in each simple cubic lattice we would compute L^2 row sums in the x-direction, L^2 row sums in the y-direction and L^2 row sums in the z-direction. Each of these row sums would be a sum of L spins. What we are essentially doing is averaging the spins in each row parallel to the three different directions in real space.

When we examine these sums, we often find information that is helpful in determine which, if any, directions in spin space are distinguished in a given state. For example, sometimes the row sums in one direction will all be parallel to a certain direction, say $\hat{\mathbf{n}}$. Then in the basis we construct for spin space we would set $\hat{\mathbf{C}}_0 = \hat{\mathbf{n}}$ and take two vectors from the plane perpendicular to $\hat{\mathbf{n}}$ to be $\hat{\mathbf{A}}_0$ and $\hat{\mathbf{B}}_0$. This is exactly the situation for the new variety of Double-Twist state discussed in section 2.4, so we use this technique to find a good basis to express that state in.

1.3.6.2 If Spins Point Towards the Corners of a Cube

One specific case in which one can construct a nice basis for spin space is the case in which the spins are actually pointing towards the eight corners of a cube. The tell-tale sign of this kind of situation is that one finds eight spins directions, say $\{\hat{\mathbf{n}}_i\}_{i=1,\ldots,8}$ with $\hat{\mathbf{n}}_2 = -\hat{\mathbf{n}}_1$, $\hat{\mathbf{n}}_4 = -\hat{\mathbf{n}}_3$, $\hat{\mathbf{n}}_6 = -\hat{\mathbf{n}}_5$, $\hat{\mathbf{n}}_8 = -\hat{\mathbf{n}}_7$, whose dot products satisfy

$$\begin{aligned} \hat{\mathbf{n}}_1 \cdot \hat{\mathbf{n}}_3 &= \hat{\mathbf{n}}_1 \cdot \hat{\mathbf{n}}_5 = \hat{\mathbf{n}}_1 \cdot \hat{\mathbf{n}}_7 = \frac{1}{3} \\ \hat{\mathbf{n}}_3 \cdot \hat{\mathbf{n}}_5 &= \hat{\mathbf{n}}_3 \cdot \hat{\mathbf{n}}_7 = \hat{\mathbf{n}}_5 \cdot \hat{\mathbf{n}}_7 = -\frac{1}{3} \, . \end{aligned}$$

Then one can construct a new basis in spin space in which these eight directions are all $\langle 111 \rangle$ directions. One possible choice of basis is

$$\hat{\mathbf{A}}_0 = \frac{\hat{\mathbf{n}}_1 + \hat{\mathbf{n}}_4 + \hat{\mathbf{n}}_5 + \hat{\mathbf{n}}_7}{|\hat{\mathbf{n}}_1 + \hat{\mathbf{n}}_4 + \hat{\mathbf{n}}_5 + \hat{\mathbf{n}}_7|} \tag{1.35a}$$

$$\hat{\mathbf{B}}_0 = \frac{\hat{\mathbf{n}}_1 + \hat{\mathbf{n}}_3 + \hat{\mathbf{n}}_6 + \hat{\mathbf{n}}_7}{|\hat{\mathbf{n}}_1 + \hat{\mathbf{n}}_3 + \hat{\mathbf{n}}_6 + \hat{\mathbf{n}}_7|} \tag{1.35b}$$

$$\hat{\mathbf{C}}_0 = \hat{\mathbf{A}}_0 \times \hat{\mathbf{B}}_0 \tag{1.35c}$$

but other choices are possible as well.

2. The J_1-J_2 Phase Diagram

A large part of our study was focused on getting a complete understanding of the ground states of equation (1.1) with only first and second nearest neighbor interactions J_1 and J_2. A rich variety of different coplanar and non-coplanar states exist in the J_1-J_2 phase diagram, which is slightly surprising since only two interactions are involved. The J_1-J_2 phase diagram for the ground states of (1.1) is shown in figure 2.1 and a summary of all the different ground states found in the phase diagram is given in table 2.1.

In the region $J_1 > 0$, $J_2 > 0$ the ground state is ferromagnetic (F.M.), since interactions between every spin are ferromagnetic. This is true even in the case of a pure $J_1 > 0$ or a pure $J_2 > 0$, as the J_1 and J_2 interactions act between spins in different F.C.C. sublattices, so all the spins in the lattice are coupled together and they all point in the same direction.

Figure 2.1: The J_1-J_2 Phase Diagram for the Pyrochlore Lattice.

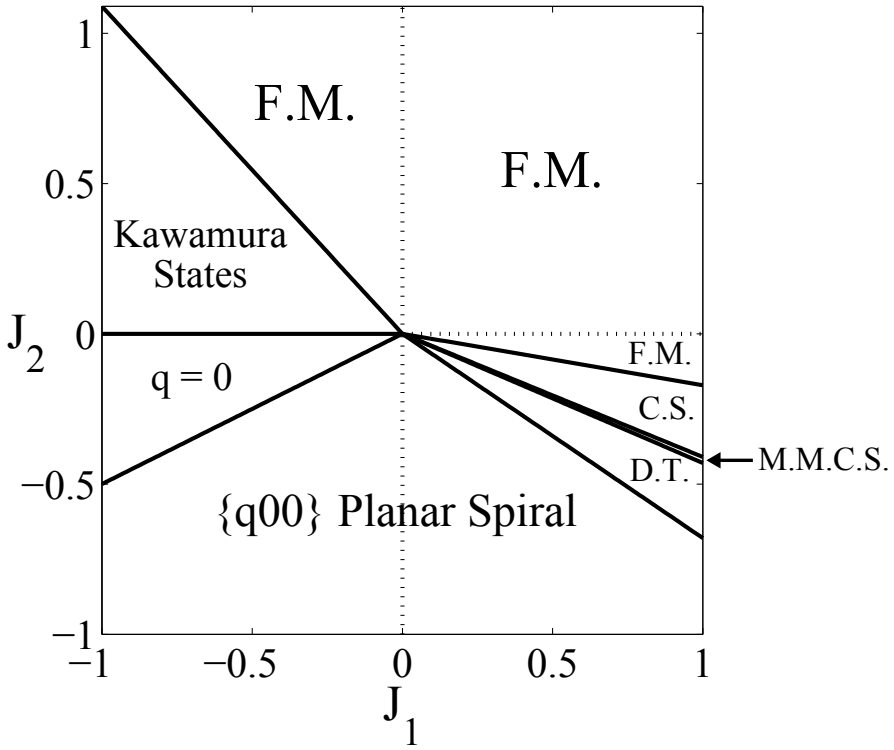

State	Location (by quadrant)	Collinear, Coplanar or Non-coplanar?	Ordering Wavevectors (* = L.T. wavevector)
Ferromagnetic (F.M.)	I, II, and IV	Collinear	$(0,0,0)^*$
$J_1 < 0$	$J_2 = 0$	Collinear	Any
$\{q00\}$ Planar Spiral	III and IV	Coplanar	$\mathbf{q} = (0,0,q)^*$ with $\cos\left(\frac{q}{4}\right) = -\frac{j_1}{4j_2}$
$\mathbf{q} = \mathbf{0}$	III	Collinear	$(0,0,0)^*$
Cuboctahedral Stack (C.S.)	IV	Non-coplanar	$\left\{\frac{1}{2}\frac{1}{2}\frac{1}{2}\right\}^*$
Kawamura States	II	Non-coplanar	$\left\{\frac{3}{4}\frac{3}{4}0\right\}^*$
Double-Twist (D.T.)	IV	Non-coplanar	$\left\{\frac{3}{4}\frac{3}{4}0\right\}^*$
Multiply-Modulated Commensurate Spiral (M.M.C.S.)	IV	Non-coplanar	$\left\{\frac{3}{4}\frac{1}{2}\frac{1}{4}\right\}^*$ and $\left\{\frac{3}{4}\frac{3}{4}0\right\}$

Table 2.1: Summary of States Found in the J_1-J_2 Phase Diagram.

For a pure antiferromagnetic first nearest neighbor interaction $J_1 < 0$, the ground state is the set of all states in which the sum of the four spins on every tetrahedron is zero. We classify this ground state as collinear, because the set of all states in which the four spins on every tetrahedron sum to zero includes a number of collinear states, which have the same energy as any non-collinear states which are also in that set.

For a pure antiferromagnetic second nearest neighbor interaction $J_2 < 0$, the ground state is a 120° planar spiral which is stacked in a $\langle 100 \rangle$ direction. This state is just a special case of the $\{q00\}$ planar spiral state found in the two quadrants with $J_2 < 0$.

In the region $J_1 < 0$, $J_2 > 0$ we find two different kinds of ground states. For $J_2 < 1.09\,|J_1|$ the ground states are the three non-coplanar states studied by Kawamura et al and Chern et al (see [9], [10] and [8]). We refer to these states as "Kawamura States" because of the progress made by the Kawamura group in understanding these states. These states are mainly composed of a subset of the six different kinds of $\left\{\frac{3}{4}\frac{3}{4}0\right\}$ wavevectors. We have focused our study on one of these states, the Kawamura Sextuplet-q state, which uses all six $\left\{\frac{3}{4}\frac{3}{4}0\right\}$ wavevectors in equal amounts. When the ratio of J_2 to $|J_1|$ becomes large enough the ground state in this region transitions to a ferromagnetic state. This transition occurs at

Figure 2.2: Largest L.T. eigenvalues vs. $J_2/|J_1|$ for the ferromagnetic and Kawamura states in the region $J_1 < 0$, $J_2 > 0$.

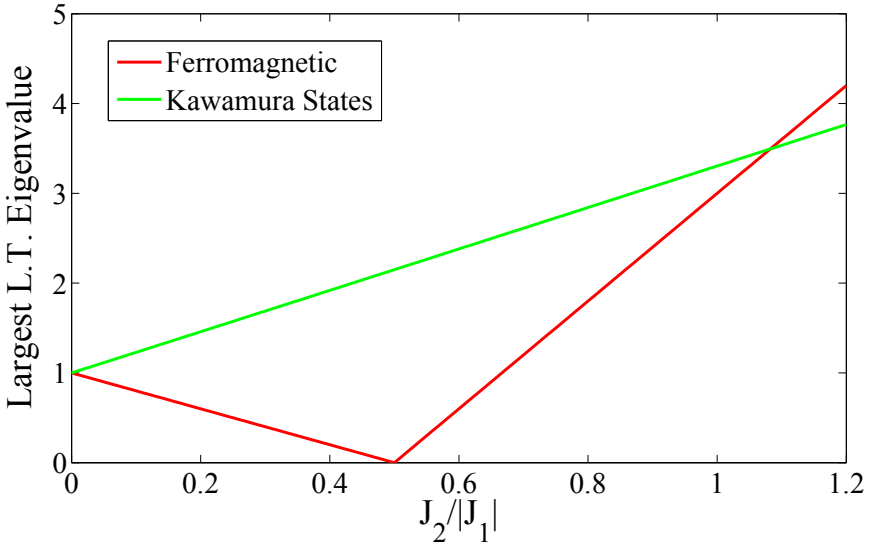

$J_2 \approx 1.09\,|J_1|$. Figure 2.2 shows the largest L.T. eigenvalues for the Kawamura States and the ferromagnetic state (really for the $\left\{\frac{3}{4}\frac{3}{4}0\right\}$ type wavevectors and the zero wavevector, the wavevectors which characterize these states) as a function of $J_2/|J_1|$ when $J_1 < 0$. We see that the largest L.T. eigenvalues for these two states are equal at $J_2 = 0$ (this degeneracy is discussed in appendix C), then the eigenvalue for the Kawamura States is larger until $J_2 \approx 1.09\,|J_1|$ where the eigenvalue for the ferromagnetic state becomes the larger one.

In the region $J_1 > 0$, $J_2 < 0$ we find five distinct ground states. The first is a ferromagnetic state. At $J_2 \approx -0.171 J_1$ (we present an exact expression for the location of this phase transition later on in this chapter) the state transitions to the non-coplanar Cuboctahedral Stack (C.S.) state, in which spins point towards the eight corners and 12 edge-midpoints of a cube. This state is made up of three $\left\{\frac{1}{2}\frac{1}{2}\frac{1}{2}\right\}$ type wavevectors and is similar to the Cuboctahedral State found on the Kagome lattice by Domenge, et al (see [7]) and the Cuboctahedral State found on the Octahedral lattice by Sklan and Henley (see [1]). At $J_2 \approx -0.40 J_1$ the state transitions to a non-coplanar state in which the spins point in 42 distinct directions, which we call a Multiply-Modulated Commensurate Spiral (M.M.C.S.) state.. This state is made up of one $\left\{\frac{1}{4}\frac{1}{4}0\right\}$ wavevector, one $\left\{\frac{3}{4}\frac{3}{4}0\right\}$ wavevector, and two

Figure 2.3: Largest L.T. eigenvalues vs. J_2/J_1 for the five ground states in the region $J_1 > 0$, $J_2 < 0$.

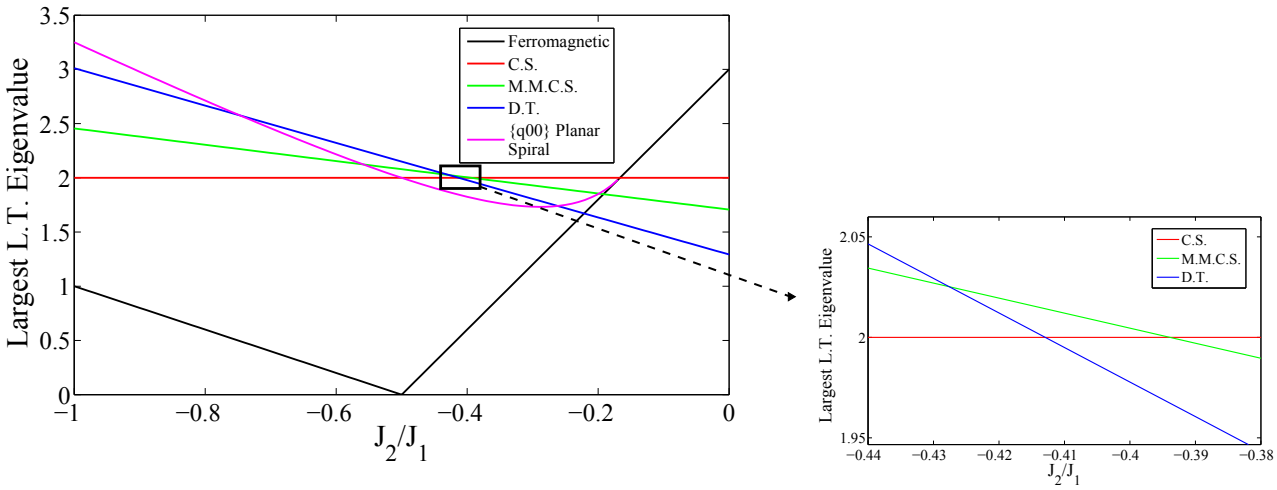

$\left\{\frac{3}{4}\frac{1}{4}\frac{1}{2}\right\}$ wavevectors. At $J_2 \approx -0.43J_1$ there is a transition to a state mainly composed of four $\left\{\frac{3}{4}\frac{3}{4}0\right\}$ type wavevectors. We call this state a new type of Double-Twist (D.T.) state because it is reminiscent of the Double-Twist state found by Sklan and Henley on the Octahedral lattice (see [1]). Finally, at $J_2 \approx -0.68$, there is a transition to a planar spiral state characterized by a wavevector of the type $\{q00\}$, so this state is stacked in a $\langle 100 \rangle$ direction in real space. This state also extends into the region $J_1 < 0$, $J_2 < 0$. Figure 2.3 shows the largest L.T. eigenvalues for the five states found in this region as a function of J_2/J_1 when $J_1 > 0$, as well as a zoomed in view of the region $-0.43 \leq J_2/J_1 \leq -0.40$ where the L.T. eigenvalue for the Multiply-Modulated Commensurate Spiral state briefly crosses above the L.T. eigenvalues for the Cuboctaheral Stack and Double-Twist states. This crossing of the largest L.T. eigenvalues in this small sliver of parameter space confirms that the ground state in this region really is a state which is distinct from the Cuboctahedral Stack and Double-Twist states, and not just an artifact of Iterative Minimization simulations.

In the region $J_1 < 0$, $J_2 < 0$ we find two distinct ground states. The first state we call the $\mathbf{q} = \mathbf{0}$ state because all spins in the same F.C.C. sublattice are parallel to each other. Furthermore, the sum of the four spin directions present (one direction from each F.C.C. sublattice) is precisely zero. This state is actually a subset of the ground states of the pure

Figure 2.4: Largest L.T. eigenvalues vs. $J_2/|J_1|$ for the $\mathbf{q} = \mathbf{0}$ and $\{q00\}$ planar spiral states found in the region $J_1 < 0$, $J_2 < 0$.

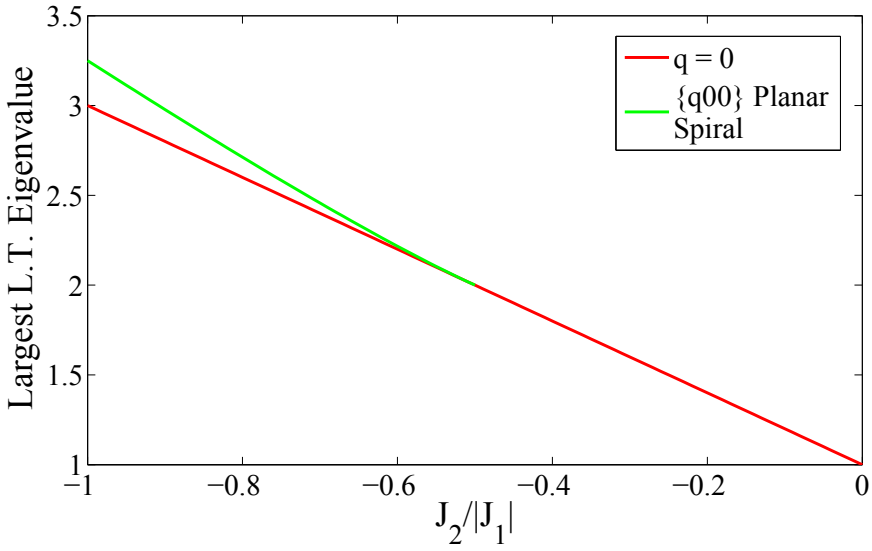

$J_1 < 0$ state, so we also classify it as a collinear state. At $J_2 = \frac{1}{2}J_1$, there is a transition to a planar spiral state characterized by a wavevector of the type $\{q00\}$, so this state is stacked along a $\langle 100 \rangle$ direction. This is the same $\{q00\}$ planar spiral state as the one found in the region $J_1 > 0$, $J_2 < 0$. Figure 2.4 shows the largest L.T. eigenvalues for the $\mathbf{q} = \mathbf{0}$ and $\{q00\}$ planar spiral states as a function of $J_2/|J_1|$ in the region $J_1 < 0$, $J_2 < 0$. We see that the planar spiral state does not exist until $J_2 = -0.5\,|J_1|$, but that when it appears it immediately becomes the dominant state for all $J_2 < -0.5\,|J_1|$.

2.1 Simple States

2.1.1 Ferromagnetic State

The simplest state we find (and the simplest possible arrangement of spins there is) is the ferromagnetic state, in which every spin points in the same direction. This state is obviously the ground state in the region where J_1 and J_2 are both greater than zero, but we also find it in the region $J_1 < 0$, $J_2 > 0$ when $J_2 \geq -1.09J_1$ and in the region $J_1 > 0$, $J_2 < 0$

when $J_2 \geq \left(-\frac{3}{8} + \frac{\sqrt{6}}{12}\right) J_1$. The energy per site of the ferromagnetic state is

$$\bar{\mathcal{E}} = -3J_1 - 6J_2 \ . \tag{2.1}$$

We use this expression for the energy of the ferromagnetic state to predict where this state transitions to competing states in the regions $J_1 > 0$, $J_2 < 0$ and $J_1 < 0$, $J_2 > 0$.

2.1.2 Pure $J_1 < 0$

In the case of a pure antiferromagnetic first neighbor interaction $J_1 < 0$, the only terms in the sum (1.1) are dot products between spins in the same tetrahedra. If we index the tetrahedra by the greek letter α and write the four spins in the α^{th} tetrahedron as $\mathbf{s}_{\alpha,0}$, $\mathbf{s}_{\alpha,1}$, $\mathbf{s}_{\alpha,2}$ and $\mathbf{s}_{\alpha,3}$ then we can rewrite equation (1.1) in the form

$$\mathcal{H} = -\frac{1}{2} J_1 \sum_{\alpha} \left(\sum_{i=0}^{3} \mathbf{s}_{\alpha,i} \right)^2 + constant \ , \tag{2.2}$$

i.e. as a sum over all tetrahedra of the squared sum of the four spins on each tetrahedron. We can see why this works by expanding the squared sum of the four spins on the α^{th} tetrahedron,

$$\frac{1}{2} \left(\sum_{i=0}^{3} \mathbf{s}_{\alpha,i} \right)^2 = 2 + \sum_{i=0}^{3} \sum_{j \neq i} \mathbf{s}_{\alpha,i} \cdot \mathbf{s}_{\alpha,j} \ . \tag{2.3}$$

The dot products between spins that appear in the sum over the α^{th} tetrahedron do not appear in the sum over any other tetrahedron (since each spin is a part of only two tetrahedra), so every term in the sum over α in (2.2) is disjoint. The factor of 2 appears because the dot product of every spin with itself is 1. To write (1.1) as a sum of terms like (2.3), we need to get rid of all of these factors of 2. That is the purpose of the constant term in (2.2).

This shows that in the case of a pure first nearest neighbor interaction J_1, (1.1) can be written in the form (2.2) as a sum of disjoint terms like (2.3). Then to minimize the total energy we can just minimize each of these disjoint terms one at a time. These terms are all greater than or equal to zero, since $J_1 < 0$ and each term is the square of a sum of four spin vectors. We see then that the minimum energy state is a state in which the sum of the four spins on every tetrahedron is equal to zero.

This method of minimizing (1.1) by simultaneously minimizing a set of similar terms is known as the cluster method (see [5]). In this case it allows us to show that the ground state in the pure $J_1 < 0$ case is a state in which the sum of the four spins on every tetrahedron is equal to zero. The site energy of each spin in the ground state is $\mathcal{E}_i = J_1$ so this state has an energy per site of

$$\bar{\mathcal{E}} = J_1 \ . \tag{2.4}$$

One can easily think of a number of geometrically distinct states which have the same total energy NJ_1 so it is clear that there is a very large number of degenerate ground states in the pure $J_1 < 0$ case. One example is a state in which all the spins in F.C.C. sublattices 0 and 1 point along the positive z-axis and all the spins in F.C.C. sublattices 2 and 3 point along the negative z-axis. Another possible state is one in which the spins in every "up" tetrahedron point towards the center of that tetrahedron along their local $\langle 111 \rangle$ axes and the spins in every "down" tetrahedron point away from the center of that tetrahedron along their local $\langle 111 \rangle$ axes. In fact, the $\mathbf{q} = \mathbf{0}$ state of subsection 2.1.3 and the Kawamura Sextuplet-q state of section 2.3.1 are both specific subsets of the set of ground states in the pure $J_1 < 0$ magnet, since the spins on every tetrahedron sum to zero in both of these states.

2.1.3 $\mathbf{q} = \mathbf{0}$ State(s)

In the region $J_1 < 0$, $\frac{1}{2}J_1 \leq J_2 \leq 0$ we find a state in which all spins in the same F.C.C. sublattice are parallel and the spins from the four F.C.C. sublattices all sum to zero. To be more precise, we have

$$\mathbf{s}_0 = \mathbf{n}_0 \tag{2.5}$$

$$\mathbf{s}_1 = \mathbf{n}_1 \tag{2.6}$$

$$\mathbf{s}_2 = \mathbf{n}_2 \tag{2.7}$$

$$\mathbf{s}_3 = \mathbf{n}_3 \tag{2.8}$$

where the $\mathbf{n}_\alpha$ are all constant unit vectors which satisfy

$$\sum_{\alpha=0}^{3} \mathbf{n}_\alpha = \mathbf{0} \ . \tag{2.9}$$

We call this state a $\mathbf{q} = \mathbf{0}$ state because the wavevector characterizing the spin configuration in each F.C.C. sublattice is the zero wavevector. This site energy for each spin in this state is $\mathcal{E}_i = J_1 + 2J_2$ so this state has an energy per site equal to

$$\bar{\mathcal{E}} = J_1 + 2J_2 \ . \tag{2.10}$$

This state can be understood as a consequence of the equivalence of a small antiferromagnetic J_2 interaction and a small ferromagnetic J_3 interaction that arises as a result of the constraint that the four spins on every tetrahedron sum to zero (see appendix D for a proof and also [8] for a different proof). Equation (D.7) shows the form the site energy of each spin takes in the case when the spins on every tetrahedron sum to zero. Because $J_2 < 0$, each spin wants to point parallel to its J_3 neighbors, so the antiferromagnetic J_2 interaction is acting like an effective ferromagnetic J_3 interaction. Because the J_3 bond links together sites which are in the same F.C.C. sublattice, all spins in the same F.C.C. sublattice will point parallel to each other, producing the observed state.

The $\mathbf{q} = \mathbf{0}$ state is not one state but is, in fact, an infinite number of states with the same total energy. The abstract space which these degenerate states occupy is a two-dimensional space spanned by two angles, θ and ϕ. This state is characterized by the four spin directions, $\mathbf{n}_0$, $\mathbf{n}_1$, $\mathbf{n}_2$ and $\mathbf{n}_3$. To construct a state, we may choose the first two directions $\mathbf{n}_0$ and $\mathbf{n}_1$ at random. Let θ be the angle between these two directions, so that $\mathbf{n}_0 \cdot \mathbf{n}_1 = \cos\theta$. The constraint equation (2.9) then implies that $\mathbf{n}_2 + \mathbf{n}_3 = -\mathbf{n}_0 - \mathbf{n}_1$, so we cannot choose $\mathbf{n}_2$ and $\mathbf{n}_3$ at random because they must add together to cancel $\mathbf{n}_0$ and $\mathbf{n}_1$. In particular, they must also satisfy $\mathbf{n}_2 \cdot \mathbf{n}_3 = \cos\theta$. Even though $\mathbf{n}_2$ and $\mathbf{n}_3$ must have a resultant that points opposite the resultant of $\mathbf{n}_0$ and $\mathbf{n}_1$, we can still rotate the plane spanned by $\mathbf{n}_2$ and $\mathbf{n}_3$ by any angle ϕ relative to the plane spanned by $\mathbf{n}_0$ and $\mathbf{n}_1$, so the degeneracy of this state is completely characterized by the two angles θ and ϕ. Taking this analysis one step further, we see that θ, $\phi \in [0, \pi]$ since θ is the smaller of the two angles between $\mathbf{n}_0$ and $\mathbf{n}_1$, and ϕ and $2\pi - \phi$ produce the same state because of the reflection symmetry through the plane spanned by $\mathbf{n}_0$ and $\mathbf{n}_1$, so we only get unique states for $\phi \in [0, \pi]$.

Because the $\mathbf{q} = \mathbf{0}$ state satisfies the constraint (2.9), this state is also a ground state of (1.1) in the case of a pure first nearest neighbor interaction $J_1 < 0$. So the set of $\mathbf{q} = \mathbf{0}$ states

Figure 2.5: L.T. eigenvalues plotted in the Brillouin zone of the F.C.C. lattice for $J_1 = -1$, $J_2 = -0.25$.

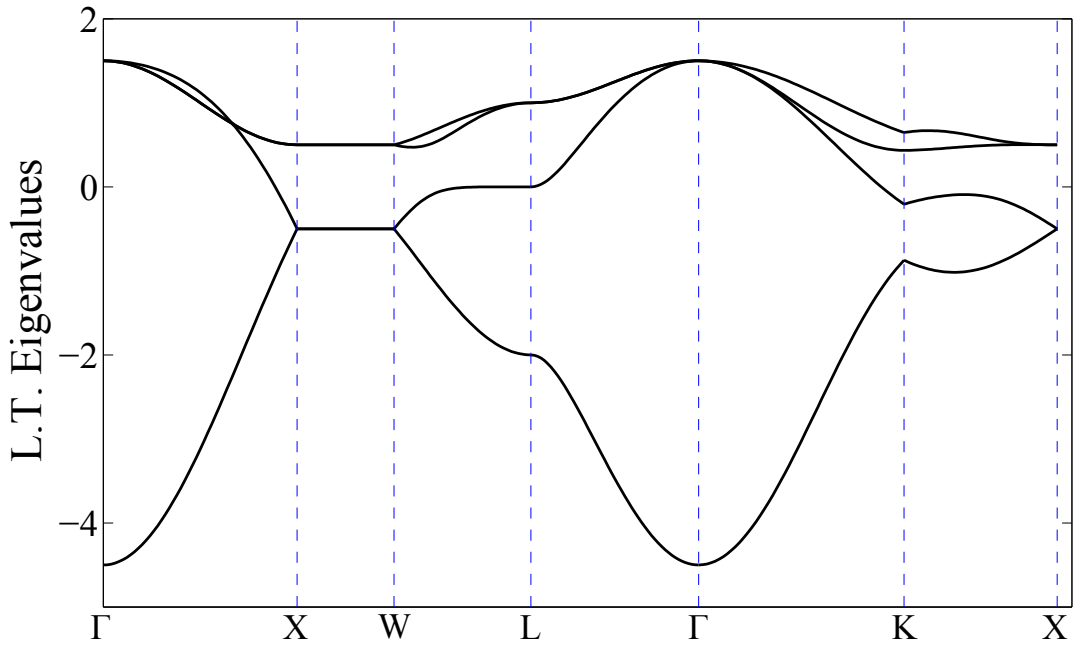

is just a subset of the states discussed in subsection 2.1.2. Adding an antiferromagnetic J_2 interaction when $J_1 < 0$ selects a specific subset of the ground states of the pure $J_1 < 0$ state.

Figure 2.5 shows the four eigenvalues of the Luttinger-Tisza matrix plotted along the $\Gamma \to X \to W \to L \to \Gamma \to K \to X$ route through the Brillouin zone of the F.C.C. lattice (discussed in subsection 1.2.4) for the parameter values $J_1 = -1$, $J_2 = -0.25$. We see that the largest Luttinger-Tisza eigenvalue has its maximum at the Γ point $\mathbf{q} = \mathbf{0}$, indicating that the optimal Luttinger-Tisza wavevector for the state with these parameter values is the zero wavevector.

2.1.4 Pure $J_2 < 0$

Next we examine the case of a purely antiferromagnetic second neighbor interaction $J_2 < 0$. In this case we find that the ground state is a 120° planar spiral stacked in a $\langle 100 \rangle$

direction. We can get an understanding of this state by *assuming* (based on evidence from Iterative Minimization simulations) that the state is stacked along a $\langle 100 \rangle$ direction and then projecting the interactions down to an equivalent one-dimensional lattice. We can then apply the Luttinger-Tisza method (see [6]) to this equivalent one-dimensional lattice to prove that the ground state is a 120° spiral in the stacking direction. We use the method outlined in subsection 1.3.5 to determine the effective interactions in the equivalent one-dimensional lattice. For simplicity we take the stacking direction to be the z-direction so that the optimal wavevector takes the form $\mathbf{q} = (0, 0, q)$.

The planes of spins perpendicular to the z-direction are separated from each other by a distance of $\frac{1}{4}$ in the z-direction. A spin has four of its second nearest neighbors in each adjacent plane (separated by a distance $\frac{1}{4}$ in the z direction) and two of its second nearest neighbors in planes which are two over (separated by a distance $\frac{1}{2}$ in the z direction). This means that in the equivalent one-dimensional lattice there is both a first neighbor interaction, $j_1 = 4J_2$, and a second nearest neighbor interaction $j_2 = 2J_2 = \frac{1}{2}j_1$. In addition, the one-dimensional lattice is a Bravais lattice, because every site in the same z plane has the same distribution of second nearest neighbors in the planes above and below it.

Applying the Luttinger-Tisza method to the one-dimensional lattice gives an expression for $\tilde{J}(\mathbf{q})$, the Fourier transform of the couplings:

$$\tilde{J}(\mathbf{q}) = 4J_2 \left(2\cos\left(\frac{q}{4}\right) + \cos\left(\frac{q}{2}\right) \right) \tag{2.11}$$

Maximizing this we find that the optimal wavenumber q is given by

$$\cos\left(\frac{q}{4}\right) = -\frac{1}{2} \tag{2.12}$$

so we have $q = \frac{8\pi}{3}$, which means that spins separated by a distance of $\frac{1}{4}$ in the z-direction (first nearest neighbors in the one-dimensional lattice) are rotated 120° from each other. So the ground state is a 120° spiral in the z-direction and we can write it as

$$\mathbf{s}_i = \cos\left(\frac{8\pi}{3}z + \phi\right)\hat{\mathbf{A}}_0 + \sin\left(\frac{8\pi}{3}z + \phi\right)\hat{\mathbf{B}}_0 \tag{2.13}$$

where ϕ can be any constant phase angle. The site energy of each spin is given by

$$\mathcal{E}_i = 3J_2 \tag{2.14}$$

We see that the 120° spiral arises naturally in the context of the one-dimensional Bravais lattice as a consequence of the fact that $j_2 = \frac{1}{2}j_1$ and both j_1 and j_2 are antiferromagnetic interactions (they are both negative). This state is actually just a special case of the more general $\{q00\}$ planar spiral state which involves both J_1 and J_2 interactions. We discuss this more general planar spiral state in the next subsection.

2.1.5 $\{q00\}$ Planar Spiral ($J_2 < 0$ and $J_1 > 0$ or $J_1 < 0$)

In the region $J_1 < 0$, $J_2 \leq \frac{1}{2}J_1$ and also in the region $J_1 > 0$, $J_2 < 0$, we find a planar spiral state which is stacked in a $\langle 100 \rangle$ direction. For simplicity we take the stacking direction to be the z-direction so that this state is characterized by a wavevector $\mathbf{q} = (0, 0, q)$.

Just like the 120° planar spiral we found in the pure $J_2 < 0$ case (subsection 2.1.4), this state can also be understood by mapping the interactions down onto an equivalent one-dimensional lattice. Because a spin in a constant z plane has two of its first nearest neighbors in each constant z plane adjacent to it, and because the second nearest neighbors of each spin are distributed in the way described in the section on the pure $J_2 < 0$ spiral, the couplings in the one-dimensional lattice have the values $j_1 = 2J_1 + 4J_2$ and $j_2 = 2J_2$. Performing the Luttinger-Tisza method on this one-dimensional lattice gives an expression for $\tilde{J}(\mathbf{q})$,

$$\tilde{J}(\mathbf{q}) = 2j_1 \cos\left(\frac{q}{4}\right) + 2j_2 \cos\left(\frac{q}{2}\right) \ . \tag{2.15}$$

Minimizing this expression with respect to q we find that the optimal wavenumber is given by

$$\cos\left(\frac{q}{4}\right) = -\frac{j_1}{4j_2} \tag{2.16}$$

or

$$\cos\left(\frac{q}{4}\right) = -\frac{J_1 + 2J_2}{4J_2} \tag{2.17}$$

in terms of the interactions in the three-dimensional lattice. These expressions show that

spins separated by a distance $\frac{1}{4}$ in the z-direction will be rotated from each other by q radians. We see that in the special case of $J_1 = 0$, $j_2 = \frac{1}{2}j_1$ and we recover the 120° spiral found in the previous section. This state has site energy for each spin equal to

$$\mathcal{E}_i = \frac{J_1^2}{4J_2} + 3J_2 \tag{2.18}$$

so $\bar{\mathcal{E}} = \mathcal{E}_i$.

Finally, we note that in order for equation (2.17) to have a solution for q, we must have $-1 \leq -\frac{J_1+2J_2}{4J_2} \leq 1$. Therefore, this spiral state can only exist in the region $J_1 < 0$ when $J_2 \leq \frac{1}{2}J_1$, and it can only exist in the region $J_1 > 0$ when $J_2 \leq -\frac{1}{6}J_1$.

2.2 Cuboctahedral Stack ($J_1 > 0$, $J_2 < 0$)

In the region $J_1 > 0$, $J_2 < 0$ we find a state that we have named the Cuboctahedral Stack because the spins in each Kagome lattice layer perpendicular to a certain $\langle 111 \rangle$ direction in real space are arranged in the Cuboctahedral state found on the Kagome lattice by Domenge, et al (see [7]) and on the Octahedral lattice by Sklan and Henley (see [1]). Those two states were called Cuboctahedral states because the spins in those states point towards the 12 vertices of a cuboctahedron (a polyhedron with 12 faces, six of which are squares and the other eight are equilateral triangles). An equivalent way of thinking about these Cuboctahedral states is that the spins in those states point towards the 12 edge-midpoints of a cube. If we choose a basis in spin space in which the sides of this cube are perpendicular to $\langle 100 \rangle$ directions, then the spins in these Cuboctahedral states point in the twelve $\langle 110 \rangle$ directions.

In the Cuboctahedral Stack state there is a distinguished direction in real space, which is one of the four $\langle 111 \rangle$ directions. In the Kagome lattice layers stacked perpendicular to this direction, the spins point towards the 12 edge-midpoints of a cube. In the triangular lattice layers between the Kagome layers, the spins point towards the eight corners of that same cube.

We find that this state is built out of three of the four $\left\{\frac{1}{2}\frac{1}{2}\frac{1}{2}\right\}$ type wavevectors. The fourth unused wavevector points in the stacking direction of the Kagome and triangular lattice layers. A Cuboctahedral Stack state in which the Kagome and triangular lattice

layers are stacked in the [111] direction can be parameterized as

$$\mathbf{s}_0 = \frac{1}{\sqrt{3}}\cos(\mathbf{q}_2\cdot\mathbf{r})\ \hat{\mathbf{A}}_0 + \frac{1}{\sqrt{3}}\cos(\mathbf{q}_3\cdot\mathbf{r})\ \hat{\mathbf{B}}_0 + \frac{1}{\sqrt{3}}\cos(\mathbf{q}_1\cdot\mathbf{r})\ \hat{\mathbf{C}}_0 \tag{2.19a}$$

$$\mathbf{s}_1 = \frac{1}{\sqrt{2}}\cos(\mathbf{q}_2\cdot\mathbf{r})\ \hat{\mathbf{A}}_0 + \frac{1}{\sqrt{2}}\cos(\mathbf{q}_3\cdot\mathbf{r})\ \hat{\mathbf{B}}_0 \tag{2.19b}$$

$$\mathbf{s}_2 = \frac{1}{\sqrt{2}}\cos(\mathbf{q}_3\cdot\mathbf{r})\ \hat{\mathbf{A}}_0 + \frac{1}{\sqrt{2}}\cos(\mathbf{q}_1\cdot\mathbf{r})\ \hat{\mathbf{C}}_0 \tag{2.19c}$$

$$\mathbf{s}_3 = \frac{1}{\sqrt{2}}\cos(\mathbf{q}_2\cdot\mathbf{r})\ \hat{\mathbf{B}}_0 + \frac{1}{\sqrt{2}}\cos(\mathbf{q}_1\cdot\mathbf{r})\ \hat{\mathbf{C}}_0 \tag{2.19d}$$

where the three wavevectors used to construct this state are $\mathbf{q}_1 = 2\pi(-\frac{1}{2},\frac{1}{2},\frac{1}{2})$, $\mathbf{q}_2 = 2\pi(\frac{1}{2},-\frac{1}{2},\frac{1}{2})$ and $\mathbf{q}_3 = 2\pi(\frac{1}{2},\frac{1}{2},-\frac{1}{2})$.

In this state it turns out that the spins in the Kagome layers have a different site energy, equation (1.2), than the spins in the triangular layers. In the above parameterization, the triangular layers consist of the spins in F.C.C. sublattice 0 and the Kagome layers consist of the spins in F.C.C. sublattices 1, 2 and 3. Using the parameterization of this state, equations (2.19a) - (2.19d), we find that the site energies for spins in the four F.C.C. sublattices are

$$\mathcal{E}_i^{(0)} = \sqrt{6}J_1 \tag{2.20}$$

$$\mathcal{E}_i^{(1,2,3)} = -J_1\left(1+\frac{\sqrt{6}}{3}\right) \tag{2.21}$$

where the superscript indexes the F.C.C. sublattices. The energy per site for this system is then

$$\bar{\mathcal{E}} = -J_1\left(\frac{3}{4}+\frac{\sqrt{6}}{2}\right)\ . \tag{2.22}$$

Evidently, the J_2 contribution to the energy of this state completely cancels out, so that the total energy depends only on J_1. To see why this happens, we need to think more about the structure of this state. Of the four spins in every tetrahedron, three of them lie in a Kagome lattice layer and the fourth lies in a triangular lattice layer. Recall that every spin in a triangular lattice layer points in a $\langle 111\rangle$ direction and every spin in a Kagome lattice layer points in a $\langle 110\rangle$ direction. To approximately satisfy the ferromagnetic first nearest neighbor interaction, the three spins on a tetrahedron in a Kagome lattice layer will point in

three $\langle 110 \rangle$ directions which surround the same corner of a cube. For example, these spins might point in the [110], [101] and [011] directions. Then the dot product between any two of these three spins will be $\frac{1}{2}$. The fourth spin on this tetrahedron, the one which lies in a triangular lattice layer, will then point in the [111] direction, the average of the directions the other three spins point in. The dot product of this fourth spin with any of the other three will then be $\frac{2}{\sqrt{6}} \approx 0.82$, which also favors the ferromagnetic first nearest neighbor interaction.

Because of this structure, the dot product between any spin in a triangular lattice layer (i.e. in F.C.C. sublattice 0) and any of its second nearest neighbors is always zero. The reason for this is that any second nearest neighbor of a spin in a triangular lattice layer will be in a Kagome lattice layer, so it will point in a $\langle 110 \rangle$ direction. Moreover, the $\langle 110 \rangle$ direction it points in will be one which surrounds a corner of the cube in spin space which is adjacent to the corner that the spin in the triangular lattice layer points towards but this $\langle 110 \rangle$ direction will not point towards the midpoint of the edge that connects these two corners of the cube in spin space. It follows from this that the dot products of a spin in a triangular layer with its second nearest neighbors are all zero.

The dot products between any spin in a Kagome lattice layer and its 12 second nearest neighbors are not all zero but they do add to zero. Of these 12 dot products, four of them are 0 (the dot products with spins in the adjacent triangular layers), four of them are $-\frac{1}{2}$ (the dot products with spins in the same Kagome layer) and four of them are $\frac{1}{2}$ (the dot products with spins in the neighboring Kagome layers which are beyond the adjacent triangular layers). Clearly these 12 dot products add to zero.

We see then that J_2 makes no contribution to the energy of the Cuboctahedral Stack state. This means that if we fix J_1 and tune the parameter J_2, the energy, equation (2.22), of the Cuboctahedral Stack state always stays the same, but the energy of any competing states (whose energy generally will depend on J_2) may become lower than that of the Cuboctahedral Stack. When this happens there will be a phase transition.

If we set the energy per site of this state, equation (2.22), equal to the energy per site of the ferromagnetic state, (2.1), which is also found in the region $J_1 > 0$, $J_2 < 0$, we find that the transition from the ferromagnetic state to the Cuboctahedral Stack should

Figure 2.6: L.T. eigenvalues plotted in the Brillouin zone of the F.C.C. lattice for $J_1 = 1$, $J_2 = -0.2$.

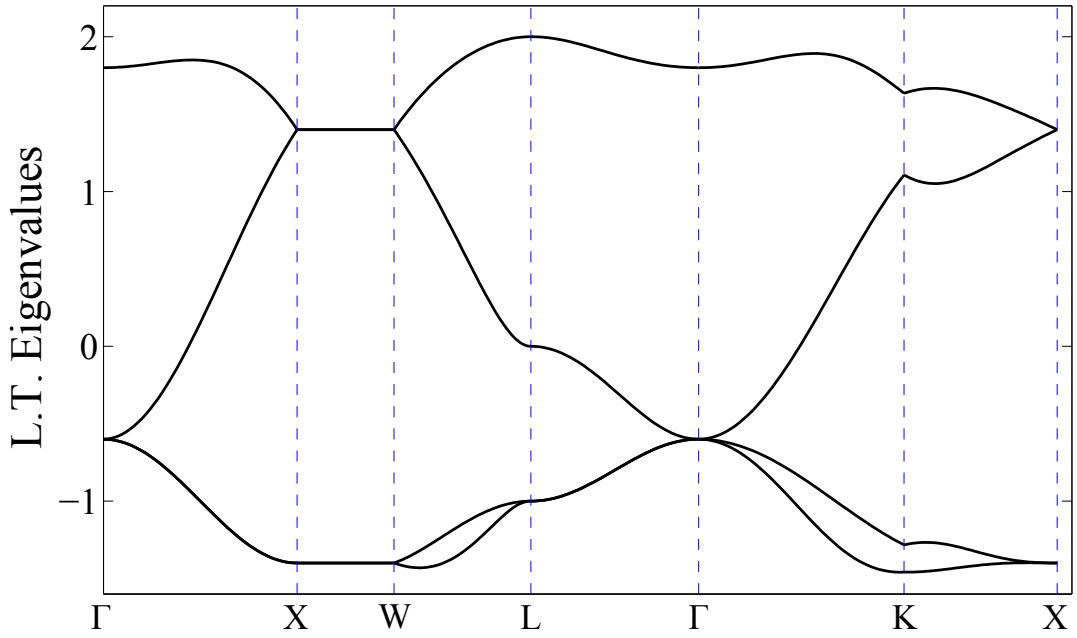

occur at $J_2 = \left(-\frac{3}{8} + \frac{\sqrt{6}}{12}\right) J_1$ or $J_2 \approx -0.171 J_1$. This is very close to the location where we observe the transition in our simulations. Simulations also show that this state transitions to a Multiply-Modulated Commensurate Spiral state (section 2.5) near $J_2 = -0.41 J_1$.

Figure 2.6 shows the four eigenvalues of the Luttinger-Tisza matrix plotted along the $\Gamma \to X \to W \to L \to \Gamma \to K \to X$ route through the Brillouin zone of the F.C.C. lattice (discussed in subsection 1.2.4) for the parameter values $J_1 = 1$, $J_2 = -0.2$. We see that the largest Luttinger-Tisza eigenvalue has its maximum at the L point $\mathbf{q} = 2\pi(\frac{1}{2}, \frac{1}{2}, \frac{1}{2})$, indicating that the optimal Luttinger-Tisza wavevectors for the state with these parameter values are wavevectors of the type $\left\{\frac{1}{2}\frac{1}{2}\frac{1}{2}\right\}$.

2.3 Kawamura States

In a study of the ground states of (1.1) on the Pyrochlore lattice with a large antiferromagnetic first nearest neighbor interaction $J_1 < 0$ and a small ferromagnetic second

nearest neighbor interaction $J_2 = 0.1\,|J_1|$, Kawamura, et al (see [10]) found three distinct ground states, which they called the Sextuplet-q state, the Quadruplet-q state of type 1 and the Quadruplet-q state of type 2. Each of these states mainly consists of wavevectors of the type $\left\{\frac{3}{4}\frac{3}{4}0\right\}$. The ground states in this region had been previously studied by Kawamura, et al (see [9]) and by Chern, et al (see [8]).

The Sextuplet-q state is composed from equal amounts of all six $\left\{\frac{3}{4}\frac{3}{4}0\right\}$ wavevectors. The Quadruplet-q state of type 1 is composed from equal amounts of four of the $\left\{\frac{3}{4}\frac{3}{4}0\right\}$ wavevectors which lie in the same plane in reciprocal space. For example, the Quadruplet-q state might be made up of the wavevectors $2\pi(\frac{3}{4}, \frac{3}{4}, 0)$, $2\pi(\frac{3}{4}, -\frac{3}{4}, 0)$, $2\pi(\frac{3}{4}, 0, \frac{3}{4})$ and $2\pi(\frac{3}{4}, 0, -\frac{3}{4})$. Finally, the Quadruplet-q state of type 2 is composed from unequal amounts of four of the $\left\{\frac{3}{4}\frac{3}{4}0\right\}$ wavevectors which all lie in the same plane. For example, it might consist principally of the wavevectors $2\pi(\frac{3}{4}, \frac{3}{4}, 0)$ and $2\pi(\frac{3}{4}, -\frac{3}{4}, 0)$ but also have a slightly smaller contribution from the wavevectors $2\pi(\frac{3}{4}, 0, \frac{3}{4})$ and $2\pi(\frac{3}{4}, 0, -\frac{3}{4})$. Luttinger-Tisza analysis confirms that wavevectors of the type $\left\{\frac{3}{4}\frac{3}{4}0\right\}$ are the optimal wavevectors for this state.

These three states very nearly satisfy the constraint that the sum of the four spins on every tetrahedron is equal to zero, so we consider these states to be a subset of the ground states of the pure $J_1 < 0$ antiferromagnet discussed in subsection 2.1.2.

Our Iterative Minimization simulations in the $J_1 < 0$, $J_2 > 0$ region of the phase diagram (figure 2.1) show that these three states are very nearly degenerate for these parameter values. In fact, Iterative Minimization simulations in this region find these three states as well as other states with only slightly higher energy and with very similar wavevector content. For this reason, we suspect that the energy landscape near these three states consists of three relative minima (the three Kawamura states) sitting in a sort of canyon with a very gently sloping floor. Iterative Minimization simulations mostly find these three minima but they sometimes find states which sit on the canyon floor slightly upslope from the three minima and which have slightly higher energy.

Figure 2.7 shows the four eigenvalues of the Luttinger-Tisza matrix plotted along the $\Gamma \to X \to W \to L \to \Gamma \to K \to X$ route through the Brillouin zone of the F.C.C. lattice (discussed in subsection 1.2.4) for the parameter values $J_1 = -1$, $J_2 = 0.1$. We see that

Figure 2.7: L.T. eigenvalues plotted in the Brillouin zone of the F.C.C. lattice for $J_1 = -1$, $J_2 = 0.1$.

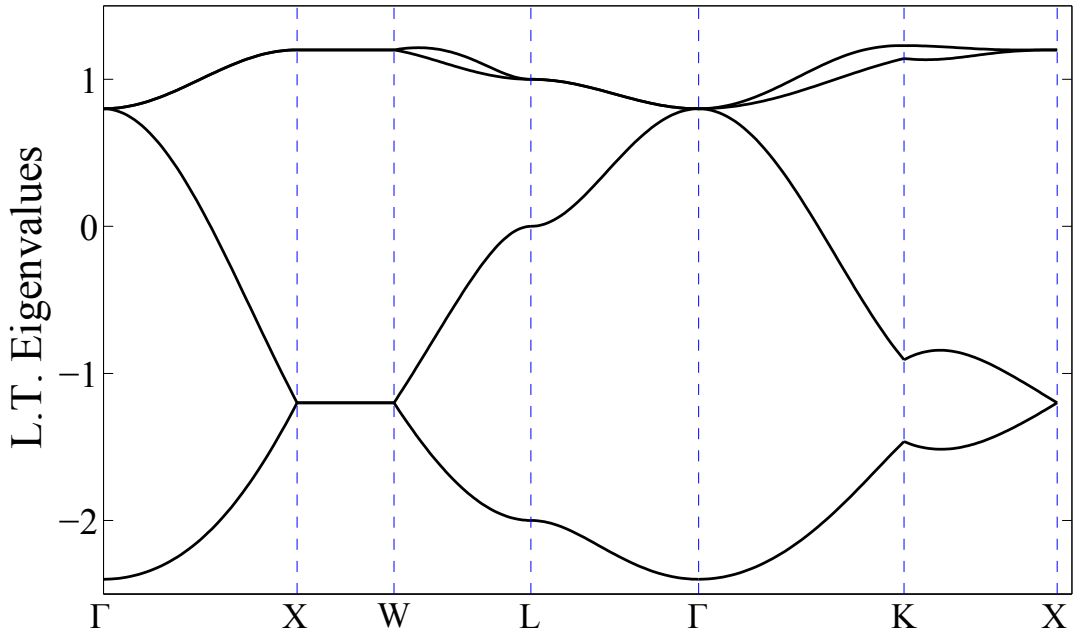

the largest Luttinger-Tisza eigenvalue has its maximum at the K point $\mathbf{q} = 2\pi(\frac{3}{4}, \frac{3}{4}, 0)$, indicating that the optimal Luttinger-Tisza wavevectors for the state with these parameter values are wavevectors of the type $\left\{\frac{3}{4}\frac{3}{4}0\right\}$.

We have focused our study of the structure of these three states almost exclusively on the Kawamura Sextuplet-q state because it seems to have the most symmetry in real space and spin space of the three states found in this region.

2.3.1 Kawamura Sextuplet-q State

As we mentioned above, one of the nearly degenerate ground states found in the region $J_1 < 0$, $J_2 > 0$ is the Kawamura Sextuplet-q state, a complicated non-coplanar state which is mostly composed of equal amounts of the six $\left\{\frac{3}{4}\frac{3}{4}0\right\}$ type wavevectors. This state transitions into a ferromagnetic state at $J_2 \approx -1.09J_1$, when the ferromagnetic J_2 interaction becomes strong enough to overcome the antiferromagnetic first nearest neighbor interaction

Sublattice	$\mathcal{E}_i$	# of spins
1	-1.1053	192
2	-1.1841	192
3	-1.2103	192
4	-1.2672	64
5	-1.2753	192
6	-1.2902	192

Table 2.2: Site Energies of the Kawamura Sextuplet-q State with $J_1 = -1$, $J_2 = 0.1$, $seed = 67$.

J_1.

First we present an example of the Kawamura Sextuplet-q state which we found in Iterative Minimization simulations in this region at the parameter values $J_1 = -1$, $J_2 = 0.1$, $seed = 67$, $L = 4$ (so $N = 1024$ spins). In this state, it turns out that the site energy $\mathcal{E}_i$ of the spins takes on only six different values: thus we can organize the spins by site energy into six sublattices in real space. The site energy of the spins in the six sublattices, as well as the number of spins in each of the six sublattices is shown in table 2.2 for this example.

Each of the six sublattices has a cubic unit cell of size $2 \times 2 \times 2$. The positions of sites within the unit cell of each sublattice are given in Appendix E. One can see that the sublattices are clearly not Bravais sublattices.

Sublattices 3 and 4 are the two distinguished sublattices in this configuration. They are each made up of tetrahedra of spins. The midpoints of the tetrahedra in sublattice 4 sit on the sites of a body-centered cubic (B.C.C.) lattice with a unit cell of size $2 \times 2 \times 2$. The tetrahedra of spins in sublattice 3 combine with those in sublattice 4 to create a simple cubic lattice of tetrahedra with a unit cell of size $1 \times 1 \times 1$. These two sublattices are unique because the spins in these two sublattices point towards the high symmetry directions of a cube in spin space. The spins in sublattice 3 point towards the 12 edge-midpoints of a cube and the spins in sublattice 4 point towards the eight corners of that same cube.

The nearest neighbors of the spins in sublattices 3 and 4 are distributed throughout the six sublattices. Because sublattices 3 and 4 are made up of tetrahedra, three of the six nearest neighbors of every spin lie in the same sublattice as that spin. The other three nearest neighbors of the spins in sublattice 4 (there are $192 = 3{\times}64$ of them) are contained

in sublattice 5. These are the only spins in sublattice 5. The missing three nearest neighbors of the spins in sublattice 3 (there are $576 = 3\times192$ of them) are distributed throughout sublattices 1, 2 and 6.

Using the technique outlined in subsubsection 1.3.6.2, we can use the eight spin directions in sublattice 4 to define a more symmetrical basis in spin space to use to parameterize this state.

With the spins in this state rotated into this new basis we then perform a least square fit of this state to functions of the form $A\sin(\mathbf{q}\cdot\mathbf{r}+\phi)$ where $\mathbf{q}$ is one of the wavevectors of type $\left\{\frac{3}{4}\frac{3}{4}0\right\}$. We have idealized this state by taking averages of phases and numerical coefficients which were very close to the same value. We find that the final state can be written in terms of two constants, $c_1 \approx 0.73$ and $c_2 \approx 0.27$, and two phase angles, $\frac{\pi}{8}$ and $\frac{\pi}{4}$. We use the notation

$$\Phi_{xy} = 2\pi\left(\frac{3}{4}x+\frac{3}{4}y\right) \tag{2.23a}$$

$$\bar{\Phi}_{xy} = 2\pi\left(\frac{3}{4}x-\frac{3}{4}y\right) \tag{2.23b}$$

and a similar notation for arguments involving x and z and y and z to simplify the presentation of this state. Our parameterization then takes the form

$$
\begin{aligned}
\mathbf{s}_0 &= \left\{-c_1 \sin\left(\Phi_{yz} - \frac{\pi}{8}\right) + c_2 \sin\left(\bar{\Phi}_{yz}\right)\right\} \hat{\mathbf{A}}_0 \\
&+ \left\{-c_1 \sin\left(\Phi_{xz} + \frac{\pi}{8}\right) - c_2 \sin\left(\bar{\Phi}_{xz} + \frac{\pi}{4}\right)\right\} \hat{\mathbf{B}}_0 \\
&+ \left\{c_1 \sin\left(\Phi_{xy} + \frac{\pi}{8}\right) - c_2 \sin\left(\bar{\Phi}_{xy} + \frac{\pi}{4}\right)\right\} \hat{\mathbf{C}}_0 \qquad (2.24a) \\
\mathbf{s}_1 &= \left\{-c_1 \sin\left(\Phi_{yz} - \frac{\pi}{8}\right) + c_2 \sin\left(\bar{\Phi}_{yz}\right)\right\} \hat{\mathbf{A}}_0 \\
&+ \left\{c_2 \sin\left(\Phi_{xz} + \frac{\pi}{8}\right) + c_1 \sin\left(\bar{\Phi}_{xz} + \frac{\pi}{4}\right)\right\} \hat{\mathbf{B}}_0 \\
&+ \left\{-c_2 \sin\left(\Phi_{xy} + \frac{\pi}{8}\right) + c_1 \sin\left(\bar{\Phi}_{xy} + \frac{\pi}{4}\right)\right\} \hat{\mathbf{C}}_0 \qquad (2.24b) \\
\mathbf{s}_2 &= \left\{c_2 \sin\left(\Phi_{yz} - \frac{\pi}{8}\right) - c_1 \sin\left(\bar{\Phi}_{yz}\right)\right\} \hat{\mathbf{A}}_0 \\
&+ \left\{-c_1 \sin\left(\Phi_{xz} + \frac{\pi}{8}\right) - c_2 \sin\left(\bar{\Phi}_{xz} + \frac{\pi}{4}\right)\right\} \hat{\mathbf{B}}_0 \\
&+ \left\{-c_2 \sin\left(\Phi_{xy} + \frac{\pi}{8}\right) + c_1 \sin\left(\bar{\Phi}_{xy} + \frac{\pi}{4}\right)\right\} \hat{\mathbf{C}}_0 \qquad (2.24c) \\
\mathbf{s}_3 &= \left\{c_2 \sin\left(\Phi_{yz} - \frac{\pi}{8}\right) - c_1 \sin\left(\bar{\Phi}_{yz}\right)\right\} \hat{\mathbf{A}}_0 \\
&+ \left\{c_2 \sin\left(\Phi_{xz} + \frac{\pi}{8}\right) + c_1 \sin\left(\bar{\Phi}_{xz} + \frac{\pi}{4}\right)\right\} \hat{\mathbf{B}}_0 \\
&+ \left\{c_1 \sin\left(\Phi_{xy} + \frac{\pi}{8}\right) - c_2 \sin\left(\bar{\Phi}_{xy} + \frac{\pi}{4}\right)\right\} \hat{\mathbf{C}}_0 \ . \qquad (2.24d)
\end{aligned}
$$

We now present another parameterization of this same state, which was found in an Iterative Minimization simulation at the parameter values $J_1 = -1$, $J_2 = 0.5$, $L = 4$ and $seed = 84$ (so that $J_2 = 0.5\,|J_1|$). The spins in this state can also be sorted by their site energy $\mathcal{E}_i$ into six sublattices in real space. The site energies and number of spins in each of these six sublattices are shown in table 2.3 for this example.

In this example the distinguished sublattices are sublattices 5 and 6. The spins in sublattice 5 point towards the 12 edge-midpoints of a cube in spin space and the spins in sublattice 6 point towards the eight corners of that same cube, so sublattices 5 and 6 in this example correspond to sublattices 3 and 4 in the previous example which is parameterized in equation (2.24).

Because the spins in sublattice 6 point towards the eight corners of a cube, we can again use the technique of subsubsection 1.3.6.2 to find a nice basis for this state in spin space. We then perform a least square fit of this state to sines and cosines of the $\left\{\frac{3}{4}\frac{3}{4}0\right\}$

Sublattice	$\mathcal{E}_i$	# of spins
1	-1.6730	192
2	-1.9787	192
3	-2.0640	192
4	-2.3381	192
5	-2.3446	192
6	-2.3934	64

Table 2.3: Site Energies of the Kawamura Sextuplet-q State with $J_1 = -1$, $J_2 = 0.5$, $seed = 84$.

type wavevectors. Our parameterization of this state uses the two coefficients $c_1 \approx 0.75$ and $c_2 \approx 0.26$. With these coefficients the parameterization takes the form

$$\begin{aligned}
\mathbf{s}_0 &= \left\{c_1 \sin\left(\Phi_{yz} - \frac{\pi}{8}\right) - c_2 \cos\left(\bar{\Phi}_{yz}\right)\right\} \hat{\mathbf{A}}_0 \\
&+ \left\{c_1 \sin\left(\Phi_{xz} + \frac{3\pi}{8}\right) - c_2 \sin\left(\bar{\Phi}_{xz}\right)\right\} \hat{\mathbf{B}}_0 \\
&+ \left\{c_1 \sin\left(\Phi_{xy} - \frac{\pi}{8}\right) + c_2 \cos\left(\bar{\Phi}_{xy}\right)\right\} \hat{\mathbf{C}}_0 \qquad (2.25a) \\
\mathbf{s}_1 &= \left\{c_1 \sin\left(\Phi_{yz} - \frac{\pi}{8}\right) - c_2 \cos\left(\bar{\Phi}_{yz}\right)\right\} \hat{\mathbf{A}}_0 \\
&+ \left\{-c_2 \sin\left(\Phi_{xz} + \frac{3\pi}{8}\right) + c_1 \sin\left(\bar{\Phi}_{xz}\right)\right\} \hat{\mathbf{B}}_0 \\
&+ \left\{-c_2 \sin\left(\Phi_{xy} - \frac{\pi}{8}\right) - c_1 \cos\left(\bar{\Phi}_{xy}\right)\right\} \hat{\mathbf{C}}_0 \qquad (2.25b) \\
\mathbf{s}_2 &= \left\{-c_2 \sin\left(\Phi_{yz} - \frac{\pi}{8}\right) + c_1 \cos\left(\bar{\Phi}_{yz}\right)\right\} \hat{\mathbf{A}}_0 \\
&+ \left\{c_1 \sin\left(\Phi_{xz} + \frac{3\pi}{8}\right) - c_2 \sin\left(\bar{\Phi}_{xz}\right)\right\} \hat{\mathbf{B}}_0 \\
&+ \left\{-c_2 \sin\left(\Phi_{xy} - \frac{\pi}{8}\right) - c_1 \cos\left(\bar{\Phi}_{xy}\right)\right\} \hat{\mathbf{C}}_0 \qquad (2.25c) \\
\mathbf{s}_3 &= \left\{-c_2 \sin\left(\Phi_{yz} - \frac{\pi}{8}\right) + c_1 \cos\left(\bar{\Phi}_{yz}\right)\right\} \hat{\mathbf{A}}_0 \\
&+ \left\{-c_2 \sin\left(\Phi_{xz} + \frac{3\pi}{8}\right) + c_1 \sin\left(\bar{\Phi}_{xz}\right)\right\} \hat{\mathbf{B}}_0 \\
&+ \left\{c_1 \sin\left(\Phi_{xy} - \frac{\pi}{8}\right) + c_2 \cos\left(\bar{\Phi}_{xy}\right)\right\} \hat{\mathbf{C}}_0 \qquad (2.25d)
\end{aligned}$$

where we again use the condensed notation for the arguments of the sines and cosines defined in (2.23).

We have already mentioned that the Kawamura Sextuplet-q state satisfies the constraint that the sum of the four spins on every tetrahedron is equal to zero. It follows from this fact that this state has no net magnetic moment. Our two parameterizations of this state give us an alternate way of seeing that this is true. We note that in equations (2.24) and (2.25) the expressions for the spins in each F.C.C. sublattice have the form

$$\mathbf{s}_i = f(y,z)\hat{\mathbf{A}}_0 + g(x,z)\hat{\mathbf{B}}_0 + h(x,y)\hat{\mathbf{C}}_0 \ . \tag{2.26}$$

Taking inspiration from the Coulomb Phase ([4]), we can think of the spin parameterization as a coarse-grained vector field that fills all of space. We immediately see that the divergence of this vector field is zero, since

$$\nabla \cdot \mathbf{s}_i = \frac{\partial f(y,z)}{\partial x} + \frac{\partial g(x,z)}{\partial y} + \frac{\partial h(x,y)}{\partial z} = 0 \ , \tag{2.27}$$

so that if we calculated the flux of this vector field out of any volume in the crystal we would get zero. This shows that the state has zero net magnetic moment. In particular, if we calculated the flux out of a surface surrounding a tetrahedron, we find that four spins on every tetrahedron add to zero. This is the condition satisfied by all ground states of (1.1) with only an antiferromagnetic J_1 interaction, so we see again that this state is a subset of the ground states of the pure $J_1 < 0$ antiferromagnet.

We can also see that if one fixes the x and y coordinates and moves in the z-direction, then the spin configuration looks roughly like a superposition of two distorted conic spirals about the z-axis. A similar statement holds if one fixes the x and z coordinates and moves in the y-direction or fixes the y and z coordinates and moves in the x-direction.

Although parameterizations (2.24) and (2.25) look relatively clean, they are not normalized on all of the lattice sites. This implies that the Kawamura Sextuplet-q state is not made up of only wavevectors of the type $\left\{\frac{3}{4}\frac{3}{4}0\right\}$. A closer look at the Fourier Transform of the state found in Iterative Minimization simulations (before it is projected down onto the optimal LT wavevectors) shows that it also contains small contributions from wavevectors like $2\pi(\frac{1}{4},\frac{1}{2},\frac{3}{4})$, $2\pi(\frac{1}{4},\frac{1}{2},-\frac{3}{4})$ and $2\pi(\frac{1}{2},\frac{1}{4},-\frac{1}{4})$, even though these are not optimal wavevectors in the Luttinger-Tisza sense.

But we can see that wavevectors of these types are actually just linear combinations of three of the optimal LT wavevectors. For example, we can write $2\pi(\frac{3}{4},-\frac{3}{4},0)+2\pi(\frac{3}{4},-\frac{3}{4},0)+2\pi(\frac{3}{4},0,\frac{3}{4}) = 2\pi(\frac{9}{4},-\frac{3}{2},\frac{3}{4})$. But we may add to this wavevector a reciprocal lattice vector of the form $2\pi(-2,2,0)$ to map it back to a wavevector in the first Brillouin zone. We see then that this linear combination of optimal LT wavevectors is equivalent to the wavevector $2\pi(\frac{1}{4},\frac{1}{2},\frac{3}{4})$. It turns out that the small contributions from these three kinds of new wavevectors can be accounted for by looking at what happens to our parameterization when we normalize it.

Above we have two parameterizations, equations (2.24) and (2.25), for this state that are not normalized. To normalize them, we would compute

$$\hat{\mathbf{s}}_i = \frac{\mathbf{s}_i}{\sqrt{|\mathbf{s}_i|^2}} \tag{2.28}$$

for every spin. We can rewrite the magnitude of the spin $\mathbf{s}_i$ as $\sqrt{|\mathbf{s}_i|^2} = \sqrt{1+\left(|\mathbf{s}_i|^2-1\right)}$. Then we can Taylor expand the reciprocal of this quantity about the point $|\mathbf{s}_i|^2 = 1$ (where the state is normalized) to find

$$\hat{\mathbf{s}}_i = \mathbf{s}_i\left[1-\frac{1}{2}\left(|\mathbf{s}_i|^2-1\right)+\ldots\right] . \tag{2.29}$$

So the first order correction to the spin $\mathbf{s}_i$ includes a term $|\mathbf{s}_i|^2\,\mathbf{s}_i$. It is from this cubic term that we get corrections to the state that involve wavevectors which are a linear combination of three of the optimal Luttinger-Tisza wavevectors (if we wrote out $\mathbf{s}_i$ as a exponential Fourier series, we would see the addition of wavevectors happening in the exponents).

2.4 A New Variety of Double-Twist State

In the region $J_1 > 0$, $-.68 \leq J_2 \leq -.43$, we find a state which is chiefly composed of a dominant set of two of the six $\left\{\frac{3}{4}\frac{3}{4}0\right\}$ wavevectors and a sub-dominant set of two of the other wavevectors of this type, with the constraint that these four wavevectors lie in the same plane in reciprocal space. For example, this state might be made from the wavevectors $2\pi(\frac{3}{4},\frac{3}{4},0)$, $2\pi(\frac{3}{4},-\frac{3}{4},0)$, $2\pi(\frac{3}{4},0,\frac{3}{4})$ and $2\pi(\frac{3}{4},0,-\frac{3}{4})$ with the Fourier amplitudes of the first

two wavevectors begin approximately 1.40 times the Fourier amplitude of the second two wavevectors. Luttinger-Tisza analysis confirms that wavevectors of the type $\left\{\frac{3}{4}\frac{3}{4}0\right\}$ are the optimal wavevectors for this state. Interestingly, these are the same kind of wavevectors which make up the Kawamura states discussed in section 2.3, although this state uses the wavevectors in a different way. It is especially interesting because these states are located roughly diagonally opposite each other in the J_1-J_2 phase diagram.

Although this state is mostly constructed from $\left\{\frac{3}{4}\frac{3}{4}0\right\}$ wavevectors, it also contains small contributions from $\left\{\frac{3}{4}\frac{1}{4}0\right\}$ wavevectors. These extra wavevectors aid in normalizing this state, since one cannot construct a normalized state from $\left\{\frac{3}{4}\frac{3}{4}0\right\}$ wavevectors alone.

We call this state a new variety of Double-Twist state because it is reminiscent of the Double-Twist state found on the Octahedral lattice by Sklan and Henley (see [1]). Here we list a few characteristic of the Double-Twist state. Firstly, there is a distinguished direction $\hat{\mathbf{m}}$ in real space and also a distinguished direction $\hat{\mathbf{C}}_0$ in spin space. This state can be written using a basis for spin space that uses the fixed basis vector $\hat{\mathbf{C}}_0$ and two rotating basis vectors $\hat{\mathbf{A}}(\mathbf{r}\cdot\hat{\mathbf{m}})$ and $\hat{\mathbf{B}}(\mathbf{r}\cdot\hat{\mathbf{m}})$ which lie in the plane perpendicular to $\hat{\mathbf{C}}_0$, so that $\hat{\mathbf{A}}(\mathbf{r}\cdot\hat{\mathbf{m}})\times\hat{\mathbf{B}}(\mathbf{r}\cdot\hat{\mathbf{m}})=\hat{\mathbf{C}}_0$. As one moves in the $\hat{\mathbf{m}}$ direction in real space the rotating basis vectors $\hat{\mathbf{A}}(\mathbf{r}\cdot\hat{\mathbf{m}})$ and $\hat{\mathbf{B}}(\mathbf{r}\cdot\hat{\mathbf{m}})$ spiral about the fixed vector $\hat{\mathbf{C}}_0$ in spin space (since they are functions of the coordinate in real space parallel to $\hat{\mathbf{m}}$). Thirdly, there is a second direction $\hat{\mathbf{n}}$ in real space, with $\hat{\mathbf{m}}\cdot\hat{\mathbf{n}}=0$, with the property that that spins will also spiral as one moves in the $\hat{\mathbf{n}}$ direction (although not about the $\hat{\mathbf{C}}_0$ axis), even though the rotating basis vectors stay put as one moves in the $\hat{\mathbf{n}}$ direction. Finally, these two distinct kinds of spiraling behavior are controlled by the same type of wavevector.

To summarize, this state gets its name, the "Double-Twist" state, from the fact that the spins are tracing out two different kinds of spirals in two directions which are perpendicular to each other, but these two spirals are controlled by the same type of wavevector.

In the Double-Twist state that we find on the Pyrochlore lattice, the distinguished direction $\hat{\mathbf{m}}$ in real space is a $\langle 100\rangle$ direction, which we take to be the z-direction in our discussion of this state. In addition to the spiraling that the spins do as one moves in the z-direction, we see that the spins also spiral as one moves in the x or y-direction, but that these two spirals are both controlled by wavevectors of the type $\left\{\frac{3}{4}00\right\}$.

To get a better understanding of this state, we take two example ground states found in Iterative minimization simulations and perform a least squares fit of these states to sines and cosines of the optimal LT wavevectors $\left\{\frac{3}{4}\frac{3}{4}0\right\}$. To find a good basis in spin space to express these states in we used the technique of taking row sums of the spins in the SC sublattices outlined in subsubsection 1.3.6.1. We found for this state that the row sums in one direction were all parallel to a certain direction, say $\hat{\mathbf{n}}$, the row sums in a second direction were all zero and the row sums in the third direction were spiraling in the plane perpendicular to $\hat{\mathbf{n}}$. To construct a good basis in spin space, we picked two perpendicular vectors in the plane perpendicular to $\hat{\mathbf{n}}$ to be $\hat{\mathbf{A}}_0$ and $\hat{\mathbf{B}}_0$ and we set $\hat{\mathbf{C}}_0 = \hat{\mathbf{n}}$.

In this section we used the condensed notation

$$\Phi_{xy} = 2\pi\left(\frac{3}{4}x + \frac{3}{4}y\right) \tag{2.30a}$$

$$\bar{\Phi}_{xy} = 2\pi\left(\frac{3}{4}x - \frac{3}{4}y\right) \tag{2.30b}$$

$$\Phi_{x} = 2\pi\left(\frac{3}{4}x\right) \tag{2.30c}$$

(with similar notations for arguments using y and z) to more concisely present the parameterizations of these states.

Our first example of this state comes from the result of an Iterative Minimization simulation at the parameter values $J_1 = 1$, $J_2 = -0.6$, $L = 4$ and $seed = 65$. This state has an energy per site $\bar{\mathcal{E}} = -2.2780$. The two dominant $\left\{\frac{3}{4}\frac{3}{4}0\right\}$ wavevectors making up this state are $2\pi(\frac{3}{4}, \frac{3}{4}, 0)$ and $2\pi(\frac{3}{4}, -\frac{3}{4}, 0)$ and the two sub-dominant wavevectors making up this state are $2\pi(\frac{3}{4}, 0, \frac{3}{4})$ and $2\pi(\frac{3}{4}, 0, -\frac{3}{4})$. Our parameterization of this state uses the four coefficients $c_1 \approx 0.23$, $c_2 \approx 0.76$, $c_3 \approx 0.26$ and $c_4 \approx 0.75$, and the eight phase angles $\phi_1 \approx 5.0°$, $\phi_2 \approx 3.8°$, $\phi_3 \approx 31.0°$, $\phi_4 \approx 4.5°$, $\phi_5 \approx 17.7°$, $\phi_6 \approx 7.4°$, $\phi_7 \approx 18.4°$, $\phi_8 \approx 17.3°$. We express this state in terms of the two rotating basis vectors

$$\hat{\mathbf{A}}(z) = \cos\left(\Phi_z\right)\hat{\mathbf{A}}_0 + \sin\left(\Phi_z\right)\hat{\mathbf{B}}_0 \tag{2.31}$$

$$\hat{\mathbf{B}}(z) = -\sin\left(\Phi_z\right)\hat{\mathbf{A}}_0 + \cos\left(\Phi_z\right)\hat{\mathbf{B}}_0 \tag{2.32}$$

which have been chosen so that $\hat{\mathbf{A}}(z) \times \hat{\mathbf{B}}(z) = \hat{\mathbf{C}}_0$. The parameterization of this state takes

the form

$$\begin{aligned}
\mathbf{s}_0 &= \{c_1 \sin(\Phi_y + \phi_1) + c_2 \sin(\Phi_y + \phi_2)\}\, \hat{\mathbf{A}}(z) \\
&+ \{-c_1 \cos(\Phi_y + \phi_1) + c_2 \cos(\Phi_y + \phi_2)\}\, \hat{\mathbf{B}}(z) \\
&+ \left\{c_3 \sin\left(\Phi_{xy} + \frac{\pi}{4}\right) + c_4 \sin\left(\bar{\Phi}_{xy} + \frac{\pi}{8}\right)\right\} \hat{\mathbf{C}}_0 \qquad (2.33a) \\
\mathbf{s}_1 &= \{c_1 \sin(\Phi_y + \phi_3) + c_2 \sin(\Phi_y + \phi_4)\}\, \hat{\mathbf{A}}(z) \\
&+ \{-c_1 \cos(\Phi_y + \phi_3) + c_2 \cos(\Phi_y + \phi_4)\}\, \hat{\mathbf{B}}(z) \\
&+ \left\{c_4 \sin\left(\Phi_{xy} + \frac{\pi}{4}\right) + c_3 \sin\left(\bar{\Phi}_{xy} + \frac{\pi}{8}\right)\right\} \hat{\mathbf{C}}_0 \qquad (2.33b) \\
\mathbf{s}_2 &= \{c_2 \sin(\Phi_y + \phi_5) + c_1 \sin(\Phi_y - \phi_6)\}\, \hat{\mathbf{A}}(z) \\
&+ \{-c_2 \cos(\Phi_y + \phi_5) + c_1 \cos(\Phi_y - \phi_6)\}\, \hat{\mathbf{B}}(z) \\
&+ \left\{c_4 \sin\left(\Phi_{xy} + \frac{\pi}{4}\right) + c_3 \sin\left(\bar{\Phi}_{xy} + \frac{\pi}{8}\right)\right\} \hat{\mathbf{C}}_0 \qquad (2.33c) \\
\mathbf{s}_3 &= \{c_2 \sin(\Phi_y + \phi_7) + c_1 \sin(\Phi_y + \phi_8)\}\, \hat{\mathbf{A}}(z) \\
&+ \{-c_2 \cos(\Phi_y + \phi_7) + c_1 \cos(\Phi_y + \phi_8)\}\, \hat{\mathbf{B}}(z) \\
&+ \left\{c_3 \sin\left(\Phi_{xy} + \frac{\pi}{4}\right) + c_4 \sin\left(\bar{\Phi}_{xy} + \frac{\pi}{8}\right)\right\} \hat{\mathbf{C}}_0 \ . \qquad (2.33d)
\end{aligned}$$

We see that if one holds z constant and moves in the y-direction, the spins spiral (but not about the $\hat{\mathbf{C}}_0$ axis, since the $\hat{\mathbf{C}}_0$ component of the spins changes as one moves in the y-direction), and if one holds y constant and moves in the z-direction the spins spiral about the $\hat{\mathbf{C}}_0$ direction (since the basis vectors $\hat{\mathbf{A}}(z)$ and $\hat{\mathbf{B}}(z)$ change as one moves in the z-direction). In addition, both of these spirals use a wavevector of the type $\left\{\frac{3}{4}00\right\}$. So in this example the $\hat{\mathbf{m}}$ direction is the z-direction and the $\hat{\mathbf{n}}$ direction is the y-direction. So this example state has all the characteristics of the Double-Twist state found in (see [1]).

Our second example of this state comes from an Iterative Minimization simulation at the parameter values $J_1 = 1$, $J_2 = -0.6$, $L = 4$ and $seed = 63$. It has an energy per site of $\bar{\mathcal{E}} = -2.2780$. The two dominant $\left\{\frac{3}{4}\frac{3}{4}0\right\}$ wavevectors which make up this state are $2\pi(\frac{3}{4}, \frac{3}{4}, 0)$ and $2\pi(\frac{3}{4}, -\frac{3}{4}, 0)$ and the two sub-dominant wavevectors that make up this state are $2\pi(0, \frac{3}{4}, \frac{3}{4})$ and $2\pi(\frac{3}{4}, 0, -\frac{3}{4})$. Like the first state (2.33), the parameterization of this state also uses four coefficients and eight phase angles. The four coefficients are $c_1 \approx 0.23$, $c_2 \approx 0.76$, $c_3 \approx 0.26$ and $c_4 \approx 0.76$, and the eight phase angles are $\phi_1 \approx 5.0°$, $\phi_2 \approx 3.8°$,

$\phi_3 \approx 17.7°$, $\phi_4 \approx 8.65°$, $\phi_5 \approx 31.0°$, $\phi_6 \approx 4.5°$, $\phi_7 \approx 18.9°$, $\phi_8 \approx 17.3°$. We see that these coefficients and phase angles are very similar to those used in the parameterization (2.33) of the first state. The parameterization of this state uses the two rotating basis vectors

$$\hat{\mathbf{A}}(z) = \cos(\Phi_z)\,\hat{\mathbf{A}}_0 - \sin(\Phi_z)\,\hat{\mathbf{B}}_0 \tag{2.34a}$$

$$\hat{\mathbf{B}}(z) = \sin(\Phi_z)\,\hat{\mathbf{A}}_0 + \cos(\Phi_z)\,\hat{\mathbf{B}}_0 \tag{2.34b}$$

which have been chosen so that $\hat{\mathbf{A}}(z) \times \hat{\mathbf{B}}(z) = \hat{\mathbf{C}}_0$. Then the parameterization of this state has the form

$$\begin{aligned}
\mathbf{s}_0 &= \{-c_1\cos(\Phi_x - \phi_1) + c_2\cos(\Phi_x - \phi_2)\}\,\hat{\mathbf{A}}(z) \\
&+ \{c_1\sin(\Phi_x - \phi_1) + c_2\sin(\Phi_x - \phi_2)\}\,\hat{\mathbf{B}}(z) \\
&+ \left\{-c_3\sin\left(\Phi_{xy} - \frac{\pi}{4}\right) + c_4\sin\left(\bar{\Phi}_{xy} + \frac{\pi}{8}\right)\right\}\hat{\mathbf{C}}_0 \qquad (2.35a) \\
\mathbf{s}_1 &= \{-c_2\cos(\Phi_x - \phi_3) + c_1\cos(\Phi_x + \phi_4)\}\,\hat{\mathbf{A}}(z) \\
&+ \{c_2\sin(\Phi_x - \phi_3) + c_1\sin(\Phi_x + \phi_4)\}\,\hat{\mathbf{B}}(z) \\
&+ \left\{-c_4\sin\left(\Phi_{xy} - \frac{\pi}{4}\right) + c_3\sin\left(\bar{\Phi}_{xy} + \frac{\pi}{8}\right)\right\}\hat{\mathbf{C}}_0 \qquad (2.35b) \\
\mathbf{s}_2 &= \{-c_1\cos(\Phi_x - \phi_5) + c_2\cos(\Phi_x - \phi_6)\}\,\hat{\mathbf{A}}(z) \\
&+ \{c_1\sin(\Phi_x - \phi_5) + c_2\sin(\Phi_x - \phi_6)\}\,\hat{\mathbf{B}}(z) \\
&+ \left\{-c_4\sin\left(\Phi_{xy} - \frac{\pi}{4}\right) + c_3\sin\left(\bar{\Phi}_{xy} + \frac{\pi}{8}\right)\right\}\hat{\mathbf{C}}_0 \qquad (2.35c) \\
\mathbf{s}_3 &= \{-c_2\cos(\Phi_x - \phi_7) + c_1\cos(\Phi_x - \phi_8)\}\,\hat{\mathbf{A}}(z) \\
&+ \{c_2\sin(\Phi_x - \phi_7) + c_1\sin(\Phi_x - \phi_8)\}\,\hat{\mathbf{B}}(z) \\
&+ \left\{-c_3\sin\left(\Phi_{xy} - \frac{\pi}{4}\right) + c_4\sin\left(\bar{\Phi}_{xy} + \frac{\pi}{8}\right)\right\}\hat{\mathbf{C}}_0\ . \qquad (2.35d)
\end{aligned}$$

We see that in this example if one holds z constant and moves in the x-direction the spins spiral (again, not about the $\hat{\mathbf{C}}_0$ direction since the $\hat{\mathbf{C}}_0$ component of the spins also changes as one moves in the x-direction), and if one holds x constant and moves in the z-direction the spins spiral about the $\hat{\mathbf{C}}_0$ direction. Again, both of these spirals use a wavevector of the type $\left\{\frac{3}{4}00\right\}$. In this example the $\hat{\mathbf{m}}$ direction is the z-direction and the $\hat{\mathbf{n}}$ direction is the x-direction. So this example also has all the characteristics of the Double-Twist state found

Figure 2.8: L.T. eigenvalues plotted in the Brillouin zone of the F.C.C. lattice for $J_1 = 1$, $J_2 = -0.6$.

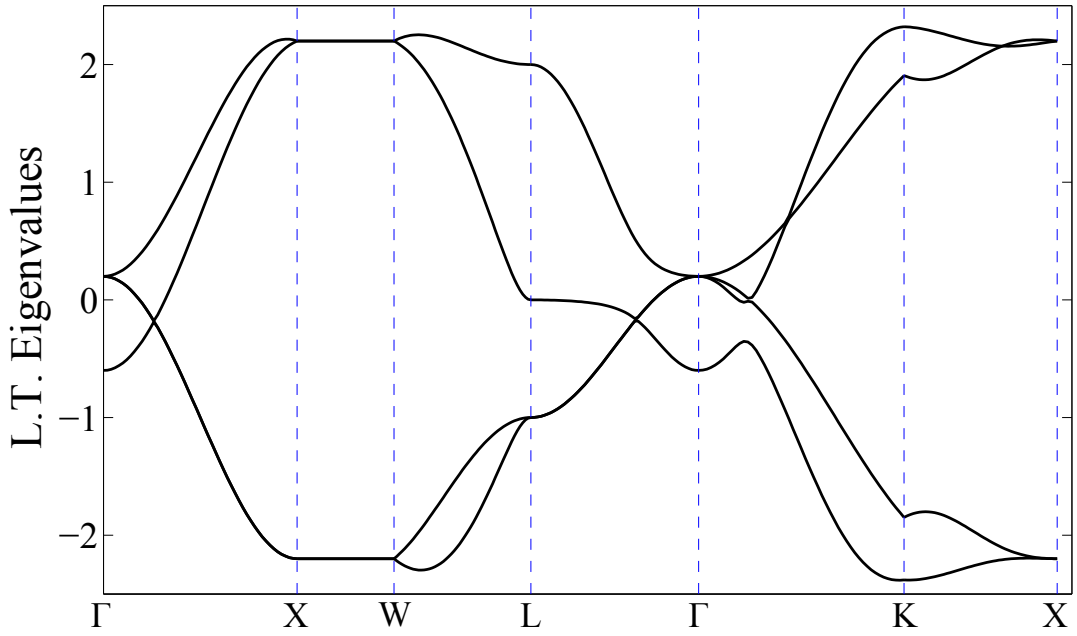

by Sklan and Henley (see [1]).

Figure 2.8 shows the four eigenvalues of the Luttinger-Tisza matrix plotted along the $\Gamma \to X \to W \to L \to \Gamma \to K \to X$ route through the Brillouin zone of the F.C.C. lattice (discussed in subsection 1.2.4) for the parameter values $J_1 = 1$, $J_2 = -0.6$. We see that the largest Luttinger-Tisza eigenvalue has its maximum at the K point $\mathbf{q} = 2\pi(\frac{3}{4}, \frac{3}{4}, 0)$, indicating that the optimal Luttinger-Tisza wavevectors for the state with these parameter values are also wavevectors of the type $\left\{\frac{3}{4}\frac{3}{4}0\right\}$, just as was the case for the Kawamura States.

2.5 Multiply-Modulated Commensurate Spirals

In the small sliver of parameter space $J_1 = 1$, $-0.43 \leq J_2 \leq -0.40$ we find a non-coplanar state with period 4 constructed solely from wavevectors of the types $\left\{\frac{3}{4}\frac{1}{4}\frac{1}{2}\right\}$, $\left\{\frac{3}{4}\frac{3}{4}0\right\}$ and $\left\{\frac{1}{4}\frac{1}{4}0\right\}$. The prototype of this state uses the four wavevectors $2\pi(\frac{3}{4}, \frac{1}{4}, \frac{1}{2})$, $2\pi(\frac{3}{4}, \frac{1}{4}, -\frac{1}{2})$, $2\pi(\frac{3}{4}, -\frac{3}{4}, 0)$, and $2\pi(\frac{1}{4}, -\frac{1}{4}, 0)$ but one can build this state from any rotation of this set of

four wavevectors by multiples of $\frac{\pi}{2}$ about the q_x, q_y or q_z axes in reciprocal space. The contribution from each kind of wavevector varies on the different FCC sublattices and the wavevectors $2\pi(\frac{3}{4},\frac{1}{4},\frac{1}{2})$ and $2\pi(\frac{3}{4},\frac{1}{4},-\frac{1}{2})$ are the optimal Luttinger-Tisza wavevectors. In fact, the largest Luttinger-Tisza eigenvalues for these wavevectors at the parameter values $J_1 = 1$, $J_2 = -0.42$ are $\lambda_{LT^*} = 2.0195$ for $2\pi(\frac{3}{4},\frac{1}{4},\pm\frac{1}{2})$, $\lambda_{LT^*} = 2.0121$ for $2\pi(\frac{3}{4},-\frac{3}{4},0)$ and $\lambda_{LT^*} = 0.9337$ for $2\pi(\frac{1}{4},-\frac{1}{4},0)$. So this state is another example of a non-coplanar state which is constructed from an optimal LT wavevector and from wavevectors which are suboptimal.

We call this state a Multiply-Modulated Commensurate Spiral (M.M.C.S.) because the spins in this state are tracing out two different spirals in two different directions which are orthogonal to each other and these spirals are controlled by two different kinds of wavevectors. The presence of two different kinds of wavevectors which control the spirals is what gives this state the descriptor "Multiply-Modulated". It is a commensurate spiral because every wavevector involved is commensurate with the lattice.

In this state there is a distinguished direction $\hat{\mathbf{m}}$ in real space and a distinguished direction $\hat{\mathbf{C}}_0$ in spin space. The spin configuration can be written using a basis in spin space that uses the one fixed basis vector $\hat{\mathbf{C}}_0$ and two rotating basis vectors $\hat{\mathbf{A}}(\mathbf{r}\cdot\hat{\mathbf{m}})$ and $\hat{\mathbf{B}}(\mathbf{r}\cdot\hat{\mathbf{m}})$, which lie in the plane perpendicular to $\hat{\mathbf{C}}_0$ and satisfy $\hat{\mathbf{A}}(\mathbf{r}\cdot\hat{\mathbf{m}})\times\hat{\mathbf{B}}(\mathbf{r}\cdot\hat{\mathbf{m}}) = \hat{\mathbf{C}}_0$. As one moves in the $\hat{\mathbf{m}}$ direction in real space these two basis vectors rotate counter-clockwise about $\hat{\mathbf{C}}_0$ in spin space.To write this state in the most concise way, we also use a second set of two rotating basis vectors $\hat{\mathbf{A}}'(\mathbf{r}\cdot\hat{\mathbf{m}})$ and $\hat{\mathbf{B}}'(\mathbf{r}\cdot\hat{\mathbf{m}})$ lying in the plane perpendicular to $\hat{\mathbf{C}}_0$ and also satisfying $\hat{\mathbf{A}}'(\mathbf{r}\cdot\hat{\mathbf{m}})\times\hat{\mathbf{B}}'(\mathbf{r}\cdot\hat{\mathbf{m}}) = \hat{\mathbf{C}}_0$, but this second set rotates clockwise about $\hat{\mathbf{C}}_0$ as one moves in the $\hat{\mathbf{m}}$ direction in real space. In this state there is also a second direction $\hat{\mathbf{n}}$ in real space, with $\hat{\mathbf{m}}\cdot\hat{\mathbf{n}} = 0$, such that the spins will spiral about about the $\hat{\mathbf{C}}_0$ direction in spin space when one moves in the $\hat{\mathbf{n}}$ direction in real space, even though the basis vectors $\hat{\mathbf{A}}(\mathbf{r}\cdot\hat{\mathbf{m}})$, $\hat{\mathbf{B}}(\mathbf{r}\cdot\hat{\mathbf{m}})$, $\hat{\mathbf{A}}'(\mathbf{r}\cdot\hat{\mathbf{m}})$ and $\hat{\mathbf{B}}'(\mathbf{r}\cdot\hat{\mathbf{m}})$ stay put as one moves in this direction. Finally, the wavevectors that control the spiraling in the $\hat{\mathbf{m}}$ and $\hat{\mathbf{n}}$ directions are not the same, so the spiraling behavior in this state is different from the spiraling behavior of the Double-Twist state of section 2.4, because the two kinds of spirals in the Double-Twist state are controlled by the same type of wavevector.

Using a diagnostic which counts the number of different spin directions present in a certain state (two spins $\mathbf{s}_i$ and $\mathbf{s}_j$ are considered to point in different directions if $\mathbf{s}_i \cdot \mathbf{s}_j < .99$), we find that the spins in this state point in 42 different directions. The spins in two of the FCC sublattices point in the same 10 directions and the spins in the other two FCC sublattices point in 32 directions which are distinct from the first 10.

Here we show two parameterizations of this state which were made by idealizing least square fits to the results of Iterative Minimization simulations. The first example parameterization uses the four wavevectors $2\pi(\frac{3}{4}, \frac{1}{4}, \frac{1}{2})$, $2\pi(\frac{3}{4}, \frac{1}{4}, -\frac{1}{2})$, $2\pi(\frac{3}{4}, -\frac{3}{4}, 0)$, and $2\pi(\frac{1}{4}, -\frac{1}{4}, 0)$ and corresponds to the parameter values $J_1 = 1$, $J_2 = -0.43$, $L = 4$, and $seed = 63$. The most concise presentation of this state uses two sets of two rotating basis vectors, all lying in the plane in spin space perpendicular to $\hat{\mathbf{C}}_0$. Defining the phase $\Phi_{xy} = 2\pi\left(\frac{3}{4}x + \frac{1}{4}y - \frac{1}{16}\right)$, we can write these four basis vectors as

$$\hat{\mathbf{A}}(x,y) = \cos\Phi_{xy}\hat{\mathbf{A}}_0 + \sin\Phi_{xy}\hat{\mathbf{B}}_0 \tag{2.36a}$$

$$\hat{\mathbf{B}}(x,y) = -\sin\Phi_{xy}\hat{\mathbf{A}}_0 + \cos\Phi_{xy}\hat{\mathbf{B}}_0 \tag{2.36b}$$

$$\hat{\mathbf{A}}'(x,y) = \cos\Phi_{xy}\hat{\mathbf{A}}_0 - \sin\Phi_{xy}\hat{\mathbf{B}}_0 \tag{2.36c}$$

$$\hat{\mathbf{B}}'(x,y) = \sin\Phi_{xy}\hat{\mathbf{A}}_0 + \cos\Phi_{xy}\hat{\mathbf{B}}_0 \tag{2.36d}$$

where we have arranged it so that $\hat{\mathbf{A}}_0 \times \hat{\mathbf{B}}_0 = \hat{\mathbf{A}}(x,y) \times \hat{\mathbf{B}}(x,y) = \hat{\mathbf{A}}'(x,y) \times \hat{\mathbf{B}}'(x,y) = \hat{\mathbf{C}}_0$. We see that $\hat{\mathbf{A}}(x,y)'$ is the reflection of $\hat{\mathbf{A}}(x,y)$ over the $\hat{\mathbf{A}}_0$ axis and $\hat{\mathbf{B}}'(x,y)$ is the reflection of $\hat{\mathbf{B}}(x,y)$ over the $\hat{\mathbf{B}}_0$ axis. The parameterization of this state uses the six coefficients $l_1 \approx 0.868$, $l_2 \approx 0.054$, $l_3 \approx 0.699$, $l_4 \approx 0.076$, $l_5 \approx 0.228$ and $l_6 \approx 0.011$. With these coefficients and the four rotating basis vectors defined above, the parameterization of this

state takes the form

$$\begin{aligned}
\mathbf{s}_0 &= l_1 \left\{ \sin(\pi z)\hat{\mathbf{A}}'(x,y) - \cos(\pi z)\hat{\mathbf{B}}'(x,y) \right\} \\
&+ l_2 \left\{ \sin(\pi z)\hat{\mathbf{A}}(x,y) - \cos(\pi z)\hat{\mathbf{B}}(x,y) \right\} \\
&+ \left\{ l_3 \sin\left[2\pi \left(\frac{3}{4}x - \frac{3}{4}y - \frac{1}{16} \right) \right] + l_4 \sin\left[2\pi \left(\frac{1}{4}x - \frac{1}{4}y - \frac{3}{16} \right) \right] \right\} \hat{\mathbf{C}}_0 \quad (2.37a) \\
\mathbf{s}_1 &= 2l_3 \cos(\pi z)\hat{\mathbf{B}}'(x,y) \\
&+ \left\{ l_5 \sin\left[2\pi \left(\frac{3}{4}x - \frac{3}{4}y - \frac{1}{16} \right) \right] + l_6 \sin\left[2\pi \left(\frac{1}{4}x - \frac{1}{4}y - \frac{3}{16} \right) \right] \right\} \hat{\mathbf{C}}_0 \quad (2.37b) \\
\mathbf{s}_2 &= \mathbf{s}_1 \quad (2.37c) \\
\mathbf{s}_3 &= l_1 \left\{ \sin(\pi z)\hat{\mathbf{A}}'(x,y) + \cos(\pi z)\hat{\mathbf{B}}'(x,y) \right\} \\
&- l_2 \left\{ \sin(\pi z)\hat{\mathbf{A}}(x,y) + \cos(\pi z)\hat{\mathbf{B}}(x,y) \right\} \\
&+ \left\{ l_3 \sin\left[2\pi \left(\frac{3}{4}x - \frac{3}{4}y - \frac{1}{16} \right) \right] + l_4 \sin\left[2\pi \left(\frac{1}{4}x - \frac{1}{4}y - \frac{3}{16} \right) \right] \right\} \hat{\mathbf{C}}_0 \ . \quad (2.37d)
\end{aligned}$$

We see that in this example $\hat{\mathbf{m}} = \frac{1}{\sqrt{10}}(3\hat{\mathbf{x}} + \hat{\mathbf{y}})$ and $\hat{\mathbf{n}} = \hat{\mathbf{z}}$. Furthermore, the spiraling in the $\hat{\mathbf{m}}$ direction is controlled by the wavevector $2\pi(\frac{3}{4}, \frac{1}{4}, 0)$ and the spiraling in the $\hat{\mathbf{n}}$ direction is controlled by the wavevector $(0, 0, \pi)$, and these two wavevectors are clearly not the same type of wavevector.

Our second example of this state is comprised of the four wavevectors $2\pi(\frac{3}{4}, \frac{1}{4}, \frac{1}{2})$, $2\pi(\frac{3}{4}, \frac{1}{4}, -\frac{1}{2})$, $2\pi(\frac{3}{4}, -\frac{3}{4}, 0)$, and $2\pi(\frac{1}{4}, -\frac{1}{4}, 0)$ and corresponds to the parameter values $J_1 = 1$, $J_2 = -0.42$, $L = 4$, and $seed = 77$. The parameterization of this state also uses six coefficients, whose values are $l_1 \approx 0.872$, $l_2 \approx 0.050$, $l_3 \approx 0.695$, $l_4 \approx 0.071$, $l_5 \approx 0.226$ and $l_6 \approx 0.014$. The parameterization of this state also uses the four rotating basis vectors (2.36a) through (2.36d) but with the phase Φ_{xy} defined to be $\Phi_{xy} = 2\pi(\frac{3}{4}x + \frac{1}{4}y + \frac{1}{16})$. The

resulting state can be written

$$\begin{aligned}
\mathbf{s}_0 &= l_1 \left\{ \sin(\pi z)\hat{\mathbf{A}}'(x,y) - \cos(\pi z)\hat{\mathbf{B}}'(x,y) \right\} \\
&+ l_2 \left\{ \sin(\pi z)\hat{\mathbf{A}}(x,y) - \cos(\pi z)\hat{\mathbf{B}}(x,y) \right\} \\
&+ \left\{ l_3 \sin\left[2\pi \left(\frac{3}{4}x - \frac{3}{4}y + \frac{1}{16} \right) \right] + l_4 \sin\left[2\pi \left(\frac{1}{4}x - \frac{1}{4}y + \frac{3}{16} \right) \right] \right\} \hat{\mathbf{C}}_0 \qquad (2.38a) \\
\mathbf{s}_1 &= 2l_3 \sin(\pi z)\hat{\mathbf{A}}'(x,y) \\
&+ \left\{ l_5 \sin\left[2\pi \left(\frac{3}{4}x - \frac{3}{4}y + \frac{1}{16} \right) \right] + l_6 \sin\left[2\pi \left(\frac{1}{4}x - \frac{1}{4}y + \frac{3}{16} \right) \right] \right\} \hat{\mathbf{C}}_0 \qquad (2.38b) \\
\mathbf{s}_2 &= \mathbf{s}_1 \qquad (2.38c) \\
\mathbf{s}_3 &= l_1 \left\{ \sin(\pi z)\hat{\mathbf{A}}'(x,y) + \cos(\pi z)\hat{\mathbf{B}}'(x,y) \right\} \\
&- l_2 \left\{ \sin(\pi z)\hat{\mathbf{A}}(x,y) + \cos(\pi z)\hat{\mathbf{B}}(x,y) \right\} \\
&+ \left\{ l_3 \sin\left[2\pi \left(\frac{3}{4}x - \frac{3}{4}y + \frac{1}{16} \right) \right] + l_4 \sin\left[2\pi \left(\frac{1}{4}x - \frac{1}{4}y + \frac{3}{16} \right) \right] \right\} \hat{\mathbf{C}}_0 \ . \qquad (2.38d)
\end{aligned}$$

This state also has $\hat{\mathbf{m}} = \frac{1}{\sqrt{10}}(3\hat{\mathbf{x}} + \hat{\mathbf{y}})$ and $\hat{\mathbf{n}} = \hat{\mathbf{z}}$. As in the previous example, (2.37), the spiraling in the $\hat{\mathbf{m}}$ direction is controlled by the wavevector $2\pi(\frac{3}{4}, \frac{1}{4}, 0)$ and the spiraling in the $\hat{\mathbf{n}}$ direction is controlled by the wavevector $(0, 0, \pi)$. We see again that the two kinds of spiral are controlled by different types of wavevector.

3. Beyond first and second nearest neighbor interactions

3.1 Cuboctahedral Stack in the J_1, J_3, J_3' Phase Diagram

The Cuboctahedral Stack state, which we first discovered in the $J_1 > 0$, $J_2 < 0$ region of the J_1, J_2 phase diagram (see section 2.2), also exists in the J_1, J_3, J_3' phase diagram for J_1, $J_3 > 0$ and $J_3' < 0$. This state is again made up of three of the four $\left\{\frac{1}{2}\frac{1}{2}\frac{1}{2}\right\}$ type wavevectors, with the fourth, unused, wavevector pointing in the stacking direction. The parameterization is exactly the same as that presented in equations (2.19a) through (2.19d). The energy per site for the Cuboctahedral Stack state with these three interactions is

$$\bar{\mathcal{E}} = -\left(\frac{3}{4} + \frac{\sqrt{6}}{2}\right) J_1 - J_3 + J_3' \tag{3.1}$$

This state will transition to a ferromagnetic state, with energy per site (2.1), when

$$J_1 = -\frac{8J_3 + 16J_3'}{9 - 2\sqrt{6}} \ . \tag{3.2}$$

Because there are no variable parameters in the parameterization of the Cuboctahedral Stack state, the transition between this state and the ferromagnetic state must be a first order phase transition (a discontinuous transition). The results of simulations show, however, that near the transition between these two states there is a "mixed" state whose Fourier Transform shows peaks at $(0, 0, 0)$ as well as at the $\left\{\frac{1}{2}\frac{1}{2}\frac{1}{2}\right\}$ wavevectors that make up the Cuboctahedral Stack. In spin space the spins are arranged around a cone so that this state does have a net magnetic moment which points along the axis of that cone.

There are two possible explanations for this behavior. The first possibility is that this observed mixing of states is not a real phenomenon but just an artifact of the Iterative Minimization simulation. We know that the Iterative Minimization algorithm sometimes has trouble finding the true ground state when there are two or more states which are nearly degenerate, which is the case near a phase transition between two states. The second possibility is that there is a third state which exists only near the transition between the

ferromagnetic and Cuboctahedral Stack states and this third state has characteristics of both neighboring states. More investigation is needed to determine which of these two explanations is the correct one.

Previously (section 2.2), we had understood the Cuboctahedral Stack as being the result of competition between a strong ferromagnetic nearest neighbor interaction J_1 and a weak antiferromagnetic second nearest neighbor interaction J_2. In this case we have no second nearest neighbor interaction, but we do have a ferromagnetic J_3 interaction and an antiferromagnetic J_3' interaction. In the Cuboctahedral Stack configuration, a spin in a triangular lattice layer has a dot product of $\frac{1}{3}$ with its six J_3 neighbors and a dot product of $-\frac{1}{3}$ with its six J_3' neighbors. A spin in a Kagome lattice layer has a dot product of 1 with two of its six J_3 neighbors (those in adjacent Kagome lattice layers) and a dot product of 0 with the other four (those in the same Kagome lattice layer) and it also has a dot product of -1 with two of its J_3' neighbors (those in the same Kagome lattice layer) and 0 with the other four (those in adjacent Kagome lattice layers). In this way the Cuboctahedral Stack serves as a compromise in which spins can have positive (or zero) dot products with their J_3 neighbors and negative (or zero) dot products with their J_3' neighbors. So the dot product between each pair of spins is either zero or has the sign that goes with the interaction between that pair of spins (e.g. dot products between J_3 neighbors are either zero or are positive, which favors the ferromagnetic J_3 interaction).

3.2 A New Kind of Alternating Conic Spiral State

In the region J_1, $J_3 > 0$ and $J_3' < 0$ we find a new type of alternating conic spiral state when the magnitude of J_3' is much larger than the magnitudes of J_1 and J_3. In an alternating conic spiral state the spins spiral about a certain axis and the component of the spins parallel to this axis also alternates in sign. Our state is distinct from the alternating conic spiral found by Sklan and Henley (see [1]) because the wavevector which controls the spiraling behavior is not parallel to the wavevector which controls the alternating behavior. This means that the spins spiral about the conic axis when you move in one direction in the lattice, and the component of the spins parallel to the conic axis alternates in sign when one moves in a completely different direction in the lattice. Our state also has one sublattice

where the spins are tracing out a planar spiral in the plane perpendicular to the conic axis and another sublattice in which the spins are all collinear and only point up or down along the conic axis.

This state is made up of two different wavevectors, $\mathbf{q}_1$ and $\mathbf{q}_2$. The first wavevector $\mathbf{q}_1$ controls the spiraling behavior and we believe that $\mathbf{q}_1$ does not have to be commensurate with the lattice (as is the case for the spiraling wavevector in the $\langle 100 \rangle$ planar spiral of subsection 2.1.5). The second wavevector $\mathbf{q}_2$ controls the alternating behavior and in order for our state to be normalized it must be commensurate with the lattice and satisfy $\cos(\mathbf{q}_2 \cdot \mathbf{r}) = \pm 1$. As we mentioned before, $\mathbf{q}_1$ and $\mathbf{q}_2$ are not parallel.

In two of the F.C.C. sublattices the spins in this state are describing a conic spiral with cone angle α in the direction parallel to $\mathbf{q}_1$ and also alternating up and down in the direction parallel to $\mathbf{q}_2$. In a third F.C.C. sublattice the spins trace out a planar spiral with the same wavevector as the conic spiral. In the fourth F.C.C. sublattice the spins are all collinear and they only alternate pointing parallel and antiparallel to the conic axis. They modulate only with the wavevector $\mathbf{q}_2$.

We can express this state most concisely using one rotating basis vector. If we define the phase $\Phi = \mathbf{q}_1 \cdot \mathbf{r}$, then we can write this basis vector as

$$\hat{\mathbf{A}}(x, y, z) = \cos(\Phi)\hat{\mathbf{A}}_0 + \sin(\Phi)\hat{\mathbf{B}}_0 \tag{3.3}$$

With this rotating basis vector the parameterization of this state takes the form

$$\begin{aligned}
\mathbf{s}_0 &= \sin\alpha\hat{\mathbf{A}}(x, y, z) + \cos\alpha\cos(\mathbf{q}_2 \cdot \mathbf{r})\ \hat{\mathbf{C}}_0 && \text{(3.4a)}\\
\mathbf{s}_1 &= \hat{\mathbf{A}}(x, y, z) && \text{(3.4b)}\\
\mathbf{s}_2 &= \sin\alpha\hat{\mathbf{A}}(x, y, z) + \cos\alpha\cos(\mathbf{q}_2 \cdot \mathbf{r})\ \hat{\mathbf{C}}_0 && \text{(3.4c)}\\
\mathbf{s}_3 &= \cos(\mathbf{q}_2 \cdot \mathbf{r})\ \hat{\mathbf{C}}_0 && \text{(3.4d)}
\end{aligned}$$

where $\hat{\mathbf{A}}_0$, $\hat{\mathbf{B}}_0$ and $\hat{\mathbf{C}}_0$ again form an orthonormal triad. In this parameterization the spins in F.C.C. sublattices 0 and 2 are performing alternating conic spirals, the spins in F.C.C. sublattice 1 are performing a planar spiral and the spins in F.C.C. sublattice 3 are alternating pointing parallel and antiparallel to the axis of the conic spiral.

For the specific parameter values $J_1 = J_3 = 1$, $J_3' = -4$, $seed = 56$, the state we found with Iterative Minimization has $\mathbf{q}_1 = 2\pi(-\frac{3}{4}, -\frac{1}{2}, \frac{1}{4})$, $\mathbf{q}_2 = 2\pi(-\frac{1}{2}, \frac{1}{2}, \frac{1}{2})$ and cone angle $\alpha \approx 0.92$. As J_3' is varied in this region, the spin structure factor still shows large peaks near $\left\{\frac{1}{2}\frac{1}{2}\frac{1}{2}\right\}$ type wavevectors. For this reason, we assume that the vector $\mathbf{q}_2$, which controls the alternating behavior of the state, is always a $\left\{\frac{1}{2}\frac{1}{2}\frac{1}{2}\right\}$ type wavevector (and therefore commensurate with the lattice). On the other hand, we assume that $\mathbf{q}_1$ and the cone angle α can vary continuously and so we leave them as parameters to be optimized.

We set $\mathbf{q}_1 = (q_{1x}, q_{1y}, q_{1z})$ and $\mathbf{q}_2 = 2\pi(-\frac{1}{2}, \frac{1}{2}, \frac{1}{2})$ and then compute the energy per site for this state. We find

$$\bar{\mathcal{E}} = -\frac{J_1}{8}\bar{\mathcal{E}}_{J_1} - \frac{J_3}{8}\bar{\mathcal{E}}_{J_3} - \frac{J_3'}{8}\bar{\mathcal{E}}_{J_3'} \tag{3.5}$$

where

$$\begin{aligned}
\bar{\mathcal{E}}_{J_1} &= 2\sin\alpha + 6\cos\alpha + 4\cos^2\alpha + 4\sin\alpha\cos\left(\frac{q_{1y}+q_{1z}}{4}\right) \\
&+ 2\sin\alpha\cos\left(\frac{q_{1x}-q_{1y}}{4}\right) + 2\sin^2\alpha\cos\left(\frac{q_{1x}+q_{1z}}{4}\right) \qquad (3.6a) \\
\bar{\mathcal{E}}_{J_3} &= 4\sin^2\alpha\left[\cos\left(\frac{q_{1x}}{2}\right)\cos\left(\frac{q_{1y}}{2}\right) + \cos\left(\frac{q_{1x}+q_{1z}}{2}\right) + \cos\left(\frac{q_{1y}}{2}\right)\cos\left(\frac{q_{1z}}{2}\right)\right] \\
&+ 2\cos\left(\frac{q_{1x}-q_{1y}}{2}\right) + 2\cos\left(\frac{q_{1x}-q_{1z}}{2}\right) + 2\cos\left(\frac{q_{1y}+q_{1z}}{2}\right) + 4\cos^2\alpha + 2 \qquad (3.6b) \\
\bar{\mathcal{E}}_{J_3'} &= 4\sin^2\alpha\left[\cos\left(\frac{q_{1x}}{2}\right)\cos\left(\frac{q_{1y}}{2}\right) + \cos\left(\frac{q_{1x}-q_{1z}}{2}\right) + \cos\left(\frac{q_{1y}}{2}\right)\cos\left(\frac{q_{1z}}{2}\right)\right] \\
&+ 2\cos\left(\frac{q_{1x}+q_{1y}}{2}\right) + 2\cos\left(\frac{q_{1x}+q_{1z}}{2}\right) + 2\cos\left(\frac{q_{1y}-q_{1z}}{2}\right) - 4\cos^2\alpha - 2 \qquad (3.6c)
\end{aligned}$$

and $\bar{\mathcal{E}}_{J_1}$ represents the contribution to the energy per site from the J_1 interaction, $\bar{\mathcal{E}}_{J_3}$ is the contribution from the J_3 interaction and $\bar{\mathcal{E}}_{J_3'}$ is the contribution from the J_3' interaction. To find the optimal wavevector $\mathbf{q}_1$ and cone angle α for this state, we would differentiate equation (3.5) with respect to the components of $\mathbf{q}_1$ and α, set the derivatives equal to zero, and then solve the resulting equations for the optimal wavevector $\mathbf{q}_1$ and cone angle α.

As a quick check of our formula (3.5), we calculate a theoretical value for the cone angle α for the state with $J_1 = J_3 = 1$, $J_3' = -4$, seed = 56, by taking $\mathbf{q_1} = 2\pi(-\frac{3}{4}, -\frac{1}{2}, \frac{1}{4})$ as given and optimizing (3.5) with respect to α. We find that the optimal cone angle α satisfies

$$\left(-\frac{1}{4}-\frac{3}{4}\cos\frac{\pi}{8}\right)\cos\alpha+\frac{3}{4}\sin\alpha+\left(2-\frac{1}{2\sqrt{2}}\right)\sin\alpha\cos\alpha=0\ . \tag{3.7}$$

Solving this equation numerically gives $\cos\alpha \approx 0.897$ which is close to the value which was observed in the simulation, which was $\cos\alpha \approx 0.92$. One possible cause of the discrepancy between these two values is that $\mathbf{q_1} = 2\pi(-\frac{3}{4}, -\frac{1}{2}, \frac{1}{4})$ might not be the optimal $\mathbf{q}_1$ wavevector, but just a wavevector close to the optimal one which had the periodicity of the $4 \times 4 \times 4$ block of Pyrochlore lattice unit cells we were using in our simulation.

The largest Luttinger-Tisza eigenvalues for this state with $J_1 = J_3 = 1$, and $J_3' = -4$ are $\lambda_{LT^*} = 6.8629$ for $\mathbf{q}_1 = 2\pi(-\frac{3}{4}, -\frac{1}{2}, \frac{1}{4})$ and $\lambda_{LT^*} = 7$ for $\mathbf{q}_2 = 2\pi(-\frac{1}{2}, \frac{1}{2}, \frac{1}{2})$. We see from this that this state is not only constructed from the optimal Luttinger-Tisza wavevector $\mathbf{q}_2$, but that it also contains a significant contribution from a suboptimal wavevector $\mathbf{q}_1$. We also see that these two wavevectors are nearly degenerate, because the largest Luttinger-Tisza eigenvalues for these two wavevectors are very close to each other. This supports the hypothesis advanced by Sklan and Henley (see [1]) that many non-coplanar states are made from combinations of optimal Luttinger-Tisza wavevectors and wavevectors that are only slightly suboptimal.

3.3 States Stacked Along a $\langle 111 \rangle$ Axis in Real Space

Recent neutron diffraction experiments carried out by Lee, et al (see [2]) on a material whose magnetically interacting atoms sit on the Pyrochlore lattice found a magnetically ordered state which was stacked (see subsection 1.3.5) along a particular $\langle 111 \rangle$ direction in real space. Recall that when viewed along a $\langle 111 \rangle$ axis, the Pyrochlore lattice appears as alternating layers of triangular and Kagome lattices. Since the state found in [2] is a stacked state, spins in the same plane perpendicular to the distinguished $\langle 111 \rangle$ direction are all parallel. In this state, the spins in one Kagome lattice layer point opposite the spins in the adjacent Kagome layers, and the spins in one triangular lattice layer point opposite the spins in the adjacent triangular layers. So spins have a collinear antiferromagnetic ordering as one travels along the distinguished $\langle 111 \rangle$ direction from Kagome lattice layer to Kagome lattice layer and from triangular lattice layer to triangular lattice layer. Because of this antiferromagnetic ordering, the local field of a spin in a Kagome lattice layer due to its

neighbors in adjacent triangular lattice layers is zero. The same is true of the local field of a spin in a triangular lattice layer due to its neighbors in adjacent Kagome lattice layers.

We would like to determine which couplings J_1, J_2, J_3, J_3', J_4, etc. might cause (1.1) to have a ground state like that found in [2]. A state stacked in a $\langle 111 \rangle$ direction on the Pyrochlore lattice projects down onto a one-dimensional lattice with a basis of two sites, where the first kind of site represents a triangular lattice layer and the second kind of site represents a Kagome lattice layer. This one-dimensional non-Bravais lattice with a basis of two sites is known as the chain lattice, and the ground states of the chain lattice with various couplings were studied extensively in [1]. Here we work out the details of the projection of the Pyrochlore lattice down onto the chain lattice, so that this mapping can be used in the future to try and determine the interactions that produce a state like that found in [2].

Let the chain lattice have interactions j_1 between nearest neighbors, j_2 between second nearest neighbors which correspond to triangular lattice layers in the Pyrochlore lattice and j_2' between second nearest neighbors which correspond to Kagome lattice layers in the Pyrochlore lattice. We should scale up the couplings we find for spins in a Kagome lattice layer by a factor of three, since there are three times as many spins in the Kagome lattice layers as there are in the triangular lattice layers (for every site in a triangular lattice layer we have three sites in a Kagome lattice layer, since the Kagome layers contain spins from three F.C.C. sublattices but the triangular layers only contain spins from one F.C.C. sublattice).

To find the formulas for j_1, j_2 and j_2' in terms of J_1, J_2, J_3, J_3' and J_4, we use the technique outlined in subsection 1.3.5. A site in a triangular lattice layer has three of its J_1 neighbors, six of its J_2 neighbors and six of its J_4 neighbors in each Kagome layer adjacent to it. The situation is the same for sites in the Kagome layers except the number of neighbors is scaled down by a factor of three. Scaling up the numbers for the Kagome sites give an overall first neighbor interaction of $j_1 = 3J_1 + 6J_2 + 6J_4$.

A site in a triangular lattice layer has three of its J_3 neighbors in each triangular lattice layer closest to it so $j_2 = 3J_3$. A site in a Kagome lattice layer has two of its J_2 neighbors, one of its J_3 neighbors, two of its J_3' neighbors and four of its J_4 neighbors in each Kagome lattice layer closest to it so $j_2' = 6J_2 + 3J_3 + 6J_3' + 12J_4$.

We see that with interactions in the Pyrochlore lattice out to fourth nearest neighbors

we only get interactions in the chain lattice out to second nearest neighbors. The mapping from a state in the Pyrochlore lattice stacked along a $\langle 111 \rangle$ direction to the one-dimensional chain lattice takes the form

$$\begin{bmatrix} j_1 \\ j_2 \\ j_2' \end{bmatrix} = \begin{bmatrix} 3 & 6 & 0 & 0 & 6 \\ 0 & 0 & 3 & 0 & 0 \\ 0 & 6 & 3 & 6 & 12 \end{bmatrix} \begin{bmatrix} J_1 \\ J_2 \\ J_3 \\ J_3' \\ J_4 \end{bmatrix} \tag{3.8}$$

The Luttinger-Tisza matrix for the chain lattice with these interactions is system is given by

$$\underline{\underline{\tilde{\mathbf{J}}}}(q) = \begin{bmatrix} j_2 \cos(2dq) & j_1 \cos(dq) \\ j_1 \cos(dq) & j_2' \cos(2dq) \end{bmatrix} \tag{3.9}$$

where $d = \frac{1}{2\sqrt{3}}$ is the distance between adjacent Kagome and triangular lattice layers along a $\langle 111 \rangle$ axis in the Pyrochlore lattice. We can immediately write down some necessary conditions that the interactions in the Pyrochlore lattice will have to satisfy to produce a state like that found by Lee, et al. Since spins in the same Kagome lattice layer are all parallel we need a ferromagnetic first nearest neighbor interaction, so $J_1 > 0$.Since spins in the same triangular lattice are also all parallel to each other, we need the second kind of third nearest neighbor interaction to be ferromagnetic, so $J_3' > 0$ (recall that J_3' acts between sites in the same triangular lattice layer of an F.C.C. sublattice). Finally we need the two different kinds of second nearest neighbor interactions in the chain lattice to both be antiferromagnetic, so $j_2 < 0$ and $j_2' < 0$. The condition that $j_2 < 0$ tells us that we need $J_3 < 0$ in the Pyrochlore lattice. Finally, $j_2' < 0$ tells us that we need $6J_2 + 3J_3 + 6J_3' + 12J_4 < 0$. Writing $J_3 = -|J_3|$ and $J_3' = |J_3'|$, this last condition reduces to $2J_2 + 4J_4 < |J_3| - 2|J_3'|$.

This is just a set of necessary conditions, so they should be used to guide a search for a state like that found in [2]. They are not sufficient conditions, so more work is needed here to find the right set of interactions.

4. Conclusion

We have explored the entire J_1-J_2 phase diagram (figure 2.1), and we seem to have discovered all of the phases which exist in that region of parameter space. The J_1-J_2 phase diagram contains a rich variety of interesting coplanar and non-coplanar ground states, even though this diagram represents the case of only first and second nearest neighbor interactions. Of all the states found in this phase diagram, we only have a complete understanding of the geometry of the ferromagnetic state, the $J_1 < 0$ state, the $\mathbf{q} = \mathbf{0}$ state, the $\{q00\}$ planar spiral and the Cuboctahedral Stack state. We have written down approximate parameterizations for the Kawamura Sextuplet-q state, the Double-Twist state and the Multiply-Modulated Commensurate Spiral state, but these parameterizations do not have idealized coefficients and they are not normalized. We have also not attempted to parameterize the Kawamura Quadruplet-q states.

We know from Iterative Minimization simulations that more than just $\left\{\frac{3}{4}\frac{3}{4}0\right\}$ wavevectors are needed to normalize the Kawamura States and the Double-Twist state. The Multiply-Modulated Commensurate Spiral state, however, seems to be completely constructed from the wavevectors $2\pi(\frac{3}{4}, \frac{1}{4}, \frac{1}{2})$, $2\pi(\frac{3}{4}, \frac{1}{4}, -\frac{1}{2})$, $2\pi(\frac{3}{4}, -\frac{3}{4}, 0)$, and $2\pi(\frac{1}{4}, -\frac{1}{4}, 0)$ which we used to parameterize it. One possible goal for the near future would be to look for a set of idealized coefficients which give a normalized parameterization of this state, and then to analytically calculate the energy of this idealized state and compare it to the results of Iterative Minimization simulations.

We have also briefly looked at states with interactions beyond second nearest neighbors. With the interactions J_1, J_3 and J_3' we have again found the Cuboctahedral Stack state, as well as a new kind of alternating conic spiral state in which the wavevector which controls the spiraling behavior and the wavevector which controls the alternating behavior are not parallel. The fact that we stumbled onto these two states on a brief detour outside of the J_1-J_2 phase diagram suggests that there is a rich variety of new kinds of non-coplanar ground states to be found on the Pyrochlore lattice when one incorporates further neighbor interactions. There is plenty of work that can be done exploring the vast parameter space

of interactions beyond J_1 and J_2. One specific question which we would like to know the answer to is the question of which sets of interactions J_1, J_2, J_3, J_3', J_4, etc. can give a ground state like the one found in the neutron diffraction experiments carried out by Lee, et al in [2].

There are many unanswered questions about the ground states of equation (1.1) on the Pyrochlore lattice, and this project has only opened the door to the study and characterization of the many interesting and complicated ground states of the Heisenberg Hamiltonian on the Pyrochlore lattice.

BIBLIOGRAPHY

[1] S. Sklan and C.L. Henley, unpublished (2012).

[2] M. Matsuda, J.-H. Chung, S. Park, T. J. Sato, K. Matsuno, H. Aruga-Katori, H. Takagi, K. Kakurai, K. Kamazawa, Y. Tsunoda, I. Kagomiya, C. L. Henley, and S.-H. Lee. Europhys. Lett. **82**, 37006 (2008).

[3] C. L. Henley. Phys. Rev. Lett. **62**, 2056 (1989).

[4] C. L. Henley. Ann. Rev. Condens. Matter Phys., 1, 179-210 (2010).

[5] D. H. Lyons and T. A. Kaplan. J. Phys. Chem. Solids, **25**, 645 (1964).

[6] T.A. Kaplan and N. Menyuk. Phil. Mag. **87**, 3711 (2006).

[7] J.C. Domenge, P. Sindzingre, C. Lhuillier, and L. Pierre. Phys. Rev. B **72**, 024433 (2005).

[8] G.W. Chern, R. Moessner, and O. Tchernyshyov. Phys. Rev. B **78**, 144418 (2008).

[9] D. Tsuneishi, M. Ioki, and H. Kawamura. J. Phys.: Condens. Matter **19**, 145273 (2007).

[10] T. Okubo, T. H. Nguyen, and H. Kawamura. Phys. Rev. B **84**, 144432 (2011).

[11] N.W. Ashcroft and N.D. Mermin, *Solid State Physics*. Holt, Rinehart, and Winston, New York (1976).

[12] A. P. Ramirez, M.R.S. Bulletin, Volume 30, June 2005.

APPENDIX A
Taking Fourier Transforms on an F.C.C. Lattice

Performing a Fourier Transform of the spin configuration will tell us which wavevectors are used to construct the ground state. We take Fourier Transforms of the spin arrangement on each of the four F.C.C. sublattices. We then add together the absolute squares of these Fourier Transforms to determine which wavevectors the state is composed of.

An F.C.C. lattice is composed of four simple cubic sublattices. One can take the Fourier Transform of a function defined on a simple cubic lattice using the standard three dimensional Fourier Transform in rectangular coordinates. To take the Fourier Transform of a function defined on an F.C.C. lattice, one must first take Fourier Transforms within each of the four simple cubic sublattices and then combine these four Fourier Transforms in the proper way to get the full Fourier Transform for the F.C.C. lattice.

Consider a function $f_{x,y,z}$ $(x, y, z = 0 \ldots N-1)$ defined on an $L \times L \times L$ block of F.C.C. lattice unit cells where $L = \frac{N}{2}$ and the length of each side of a cubic unit cell is 2 (N must be even). Let the four simple cubic sublattices be located at positions (0,0,0), (1,1,0), (1,0,1) and (0,1,1). Define the four functions $s_{m,n,p}$, $t_{m,n,p}$, $u_{m,n,p}$ and $v_{m,n,p}$ $(m, n, p = 0 \ldots L-1)$ to be the values of the function $f_{x,y,z}$ on the four simple cubic sublattices.

$$s_{m,n,p} = f_{2m,2n,2p} \tag{A.1a}$$

$$t_{m,n,p} = f_{2m+1,2n+1,2p} \tag{A.1b}$$

$$u_{m,n,p} = f_{2m+1,2n,2p+1} \tag{A.1c}$$

$$v_{m,n,p} = f_{2m,2n+1,2p+1} \tag{A.1d}$$

The Fourier Transforms of these four functions on the simple cubic sublattices are given by

$$\tilde{s}_{j,k,l} = \left(\frac{1}{L}\right)^{\frac{3}{2}} \sum_{m=0}^{L-1}\sum_{n=0}^{L-1}\sum_{p=0}^{L-1} s_{m,n,p}\ e^{-i\frac{2\pi}{L}(mj+nk+pl)} \tag{A.2a}$$

$$\tilde{t}_{j,k,l} = \left(\frac{1}{L}\right)^{\frac{3}{2}} \sum_{m=0}^{L-1}\sum_{n=0}^{L-1}\sum_{p=0}^{L-1} t_{m,n,p}\ e^{-i\frac{2\pi}{L}(mj+nk+pl)} \tag{A.2b}$$

$$\tilde{u}_{j,k,l} = \left(\frac{1}{L}\right)^{\frac{3}{2}} \sum_{m=0}^{L-1}\sum_{n=0}^{L-1}\sum_{p=0}^{L-1} u_{m,n,p}\ e^{-i\frac{2\pi}{L}(mj+nk+pl)} \tag{A.2c}$$

$$\tilde{v}_{j,k,l} = \left(\frac{1}{L}\right)^{\frac{3}{2}} \sum_{m=0}^{L-1}\sum_{n=0}^{L-1}\sum_{p=0}^{L-1} v_{m,n,p}\ e^{-i\frac{2\pi}{L}(mj+nk+pl)} \tag{A.2d}$$

where $j,k,l = 0\ldots L-1$. The Fourier Transform $\tilde{f}_{q_x,q_y,q_z}$ ($q_x,q_y,q_z \in \mathbb{N}$ and $q_x,q_y,q_z = 0\ldots N-1$) of the function $f_{x,y,z}$ can then be calculated from $\tilde{s}_{j,k,l}$, $\tilde{t}_{j,k,l}$, $\tilde{u}_{j,k,l}$ and $\tilde{v}_{j,k,l}$ by adding them together with the appropriate phase factors. The subscripts q_x,q_y,q_z must run from 0 to N-1 because the Brillouin zone of the F.C.C. lattice is larger than the Brillouin zone of the simple cubic lattice. Because this is twice the range of j,k and l, we must consider eight different cases when we combine the Fourier Transforms within the four simple cubic lattices to get the Fourier Transform on the F.C.C. lattice. It turns out that we only need to do four separate calculations. We find:

$$\tilde{f}_{j,k,l} = \frac{1}{2}\left(\tilde{s}_{j,k,l} + e^{-i\frac{\pi}{L}(j+k)}\ \tilde{t}_{j,k,l} + e^{-i\frac{\pi}{L}(j+l)}\ \tilde{u}_{j,k,l} + e^{-i\frac{\pi}{L}(k+l)}\ \tilde{v}_{j,k,l}\right) \tag{A.3a}$$

$$\tilde{f}_{j+L,k,l} = \frac{1}{2}\left(\tilde{s}_{j,k,l} - e^{-i\frac{\pi}{L}(j+k)}\ \tilde{t}_{j,k,l} - e^{-i\frac{\pi}{L}(j+l)}\ \tilde{u}_{j,k,l} + e^{-i\frac{\pi}{L}(k+l)}\ \tilde{v}_{j,k,l}\right) \tag{A.3b}$$

$$\tilde{f}_{j,k+L,l} = \frac{1}{2}\left(\tilde{s}_{j,k,l} - e^{-i\frac{\pi}{L}(j+k)}\ \tilde{t}_{j,k,l} + e^{-i\frac{\pi}{L}(j+l)}\ \tilde{u}_{j,k,l} - e^{-i\frac{\pi}{L}(k+l)}\ \tilde{v}_{j,k,l}\right) \tag{A.3c}$$

$$\tilde{f}_{j,k,l+L} = \frac{1}{2}\left(\tilde{s}_{j,k,l} + e^{-i\frac{\pi}{L}(j+k)}\ \tilde{t}_{j,k,l} - e^{-i\frac{\pi}{L}(j+l)}\ \tilde{u}_{j,k,l} - e^{-i\frac{\pi}{L}(k+l)}\ \tilde{v}_{j,k,l}\right) \tag{A.3d}$$

$$\tilde{f}_{j+L,k+L,l+L} = \tilde{f}_{j,k,l} \tag{A.3e}$$

$$\tilde{f}_{j,k+L,l+L} = \tilde{f}_{j+L,k,l} \tag{A.3f}$$

$$\tilde{f}_{j+L,k,l+L} = \tilde{f}_{j,k+L,l} \tag{A.3g}$$

$$\tilde{f}_{j+L,k+L,l} = \tilde{f}_{j,k,l+L} \tag{A.3h}$$

We have now calculated $\tilde{f}_{q_x,q_y,q_z}$ at all points $q_x,q_y,q_z = 0\ldots N-1$. The Fourier

Transform has been normalized so that a $\mathbf{q} = \mathbf{0}$ state with $f_{x,y,z} = f_0$ for all x,y, and z has $\tilde{f}_{0,0,0} = f_0 \frac{N^{\frac{3}{2}}}{\sqrt{2}}$, where $\frac{N^{\frac{3}{2}}}{\sqrt{2}}$ is the square root of the number of sites in this F.C.C. lattice.

When analyzing a spin configuration, we must take a Fourier Transform like this for the $\hat{\mathbf{A}}_0$, $\hat{\mathbf{B}}_0$ and $\hat{\mathbf{C}}_0$ components of each spin in each F.C.C. sublattice for a total of 48 $(3 \times 4 \times 4)$ Fourier Transforms calculated on simple cubic sublattices. Once we know the Fourier Transform of each spin component on the four simple cubic lattices, we add together their absolute squares to determine which wavevectors the observed state is composed of.

APPENDIX B
The Luttinger-Tisza Matrix for the Pyrochlore Lattice

In this appendix we present the full Luttinger-Tisza matrix for the Pyrochlore lattice, including interactions J_1, J_2, J_3, J_3' and J_4 all the way out to fourth nearest neighbors. It is a 4×4 matrix because the Pyrochlore lattice has four Bravais sublattices (four F.C.C. sublattices to be precise). We calculate the elements of this matrix using equation (1.19) . The matrix is:

$$\underline{\underline{\tilde{\mathbf{J}}}}(\mathbf{q}) = J_1\underline{\underline{\mathbf{M}_2}} + J_2\underline{\underline{\mathbf{M}_2}} + J_3\underline{\underline{\mathbf{M}_3}} + J_3'\underline{\underline{\mathbf{M}_3'}} + J_4\underline{\underline{\mathbf{M}_4}} \tag{B.1}$$

where

$$\underline{\underline{\mathbf{M}_1}} = \begin{pmatrix} 0 & \cos(\frac{q_y+q_z}{4}) & \cos(\frac{q_x+q_z}{4}) & \cos(\frac{q_x+q_y}{4}) \\ \cos(\frac{q_y+q_z}{4}) & 0 & \cos(\frac{q_x-q_y}{4}) & \cos(\frac{q_x-q_z}{4}) \\ \cos(\frac{q_x+q_z}{4}) & \cos(\frac{q_x-q_y}{4}) & 0 & \cos(\frac{q_y-q_z}{4}) \\ \cos(\frac{q_x+q_y}{4}) & \cos(\frac{q_x-q_z}{4}) & \cos(\frac{q_y-q_z}{4}) & 0 \end{pmatrix} \tag{B.2}$$

$$\underline{\underline{\mathbf{M}_2}} = 2\begin{pmatrix} 0 & \cos(\frac{q_x}{2})\cos(\frac{q_y-q_z}{4}) & \cos(\frac{q_y}{2})\cos(\frac{q_z-q_x}{4}) & \cos(\frac{q_z}{2})\cos(\frac{q_x-q_y}{4}) \\ \cos(\frac{q_x}{2})\cos(\frac{q_y-q_z}{4}) & 0 & \cos(\frac{q_z}{2})\cos(\frac{q_x+q_y}{4}) & \cos(\frac{q_y}{2})\cos(\frac{q_x+q_z}{4}) \\ \cos(\frac{q_y}{2})\cos(\frac{q_z-q_x}{4}) & \cos(\frac{q_z}{2})\cos(\frac{q_x+q_y}{4}) & 0 & \cos(\frac{q_x}{2})\cos(\frac{q_y+q_z}{4}) \\ \cos(\frac{q_z}{2})\cos(\frac{q_x-q_y}{4}) & \cos(\frac{q_y}{2})\cos(\frac{q_x+q_z}{4}) & \cos(\frac{q_x}{2})\cos(\frac{q_y+q_z}{4}) & 0 \end{pmatrix} \tag{B.3}$$

To concisely express the matrices that go with the two kinds of third nearest neighbor interaction, we introduce the condensed notation

$$C_{xy} = \cos\left(\frac{q_x+q_y}{2}\right) \tag{B.4a}$$

$$\bar{C}_{xy} = \cos\left(\frac{q_x-q_y}{2}\right) \tag{B.4b}$$

and a similar notation for cosine terms with arguments using q_y and q_z.

$$\underline{\underline{\mathbf{M}_3}} = \begin{pmatrix} C_{xy}+C_{xz}+C_{yz} & 0 & 0 & 0 \\ 0 & \bar{C}_{xy}+\bar{C}_{xz}+C_{yz} & 0 & 0 \\ 0 & 0 & \bar{C}_{xy}+C_{xz}+\bar{C}_{yz} & 0 \\ 0 & 0 & 0 & C_{xy}+\bar{C}_{xz}+\bar{C}_{yz} \end{pmatrix} \tag{B.5}$$

$$\underline{\underline{\mathbf{M}'_3}} = \begin{pmatrix} \bar{C}_{xy}+\bar{C}_{xz}+\bar{C}_{yz} & 0 & 0 & 0 \\ 0 & C_{xy}+C_{xz}+\bar{C}_{yz} & 0 & 0 \\ 0 & 0 & C_{xy}+\bar{C}_{xz}+C_{yz} & 0 \\ 0 & 0 & 0 & \bar{C}_{xy}+C_{xz}+C_{yz} \end{pmatrix} \tag{B.6}$$

$$\underline{\underline{\mathbf{M}_4}} = 2 \begin{pmatrix} 0 & \cos(\frac{q_y-q_z}{2})\cos(\frac{q_y+q_z}{4}) & \cos(\frac{q_x-q_z}{2})\cos(\frac{q_x+q_z}{4}) & \cos(\frac{q_x-q_y}{2})\cos(\frac{q_x+q_y}{4}) \\ \cos(\frac{q_y-q_z}{2})\cos(\frac{q_y+q_z}{4}) & 0 & \cos(\frac{q_x+q_y}{2})\cos(\frac{q_x-q_y}{4}) & \cos(\frac{q_x+q_z}{2})\cos(\frac{q_x-q_z}{4}) \\ \cos(\frac{q_x-q_z}{2})\cos(\frac{q_x+q_z}{4}) & \cos(\frac{q_x+q_y}{2})\cos(\frac{q_x-q_y}{4}) & 0 & \cos(\frac{q_y+q_z}{2})\cos(\frac{q_y-q_z}{4}) \\ \cos(\frac{q_x-q_y}{2})\cos(\frac{q_x+q_y}{4}) & \cos(\frac{q_x+q_z}{2})\cos(\frac{q_x-q_z}{4}) & \cos(\frac{q_y+q_z}{2})\cos(\frac{q_y-q_z}{4}) & 0 \end{pmatrix} \tag{B.7}$$

There are a few interesting things about this matrix. While the Luttinger-Tisza is generally a hermitian matrix, this matrix is symmetric because every site on the Pyrochlore lattice is a center of inversion symmetry. Secondly, only J_3 and J'_3 terms appear on the diagonals since these are the only interactions that act between spins in the same F.C.C. sublattice. The other interactions J_1, J_2 and J_4 only act between sites in different F.C.C. sublattices, so these show up only in off-diagonal terms. Because of the messy algebra involved, it is best to calculate the eigenvalues of the Luttinger-Tisza matrix numerically, except for in a few special cases, one of which we discuss in Appendix C.

APPENDIX C
Degeneracy of the Luttinger-Tisza eigenvalues for a pure first neighbor interaction J_1

In the case of a pure first neighbor interaction J_1, the matrix $\underline{\underline{\tilde{J}}}(\mathbf{q})$ simplifies enough that one can find the eigenvalues by hand. After working through the algebra and making use of many trigonometric identities, one finds that the characteristic equation is

$$det[\ \underline{\underline{\tilde{J}}}(\mathbf{q}) - \lambda \underline{\underline{I}}\ ] = \lambda^4 - J_1^2(3 + A(\mathbf{q}))\lambda^2 - 2J_1^3(1 + A(\mathbf{q}))\lambda - J_1^4 A(\mathbf{q}) = 0 \tag{C.1}$$

where

$$A(\mathbf{q}) = \cos\left(\frac{q_x}{2}\right)\cos\left(\frac{q_y}{2}\right) + \cos\left(\frac{q_x}{2}\right)\cos\left(\frac{q_z}{2}\right) + \cos\left(\frac{q_y}{2}\right)\cos\left(\frac{q_z}{2}\right) \tag{C.2}$$

and q_x, q_y, and q_z are the components of the vector $\mathbf{q}$. Separating the terms that multiply $A(\mathbf{q})$ from the terms that do not, we find

$$\lambda(\lambda^3 - 3J_1^2\lambda - 2J_1^3) - J_1^2 A(\mathbf{q})(\lambda^2 + 2J_1\lambda + J_1^2) = 0 \tag{C.3}$$

We can easily see that $\lambda^2 + 2J_1\lambda + J_1^2 = (\lambda + J_1)^2$. We might then try to look for some d such that $(\lambda + d)(\lambda + J_1)^2 = \lambda^3 - 3J_1^2\lambda - 2J_1^3$. A little algebra shows that $d = -2J_1$ makes this work. Then the characteristic equation becomes

$$(\lambda^2 - 2J_1\lambda - J_1^2 A(\mathbf{q}))(\lambda + J_1)^2 = 0 \tag{C.4}$$

so the four eigenvalues of $\underline{\underline{\tilde{J}}}(\mathbf{q})$ are

$$\lambda_1 = -J_1 \tag{C.5}$$

$$\lambda_2 = -J_1 \tag{C.6}$$

$$\lambda_3 = J_1\left(1 + \sqrt{1 + A(\mathbf{q})}\right) \tag{C.7}$$

$$\lambda_4 = J_1\left(1 - \sqrt{1 + A(\mathbf{q})}\right) \tag{C.8}$$

We see that when $J_1 < 0$ the two largest eigenvalues of $\underline{\underline{\tilde{J}}}(\mathbf{q})$ are exactly $-J_1$, and so they are not functions of $\mathbf{q}$. This means that all possible ordering wavevectors are equally favorable, as long as the resulting state satisfies the constraint that the four spins on every tetrahedron add to zero.

As a side note, we can see that in the case of a ferromagnetic first neighbor interaction $J_1 > 0$, the optimal wavevector is indeed the zero wavevector. In the ferromagnetic case the largest eigenvalue of $\underline{\underline{\tilde{J}}}(\mathbf{q})$ is $J_1 \left(1 + \sqrt{1 + A(\mathbf{q})}\right)$, and this achieves its maximum value when $\mathbf{q} = \mathbf{0}$ and $A(\mathbf{q}) = 3$. So the optimal Luttinger-Tisza wavevector in that case is the zero wavevector, as it should be.

APPENDIX D

Equivalence of small $J_2 > 0$ and small $J_3 < 0$ (and vice-versa) for large $J_1 < 0$.

When the dominant interaction is a large antiferromagnetic first neighbor exchange $J_1 < 0$, one often finds that the four spins at the vertices of each tetrahedron approximately sum to zero. One can use this constraint to replace a small second neighbor exchange J_2 with a small third neighbor exchange $J_3 = -J_2$ (an alternate proof of this fact is given in [8]). This constraint is likely to be satisfied only when the first neighbor interaction J_1 is much larger in magnitude than the second neighbor interaction J_2, or $|J_1| \gg |J_2|$.

Suppose we have a system with a large antiferromagnetic first neighbor exchange $J_1 < 0$ and a small second neighbor exchange J_2, with $|J_2| \ll |J_1|$. We can write out the site energy of one spin, $\mathbf{s}_i$, as

$$\mathcal{E}_i = -\frac{J_1}{2}\sum_{j=1}^{6} \mathbf{s}_i \cdot \mathbf{s}_j - \frac{J_2}{2}\sum_{k=1}^{12} \mathbf{s}_i \cdot \mathbf{s}_k \tag{D.1}$$

where the first sum is over the six first nearest neighbors of $\mathbf{s}_i$ and the second sum is over the 12 second nearest neighbors of $\mathbf{s}_i$. We can use the constraint that the four spins on the corner of every tetrahedron sum to zero to rewrite the sum over the 12 second nearest neighbors of $\mathbf{s}_i$ as a sum over the six J_3 neighbors of $\mathbf{s}_i$ (the first kind of third nearest neighbor).

We demonstrate this for a spin $\mathbf{s}_0$ in the zeroth FCC sublattice, although the result is the same for any spin $\mathbf{s}_i$. The six first nearest neighbors of $\mathbf{s}_0$ are contained in the two tetrahedra which also contain $\mathbf{s}_0$. Label these two tetrahedra 1 and 2. The 12 second nearest neighbors $\mathbf{s}_0$ consist of two spins each from another six different tetrahedra. Label these six tetrahedra 3, 4, 5, 6, 7 and 8. The position of these eight tetrahedra, in relation to the position of the spin $\mathbf{s}_0$ is shown in figure D.1.

Figure D.1: Location of the spin s_0 and the eight tetrahedra containing its first and second nearest neighbors.

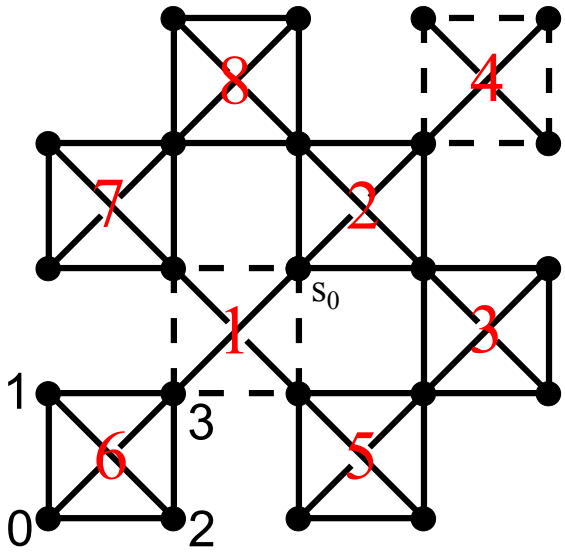

Each tetrahedron has four spins on it, one in each F.C.C. sublattice. We'll label the four spins on each tetrahedron by the F.C.C. sublattice they belong to, for example the spins on tetrahedron 1 are labeled $\vec{s}_{0,1}$, $\vec{s}_{1,1}$, $\vec{s}_{2,1}$ and $\vec{s}_{3,1}$, where the first subscript indicates which F.C.C. sublattice the spins are in and the second subscript indicates which tetrahedron the spins are on. The constraint that the sum of the spins on the corners of each tetrahedron be zero can be written as

$$\sum_{\alpha=0}^{3} \mathbf{s}_{\alpha,1} = \mathbf{0} \tag{D.2}$$

for tetrahedron 1, and likewise for the other tetrahedra. A spin in F.C.C. sublattice 0, $\mathbf{s}_0$, has two first nearest neighbors and four second nearest neighbors in each of FCC sublattices 1, 2 and 3. In terms of spins on these eight tetrahedra we can write the sums in equation

(D.1) over the first and second nearest neighbor spins as

$$\sum_{j=1}^{6} \mathbf{s}_0 \cdot \mathbf{s}_j = \mathbf{s}_0 \cdot (\mathbf{s}_{1,1} + \mathbf{s}_{2,1} + \mathbf{s}_{3,1} + \mathbf{s}_{1,2} + \mathbf{s}_{2,2} + \mathbf{s}_{3,2}) \tag{D.3}$$

$$\sum_{k=1}^{12} \mathbf{s}_0 \cdot \mathbf{s}_k = \mathbf{s}_0 \cdot (\mathbf{s}_{1,3} + \mathbf{s}_{3,3} + \mathbf{s}_{1,4} + \mathbf{s}_{2,4} + \mathbf{s}_{2,5} + \mathbf{s}_{3,5} + \mathbf{s}_{1,6} + \mathbf{s}_{2,6} + \mathbf{s}_{1,7} + \mathbf{s}_{3,7} + \mathbf{s}_{2,8} + \mathbf{s}_{3,8}) \tag{D.4}$$

Applying the constraint of equation (D.2), we immediately see that the sum in equation (D.3) is equal to -2. To calculate the second sum, we first need to deal with some redundancy in our notation. By looking at where the spins in these eight different tetrahedra are located, we see that $\mathbf{s}_{2,2} = \mathbf{s}_{2,3}$, $\mathbf{s}_{3,2} = \mathbf{s}_{3,4}$, $\mathbf{s}_{1,2} = \mathbf{s}_{1,8}$, $\mathbf{s}_{1,1} = \mathbf{s}_{1,5}$, $\mathbf{s}_{3,1} = \mathbf{s}_{3,6}$, and $\mathbf{s}_{2,1} = \mathbf{s}_{2,7}$. So these twelve spins are really only six (both spins in each pair are at the same location, so we had two labels for the same spin). Then the sum in equation (D.4) can be rewritten as

$$\sum_{k=1}^{12} \mathbf{s}_0 \cdot \mathbf{s}_k = \mathbf{s}_0 \cdot (-\mathbf{s}_{1,1} - \mathbf{s}_{2,1} - \mathbf{s}_{3,1} - \mathbf{s}_{1,2} - \mathbf{s}_{2,2} - \mathbf{s}_{3,2} - \mathbf{s}_{0,3} - \mathbf{s}_{0,4} - \mathbf{s}_{0,5} - \mathbf{s}_{0,6} - \mathbf{s}_{0,7} - \mathbf{s}_{0,8}) \tag{D.5}$$

Using the constraint of equation (D.2), this sum can be rewritten as

$$\sum_{k=1}^{12} \mathbf{s}_0 \cdot \mathbf{s}_k = 2 - \mathbf{s}_0 \cdot (\mathbf{s}_{0,3} + \mathbf{s}_{0,4} + \mathbf{s}_{0,5} + \mathbf{s}_{0,6} + \mathbf{s}_{0,7} + \mathbf{s}_{0,8}) \tag{D.6}$$

The six spins with first subscript 0 in this sum can be recognized as the six J_3 neighbors of the spin $\mathbf{s}_0$. Thus we are able to write down the site energy of $\mathbf{s}_0$ in terms of a sum over its J_3 neighbors. Finally, since this expression will be the same for spins in any F.C.C. sublattice we can rewrite equation (D.1) for any spin $\vec{s}_i$ when the constraint (D.2) holds. We get

$$\mathcal{E}_i = J_1 - J_2 + \frac{J_2}{2} \sum_{l=1}^{6} \mathbf{s}_i \cdot \mathbf{s}_l \tag{D.7}$$

where the subscript l indexes the six J_3 neighbors of the site i. This proves that when the constraint (D.2) holds, a small second nearest neighbor interaction J_2 of one sign is equivalent to a small J_3 interaction of the opposite sign.

APPENDIX E

Unit cells of the six sublattices of the Kawamura Sextuplet-q State

These are the locations of lattice sites in the unit cells of the six sublattices of the Kawamura Sextuplet-q state example with $J_1 = -1$, $J_2 = 0.1$, $L = 4$ and $seed = 67$.

1. F.C.C.0: (0,0,0), (1,1,1), (.5,0,1.5), (1.5,1,.5), (.5,1.5,0), (1.5,.5,1)
   F.C.C.1: (.5,1.25,.75), (1.5,.25,1.75), (0,.75,.75), (1,1.75,1.75), (.5,.75,1.25), (1.5,1.75,.25)
   F.C.C.2: (.25,1,.25), (1.25,0,1.25), (.75,1,1.75), (1.75,0,.75), (.25,.5,1.75), (1.25,1.5,.75)
   F.C.C.3: (.25,.25,1), (1.25,1.25,0), (.25,1.75,.5), (1.25,.75,1.5), (.75,1.75,1), (1.75,.75,0)

2. F.C.C.0: (0,1,0), (1,1,0), (1.5,0,.5), (1.5,0,1.5), (.5,.5,1), (5,1.5,1)
   F.C.C.1: (.5,.25,1.75), (.5,1.25,1.75), (0,1.75,.75), (1,1.75,.75), (1.5,.75,.25), (1.5,.75,1.25)
   F.C.C.2: (.25,0,.25), (.25,0,1.25), (.75,1,.75), (1.75,1,.75), (1.25,.5,1.75), (1.25,1.5,1.75)
   F.C.C.3: (1.25,.25,1), (1.25,1.25,1),(.25,.75,.5), (.25,.75,1.5), (.75,1.75,0), (1.75,1.75,0)

3. F.C.C.0: (0,.5,.5), (0,.5,1.5), (0,1.5,.5), (1,.5,1.5), (1,1.5,.5), (1,1.5,1.5)
   F.C.C.1: (0,.25,.25), (0,.25,1.25), (0,1.25,.25), (1,.25,1.25), (1,1.25,.25), (1,1.25,1.25)
   F.C.C.2: (.75,.5,1.25), (.75,1.5,.25), (.75,1.5,1.25), (1.75,.5,.25), (1.75,.5,1.25), (1.75,1.5,.25)
   F.C.C.3: (.75,.25,1.5), (.75,1.25,.5), (.75,1.25,1.5), (1.75,.25,.5), (1.75,.25,1.5), (1.75,1.25,.5)

4. F.C.C.0: (0,1.5,1.5), (1,.5,.5)
   F.C.C.1: (0,1.25,1.25), (1,.25,.25)
   F.C.C.2: (.75,.5,.25), (1.75,1.5,1.25)
   F.C.C.3: (.75,.25,.5), (1.75,1.25,1.5)

5. F.C.C.0: ((0,1,1), (1,0,0), (.5,0,.5), (1.5,1,1.5), (.5,.5,0), (1.5,1.5,1)
   F.C.C.1: (.5,.25,.75), (1.5,1.25,1.75), (0,1.75,1.75), (1,.75,.75), (.5,.75,.25), (1.5,1.75,1.25)
   F.C.C.2: (.25,1,1.25), (1.25,0,.25), (.75,0,.75), (1.75,1,1.75), (.25,1.5,1.75), (1.25,.5,.75)
   F.C.C.3: (.25,1.25,1), (1.25,.25,0), (.25,1.75,1.5), (1.25,.75,.5), (.75,.75,0), (1.75,1.75,1)

6. F.C.C.0: (0,0,1), (1,0,1), (.5,1.5), (.5,1,1.5), (1.5,.5,0), (1.5,1.5,0)
   F.C.C.1: (1.5,.25,.75), (1.5,1.25,.75), (0,.75,1.75), (1,.75,1.75), (.5,1.75,.25), (.5,1.75,1.25)

F.C.C.2: (1.25,1,.25), (1.25,1,1.25), (.75,0,1.75), (1.75,0,1.75), (.25,.5,.75), (.25,1.5,.75)

F.C.C.3: (.25,.25,0), (.25,1.25,0), (1.25,1.75,.5), (1.25,1.75,1.5), (.75,.75,1), (1.75,.75,1)